Интернет-семинар «Актуальные проблемы прикладной математики»

Математическое моделирование гемодинамики головного мозга

А. П. Чупахин, А. К. Хе, Д. В. Паршин, А. А. Черевко

Институт гидродинамики им. М. А. Лаврентьева СО РАН

Новосибирский государственный университет

15 мая 2020 г.
Математический центр в Академгородке, Новосибирск

Introduction. A problem

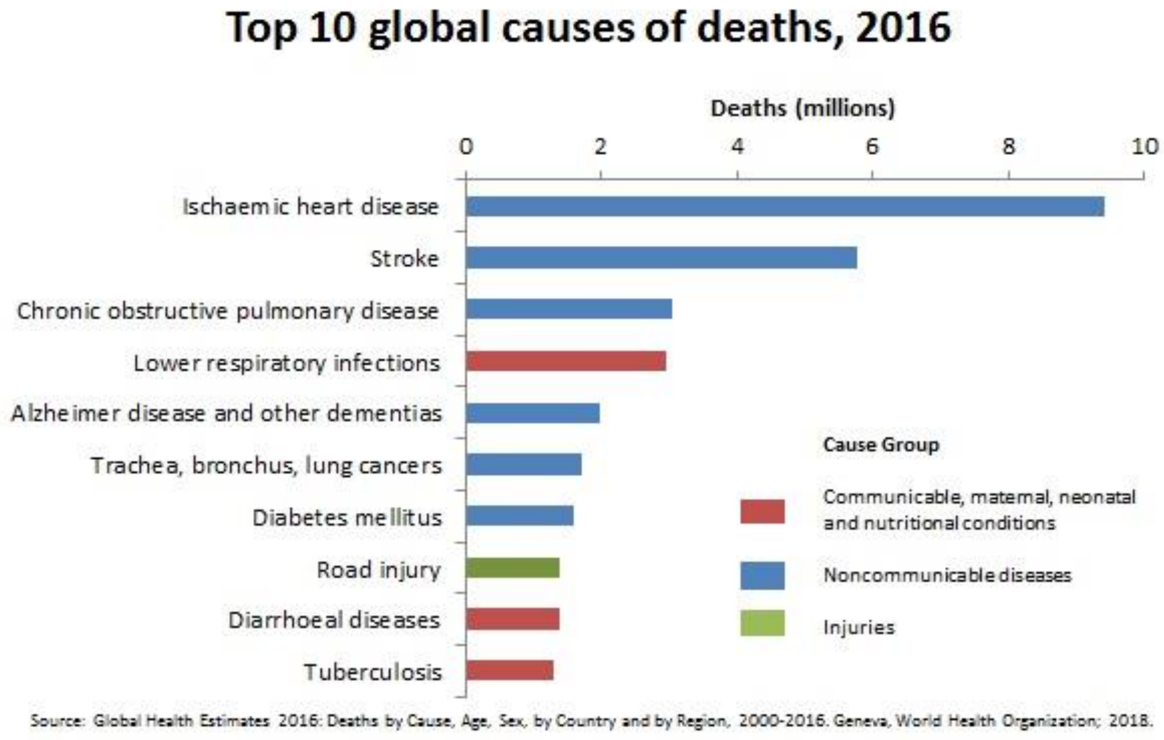

Source: Global Health Estimates 2016: Deaths by Cause, Age, Sex, by Country and by Region, 2000-2016. Geneva, World Health Organization; 2018.

© WHO

According to W.H.O. aneurysm associated diseases are among the most common causes of death in the world.

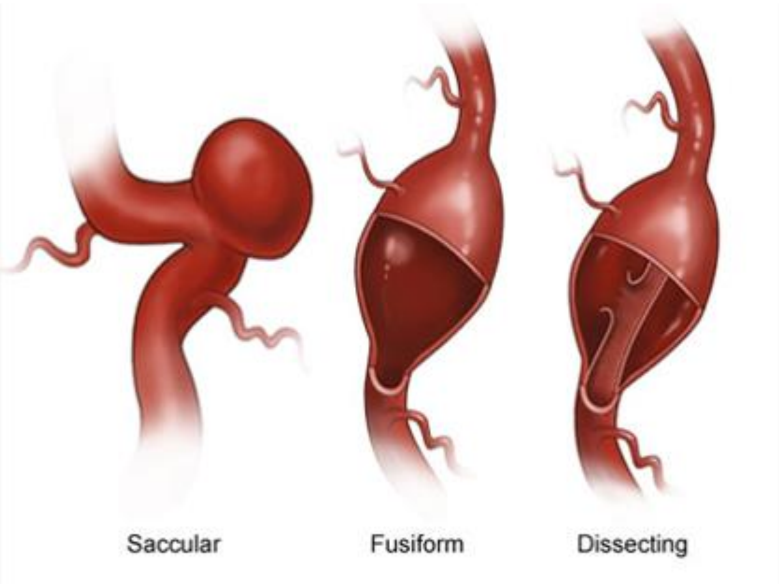

© Mayo Clinic

Types of aneurysm:

- Saccular,
- Fusiform,
- Dissecting;

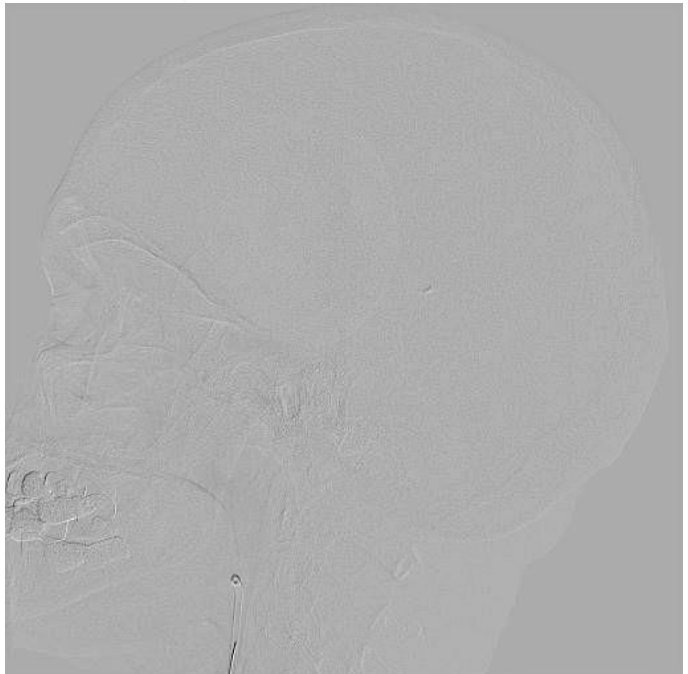

Introduction. A problem

Is surgery necessary?

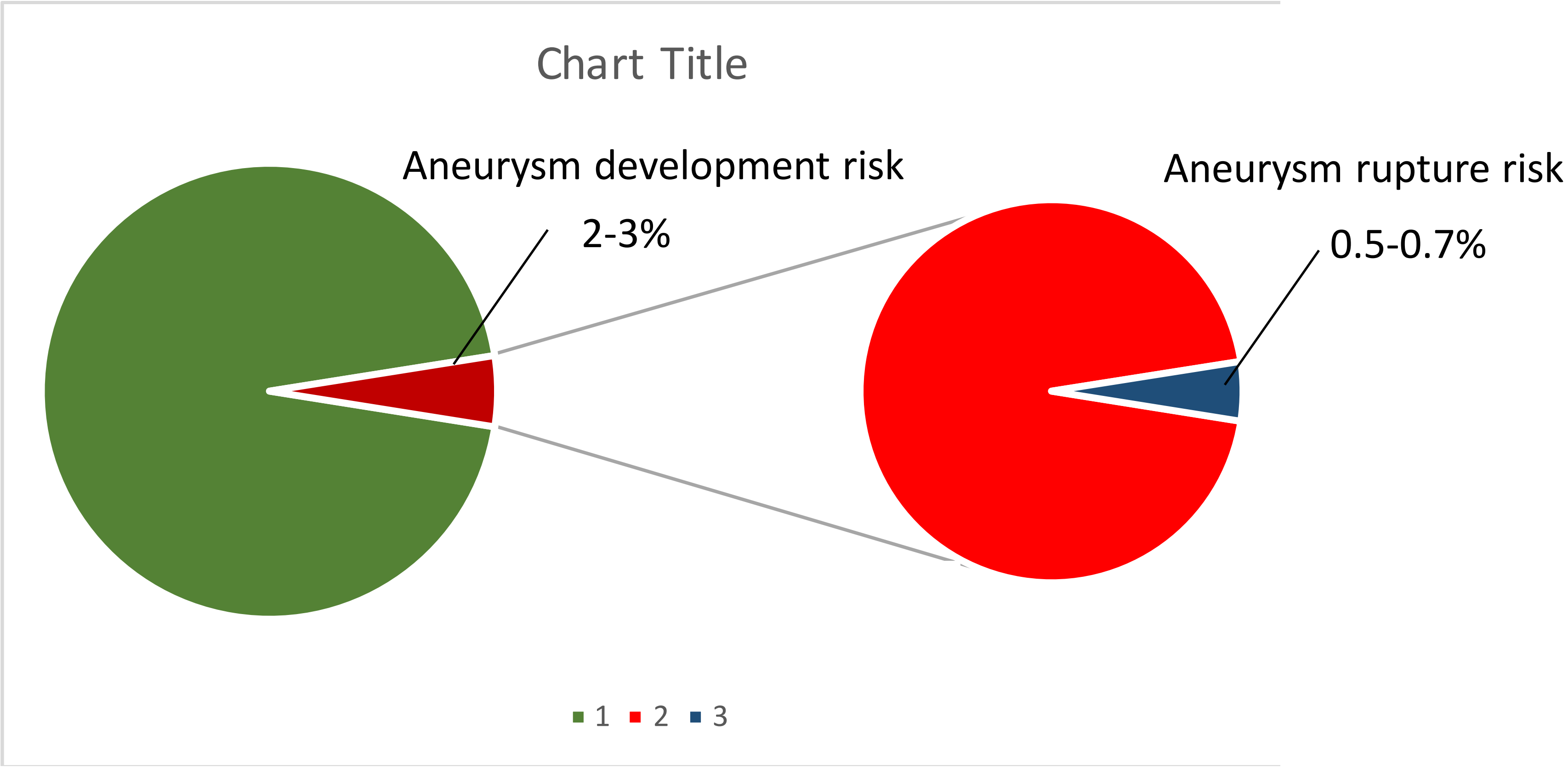

Risk of rupture ~ Risk of developing postoperative complications (0.6%)!!!

ISUIAI, *Lancet* 2003; 362: 103–10

PART I. Clinical monitoring

The aim

- Develop the measurement device and information complex for endovascular intraoperative monitoring

- Create the database for monitoring
  of the hydrodynamic parameters of blood flow

- Optimize neurosurgeon operations

Pressure and blood flow rate measurement

Pressure and velocity measurement sensor:

diameter ≈ 0.36 mm

length ≈ 1.85 m

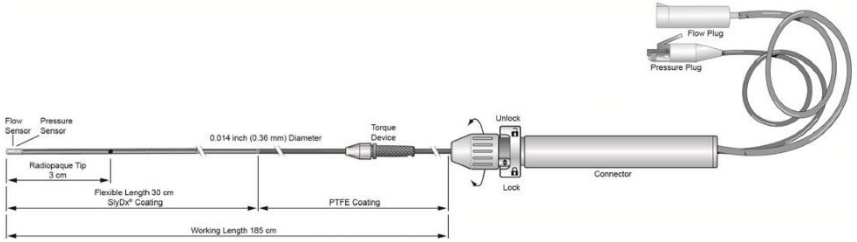

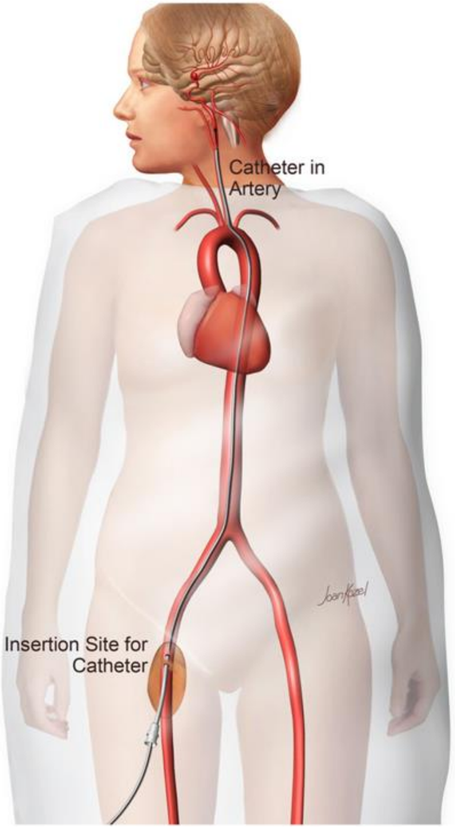

Khe, A. K., Cherevko, A. A., Chupakhin, A. P., Krivoshapkin, A. L., Orlov, K. Yu., & Panarin, V. A. (2017). Monitoring of hemodynamics of brain vessels. *Journal of Applied Mechanics and Technical Physics*, *58*(5), 763–770. https://doi.org/10.1134/S0021894417050017

Monitoring

Monitoring of neurosurgery operations includes:

- Select the data with best quality
- Clean the data - remove noise (wavelet analysis)
- Make the phase diagrams «velocity-pressure», «flow rate-flux of energy» (during neurosurgical operation)
- Make operations maps
- Make the phase diagrams «velocity-pressure», «flow rate-flux of energy» (before and after operation)

Monitoring was made for ≈50 neurosurgical operations of arteriovenous malformations and cerebral aneurysms
in Meshalkin NRICP.

Endovascular blood flow measurements

X-ray angiography

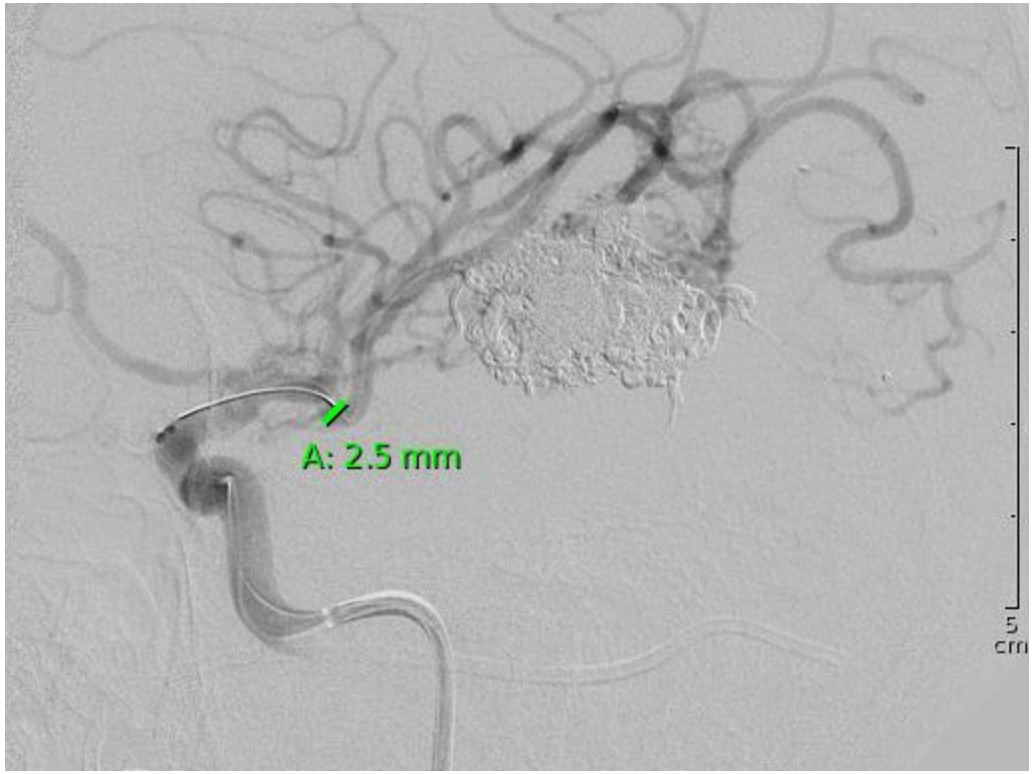

ComboMap

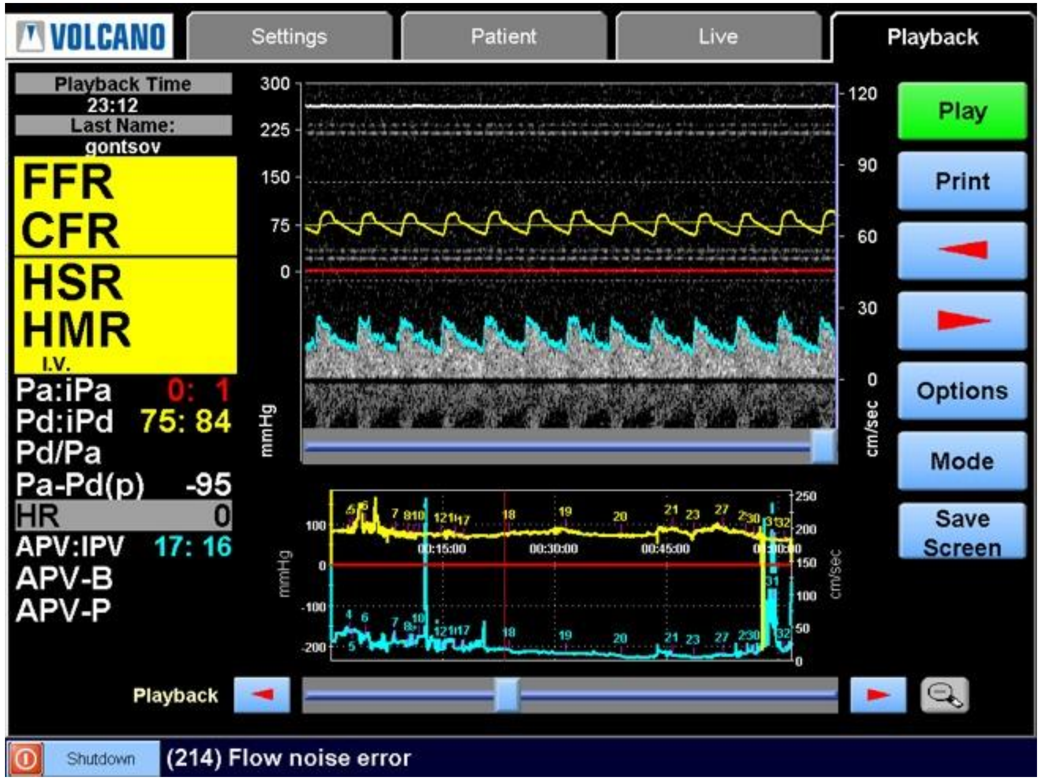

Playback Time
23:12
Last Name:
gontsov

FFR
CFR
HSR
HMR
I.V.

Pa:iPa 0: 1
Pd:iPd 75: 84
Pd/Pa
Pa-Pd(p) -95
HR 0
APV:IPV 17: 16
APV-B
APV-P

(214) Flow noise error

Intraoperative dynamics in the AVM afferent

Total embolization of an AVM

1. Before operation

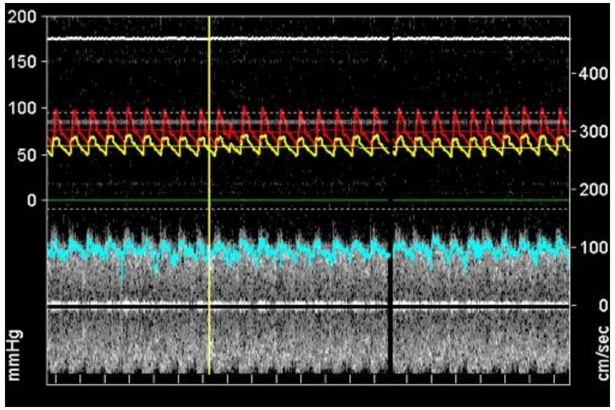

2. Onyx, 1.5 ml

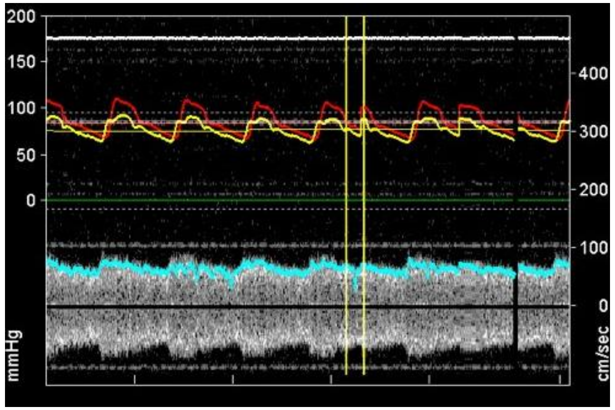

3. Onyx, 2 ml

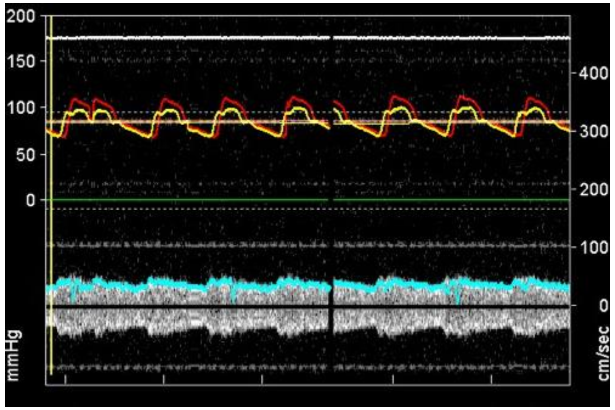

4. After operation

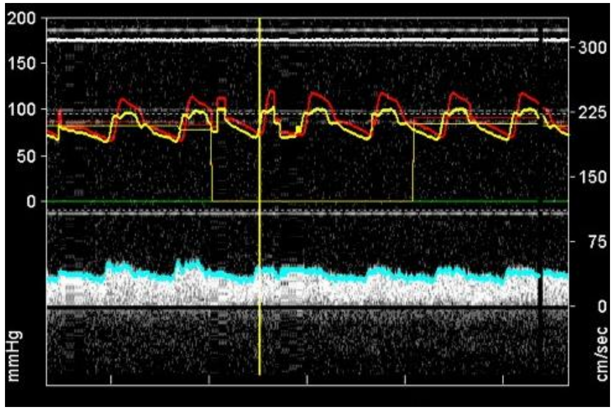

Real-time monitoring

Software for acquisition and processing data in real time

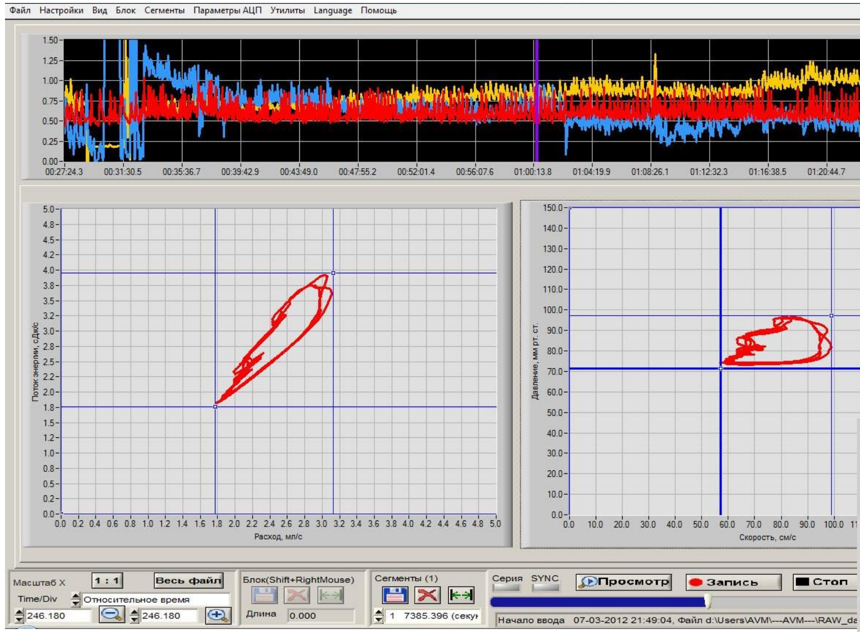

Window 1 QV-QE-03-06-01

Курсор

X 57.1165

Y 71.4115

Time/Div Относительное время

246.180

246.180

Длина 0.000

1 7385.396 (секун

Начало ввода 07-03-2012 21:49:04, Файл d:\Users\AVM\---AVM---\RAW_da

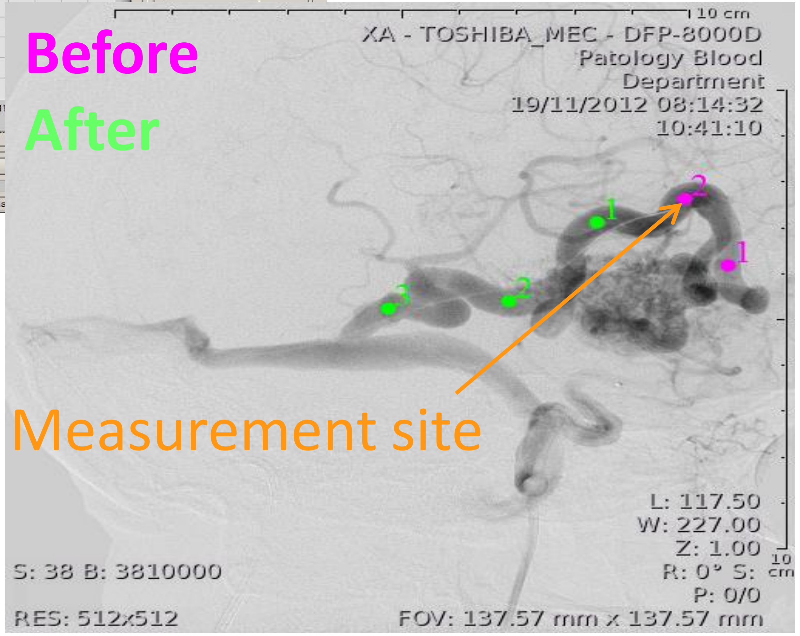

Before

After

Measurement site

The dynamics during operation

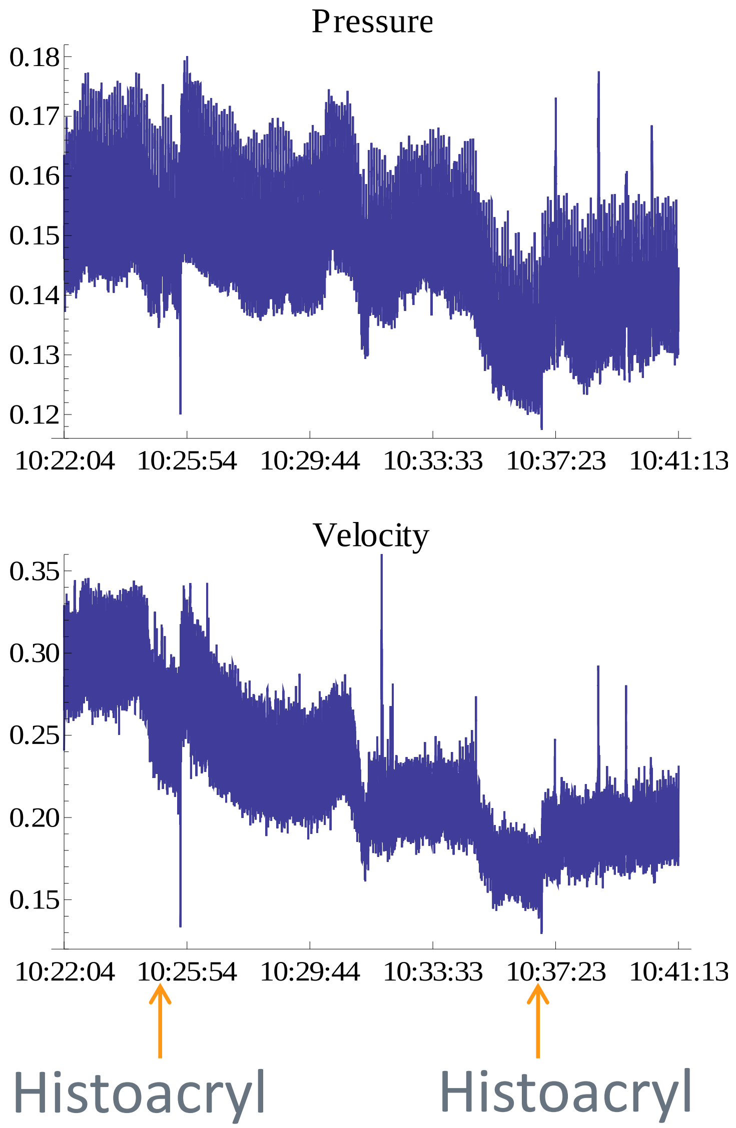

Histoacryl Histoacryl

Operation map with blood flow characteristics

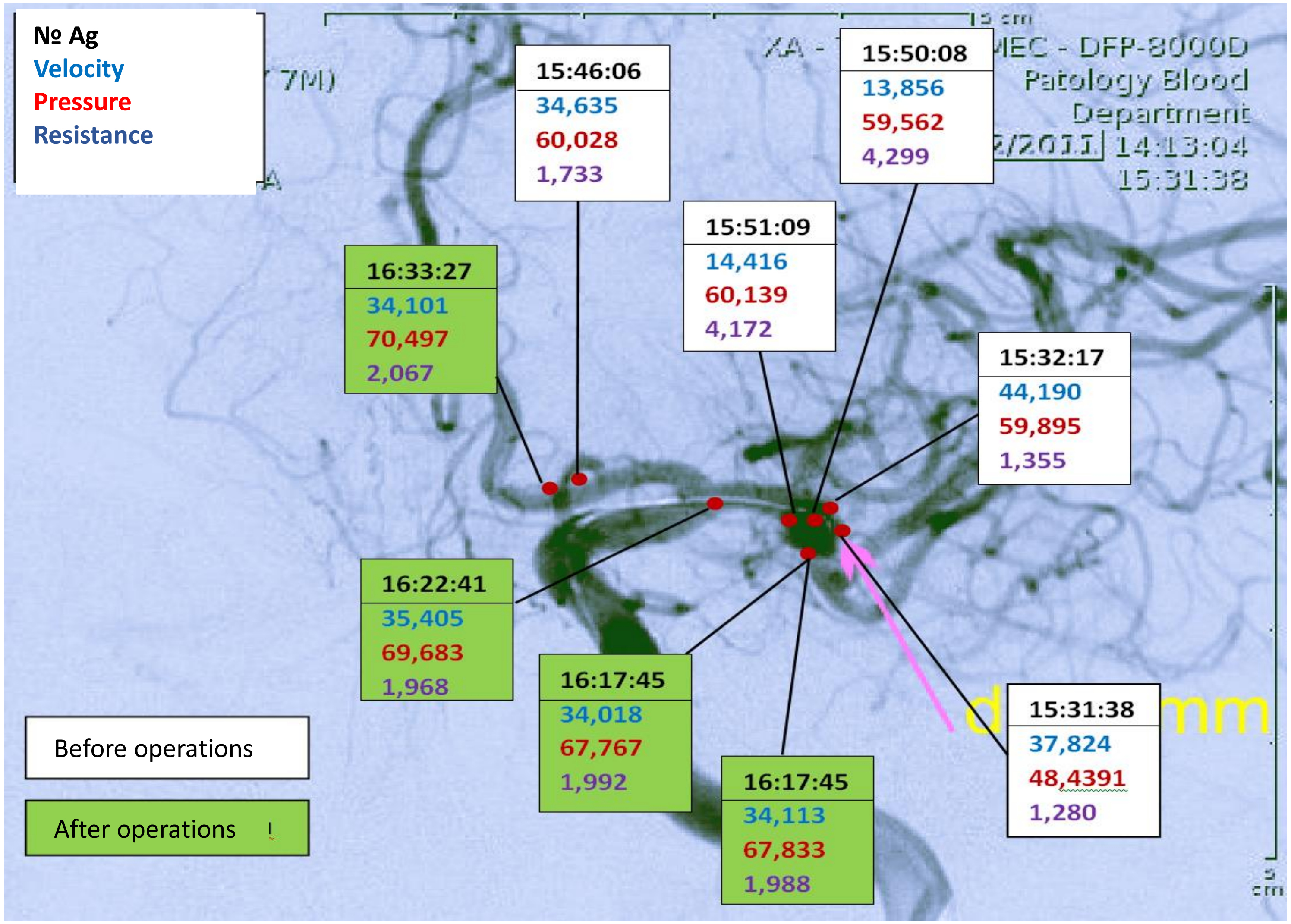

№ Ag
Velocity
Pressure
Resistance

15:46:06
34,635
60,028
1,733

15:50:08
13,856
59,562
4,299

16:33:27
34,101
70,497
2,067

15:51:09
14,416
60,139
4,172

15:32:17
44,190
59,895
1,355

16:22:41
35,405
69,683
1,968

16:17:45
34,018
67,767
1,992

15:31:38
37,824
48,4391
1,280

16:17:45
34,113
67,833
1,988

Before operations

After operations

Velocity—pressure diagrams

Arteries (AVM)

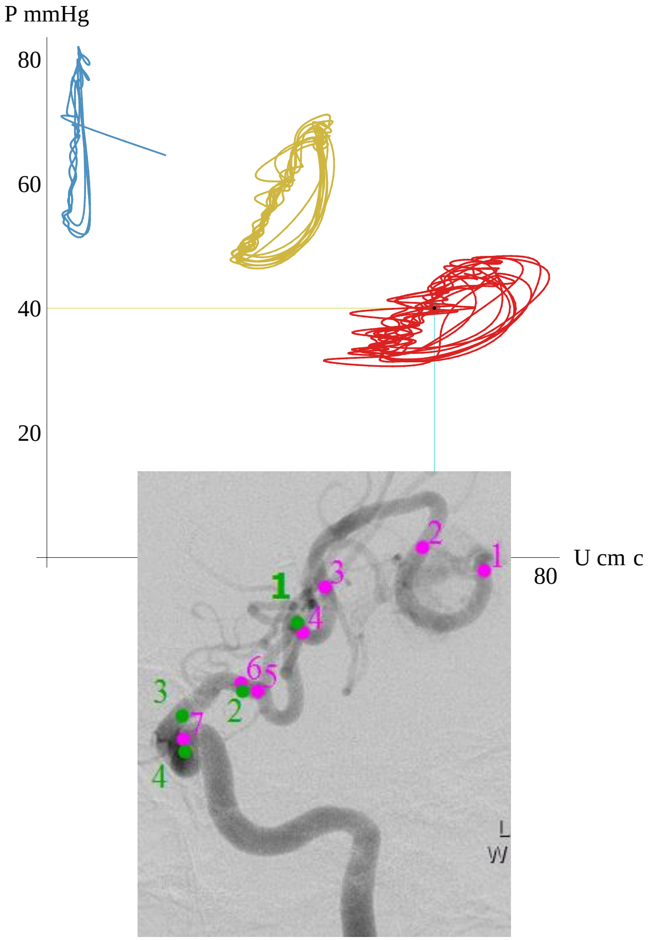

Arteries (AA)

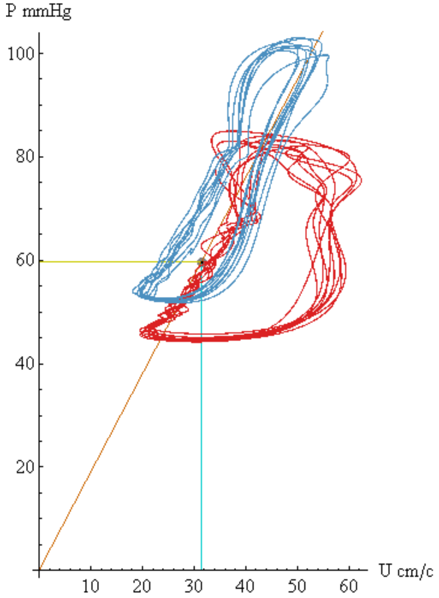

Veins

Sinuses

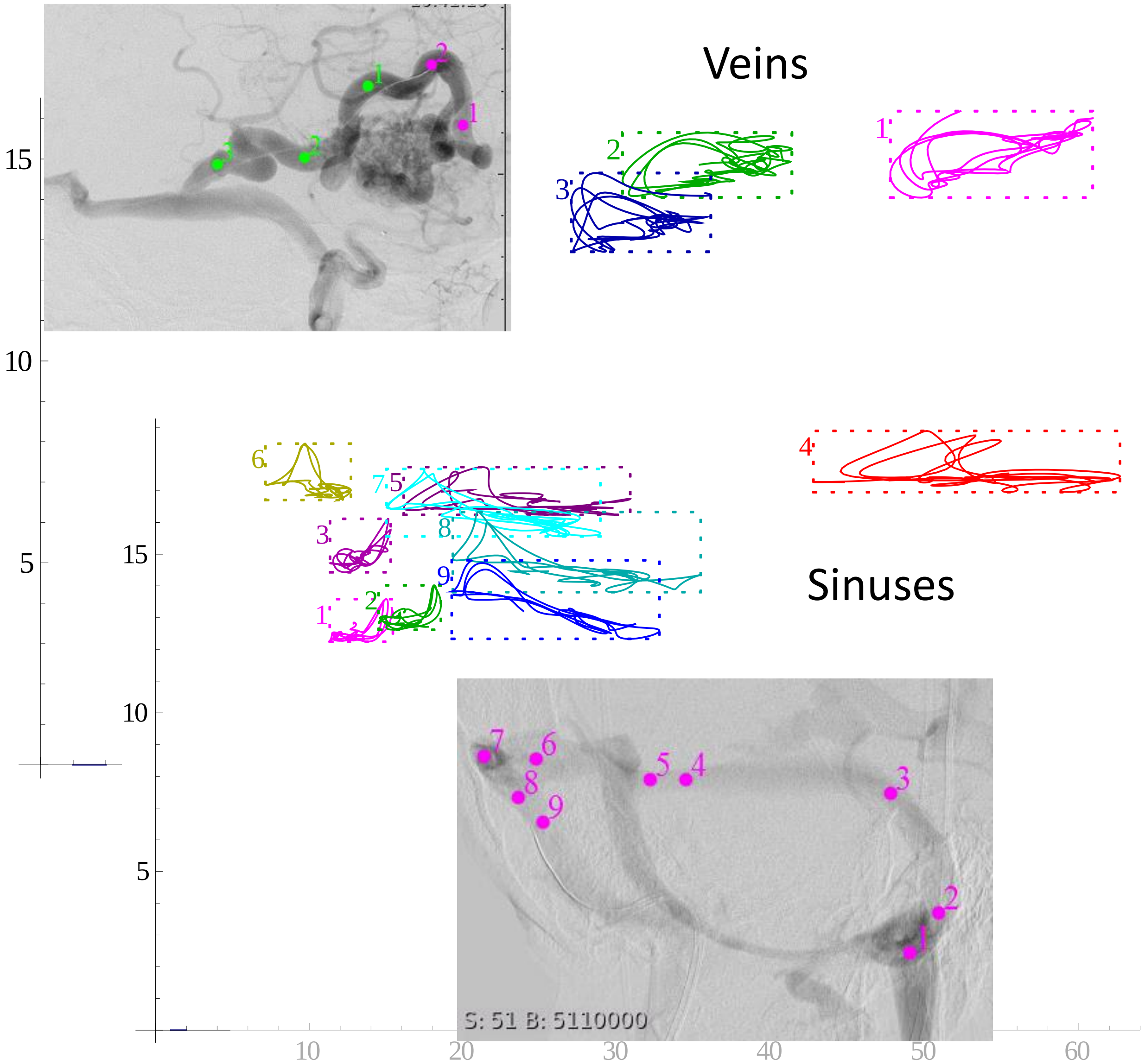

Part II. Nonlinear oscillator

The generalized equation of Van der Pol - Duffing

- To identify the character of parameters behavior in the area of pathologies we use the model of generalized equation of the Van der Pol - Duffing

$$\varepsilon q'' + \left(a_1 + a_2 q + a_3 q^2\right) q' + b_1 q + b_2 q^2 + b_3 q^3 = ku,$$

$$a_i, b_i, k \in R; \qquad i = 1,2,3;$$

- Velocity u – is given value, pressure q – the solution to the equation
- The coefficients are based on experimental data:
  b_i responds for the elastic properties of blood vessels, a_i responds for the viscous friction, ε corresponds to the relaxation character of the oscillations

Cherevko, A. A., Bord, E. E., Khe, A. K., Panarin, V. A., Orlov, K. J., & Chupakhin, A. P. (2016). Using non-linear analogue of Nyquist diagrams for analysis of the equation describing the hemodynamics in blood vessels near pathologies. *Journal of Physics: Conference Series*, *722*, 012005. DOI: 10.1088/1742-6596/722/1/012005
Parshin, D. V., Ufimtseva, I. V., Cherevko, A. A., Khe, A. K., Orlov, K. Yu., Krivoshapkin, A. L., & Chupakhin, A. P. (2016). Differential properties of Van der Pol—Duffing mathematical model of cerebrovascular haemodynamics based on clinical measurements. *Journal of Physics: Conference Series*, *722*, 012030. DOI: 10.1088/1742-6596/722/1/012030

Experimental verification of the model

- The model has been experimentally confirmed in a large number of clinical data obtained during operation in Meshalkin NRICP

- It is shown that the equation well reproduces clinical data

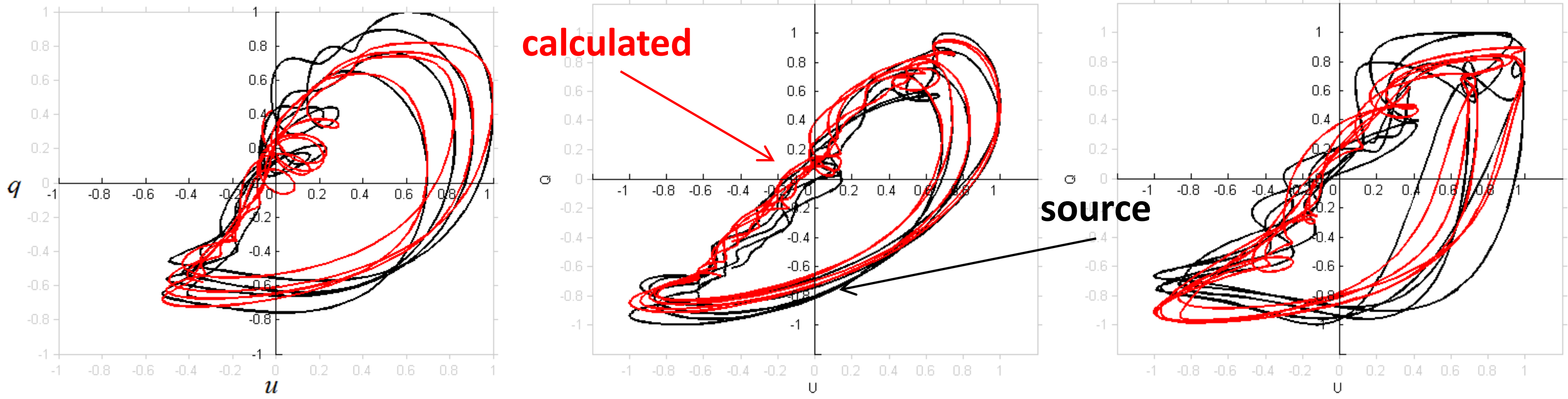

calculated

source

Part III. Assessment of the AVM embolization

Hemodynamic characteristics

- Flow rate $Q = vS$ – the volumetric flow rate through vessel cross section per unit of time
- Total pressure $P = p + \alpha\rho v^2/2$ – the energy (sum of potential and kinetic energy) which transported on one unit of blood volume;
  ρ - the density of blood, α - the Coriolis coefficient
- Energy flow rate $E = QP$ – the total energy which transported by blood through vessel cross section per unit of time
- Loads $W = E_1 - E_2$, E_1 – the amount of energy which obtain AVM through all the afferents, E_2- the amount of energy which released from AVM through draining vein
- Specific load $\mathrm{w} = \mathrm{W}/\mathrm{V}, \mathrm{V}$ – the volume of AVM

Krivoshapkin, A. L., Panarin, V. A., Orlov, K. Yu., Berestov, V. V., Shayakhmetov, T. S., Gorbatykh, A. V., Kislitsin, D. S., Chupakhin, A. P., Cherevko, A. A., Khe, A. K., Sergeev, G. S., & Chebykin, D. V. (2013). Hemodynamic hemorrhage prevention algorithm during cerebral arteriovenous malformations embolization. *The Bulletin of Siberian Branch of Russian Academy of Medical Sciences*, *33*(6), 65–73.

Dependence on the degree of AVM embolization

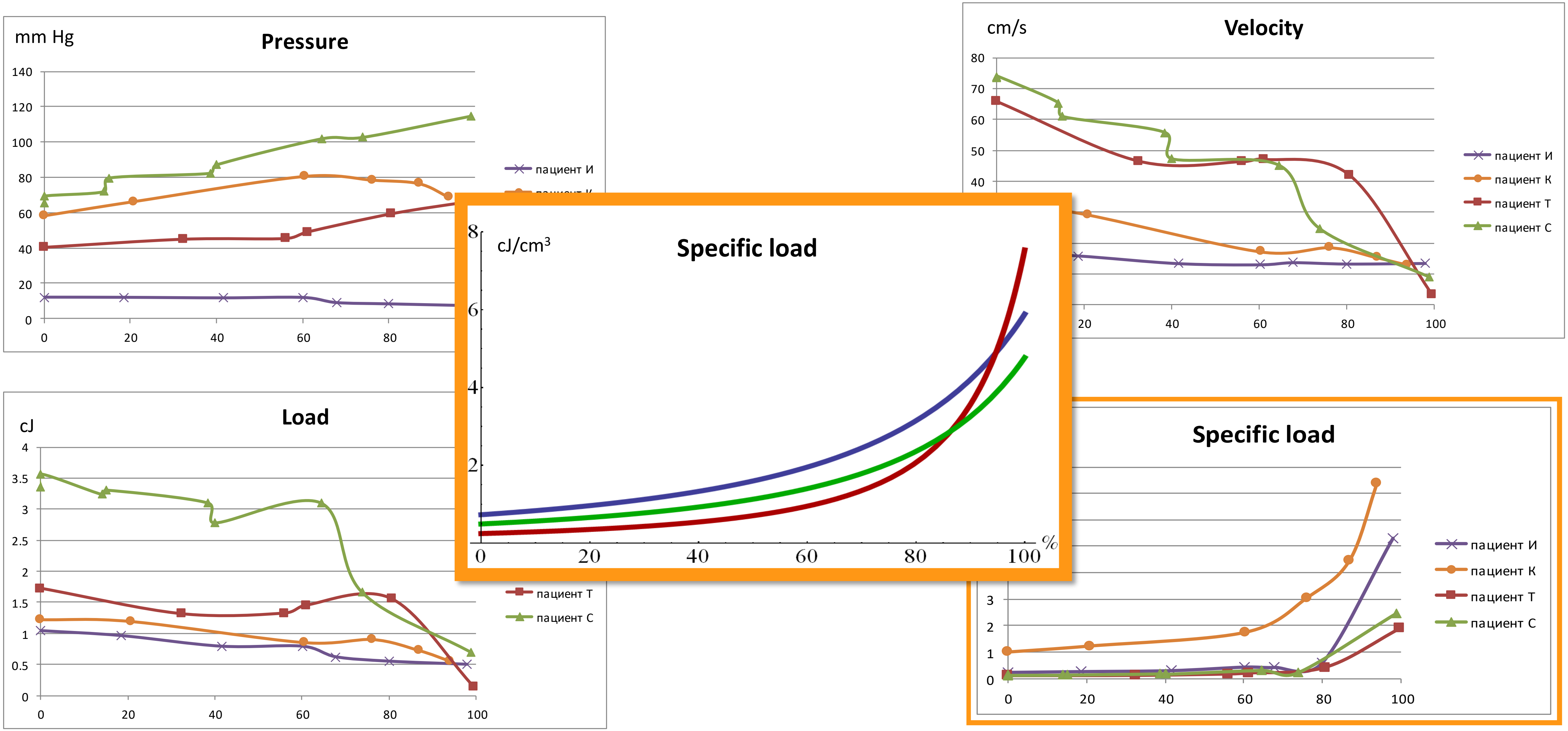

The results of treatment in groups

Signs	**Research group**	**Group of comparing**
The number of patients	30	94
The number of embolization	34	176
	11	38
	14	54
	1,27	1,42
	12	56
	1	8
	1	6
	0	4
	0	5
Hemorrhagic complications	1	11
% hemorrhagic complications/patient	**3,3%**	**11,7%**
Disability as a result of perioperative hemorrhage	0	4(4,25%)
Mortality	0	1(0,78%)

Z = 2,039; p<0,05 under ДИ 0 – 10,3

RUSSIAN FEDERATION

FEDERAL SERVICE
FOR INTELLECTUAL PROPERTY

(19) **RU** (11) **2 511 235** (13) **C2**

(51) Int. Cl.
A61B 8/06 (2006.01)

(12) ABSTRACT OF INVENTION

(21)(22) Application: 2012123062/14, 04.06.2012

(24) Effective date for property rights:
04.06.2012

Priority:
(22) Date of filing: 04.06.2012

(43) Application published: 10.12.2013 Bull. № 34

(45) Date of publication: 10.04.2014 Bull. № 10

Mail address:
630055, g.Novosibirsk, ul. Rechkunovskaja, 15,
FGBU "NNIIPK imeni akademika E.N.
Meshalkina" Minzdravsotsrazvitija Rossii

(72) Inventor(s):
Orlov Kirill Jur'evich (RU),
Panarin Vjacheslav Aleksandrovich (RU),
Berestov Vadim Vjacheslavovich (RU),
Krivoshapkin Aleksej Leonidovich (RU),
Kislitsin Dmitrij Sergeevich (RU),
Chupakhin Aleksandr Pavlovich (RU),
Baranov Viktor Il'ich (RU),
Cherevko Aleksandr Aleksandrovich (RU),
Khe Aleksandr Kancherovich (RU),
Telegina Nadezhda Jur'evna (RU)

(73) Proprietor(s):
Federal'noe gosudarstvennoe bjudzhetnoe
uchrezhdenie "Novosibirskij nauchno-
issledovatel'skij institut patologii
krovoobrashchenija imeni akademika E.N.
Meshalkina" Ministerstva zdravookhranenija i
sotsial'nogo razvitija Rossijskoj Federatsii
(FGBU "NNIIPK im. akad. E.N. Meshalkina"
Minzdravsotsrazvitija Rossii) (RU)

(54) METHOD FOR INTRAOPERATIVE DOPPLER CONTROL OF RADICALITY OF ARTERIOVENOUS MALFORMATION EMBOLISATION

(57) Abstract:

FIELD: medicine.

SUBSTANCE: invention concerns medicine, particularly neurosurgery. A DMSO-compatible microcatheter for administering the non-adhesive composition Onyx is inserted endovacularly through an arteriovenous malformation (AVM) afferent intranidally. A reinforced microcatheter of an internal diameter not less than 0.43 mm (0.17 in) is inserted into the afferent in the proximal direction from an origin of intact arteries not involved into the AVM blood flow; an intravascular conductor Combowire is inserted through the microcatheter into an arterial lumen. Immediately before an embolisation procedure and throughout the operation, Combomap apparatus is used for intravascular Doppler sonography with bypass pattern fixation; the pressure is measured in the AVM afferent at a distal end of the intravascular conductor Combowire and in a radial artery. The blood flow velocity in the AVM afferent and the pressure values in the radial artery and in the AVM afferent are indicated by Combomap apparatus with using an analogue-to-digital converter and programmed to derive hemodynamic values in the embolised AVM afferent - P and V, Q and E. The intraoperative real-time dependency diagrams of V and P, Q and E are plotted; the composition Onyx is administered until a linear blood velocity in the AVM afferent is reduced; the bypass pattern regresses completely; the AVM afferent pressure is levelled with the radial artery pressure; the plotted hemodynamic values V and P, Q and E tend to decrease. That is followed by a control angiography, and if the radicality of the AVM exclusion has been proved, an endovascular instrument is removed, and the operation is completed.

EFFECT: method enables minimising the quantity of the angiography stages that substantially reduces the intraoperative radiation exposure accompanying the endovascular operation.

2 ex, 7 dwg

Monitoring results

- Modeling the specific load during embolization;
  New concept of endovascular AVM embolization
- Quantitative description of the hysteresis parameters of blood flow in AVM embolization
- Analysis of blood flow parameters for the treatment of AA: the alignment of the resistances on various sections of the circulatory network
- Creating the database of information
- Developed protocol of AVM embolization

Part IV. Rheology and hystology of cerebral aneurysm tissue

Introduction. Causes of rupture

What affects the aneurysm growth and rupture?

Hemodynamical factors

Vs

Tissue inflammation & degeneration factors

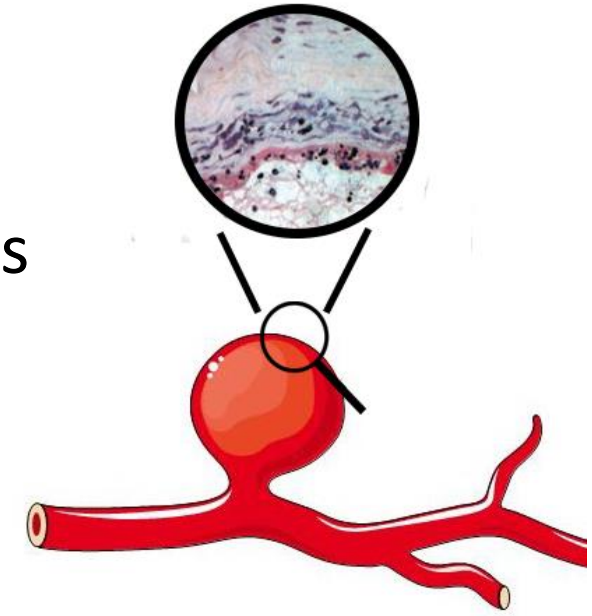

Differences in aneurysm’s and healthy vessel structure

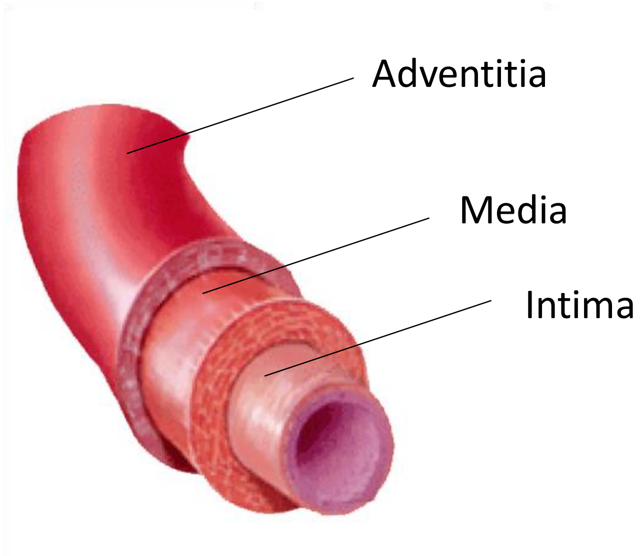

Healthy vessel

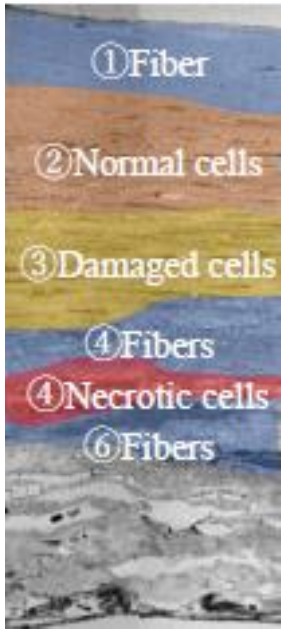

Aneurysm wall has a complex structure with alternating layers of healthy and damaged tissue.

Tobe et al, Investigation of wall thinning mechanisms in human cerebral aneurysms by pathological engineering analysis of smooth muscle cells and hemodynamics 10.1299/jsmebio.2017.29.2C42,

The history of mechanical tests

- The first mechanical test with an intracranial aneurysm wall performed by **Scott 1971**,
- Nowadays the leading position has **PUMC** with **A. Robertson** as a head of the research, and V. Costalat from University of Montpelier;

Special sessions dedicated to cerebral aneurysms held at:

- CMBE 2017
- WCB2018
- VPH2018
- CMBE2019
- ESBiomech2019
- WCBiomat2020

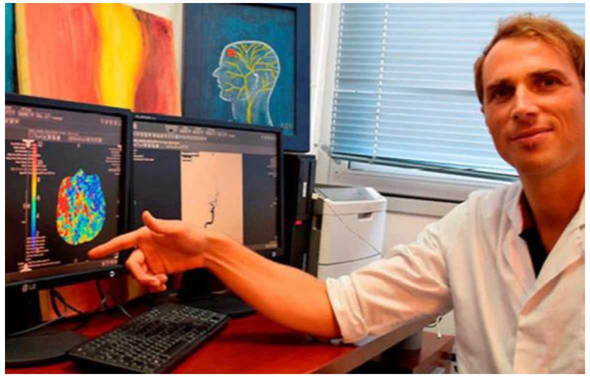

Cebral, J. R. *et al*. Wall mechanical properties and hemodynamics of unruptured intracranial aneurysms. *AJNR,* 36, 1695–1703, https://doi.org/10.3174/ajnr.A4358(2015)

Costalat, V. *et al*. Biomechanical wall properties of human intracranial aneurysms resected following surgical clipping (irras project). *Journal of Biomechanics* 44, 2685–2691, https://doi.org/10.1016/j.jbiomech.2011.07.026 (2011)

Tissue harvesting

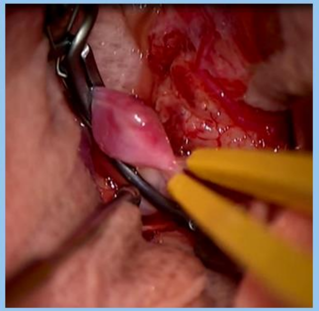

Federal Neurosurgery Center, Novosibirsk

Zwick&Roell Z10, Germany

Instron 5944

SURGERY

COLLECTING TISSUE SAMPLES

TRANSPORTATION

sodium 0.9%, +2°C-+5°C.

PERFORMING SERIES OF EXPERIMENTS ON RUPTURE MACHINE

Storage of the samples

Storage performed under temperature conditions +2C - +5C in the sodium 0.9% solute.

Note: Insignificant diversity of the results of mechanical tests for: live tissue, frozen and refrigerated and frozen samples was shown by **Stemper 2007**:

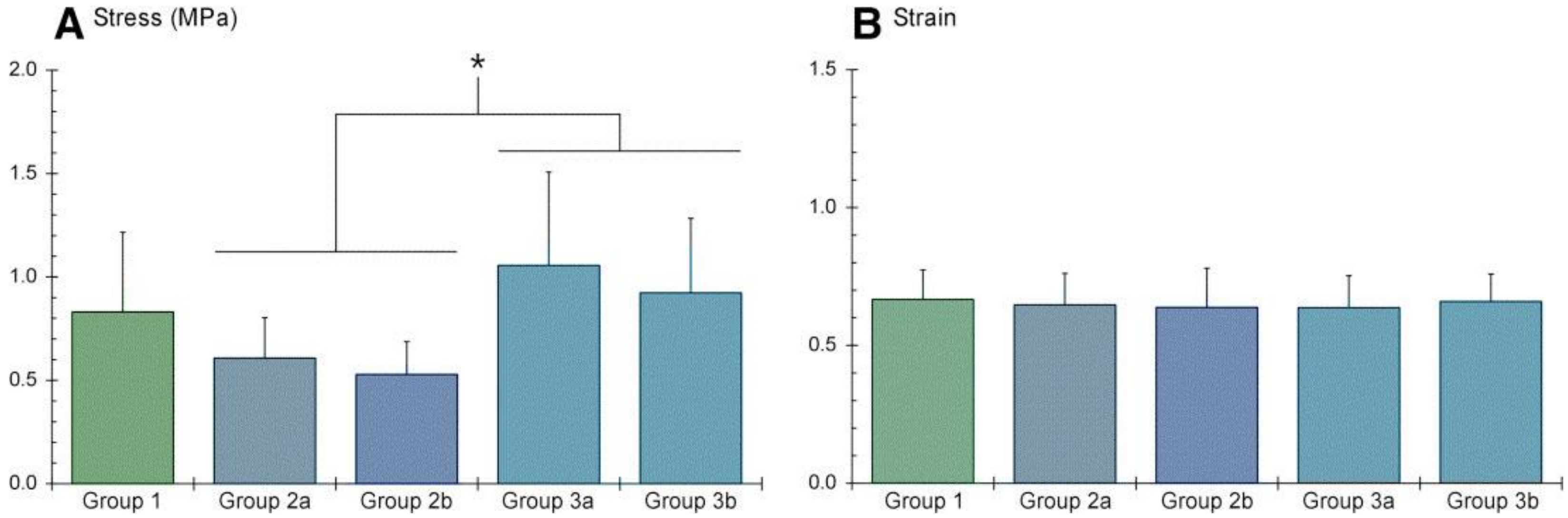

Methods. Mechanical test

Specimen before the start of the experiment.

Specimen in the *Zwick&Roell* rupture machine

Methods. Mechanical test

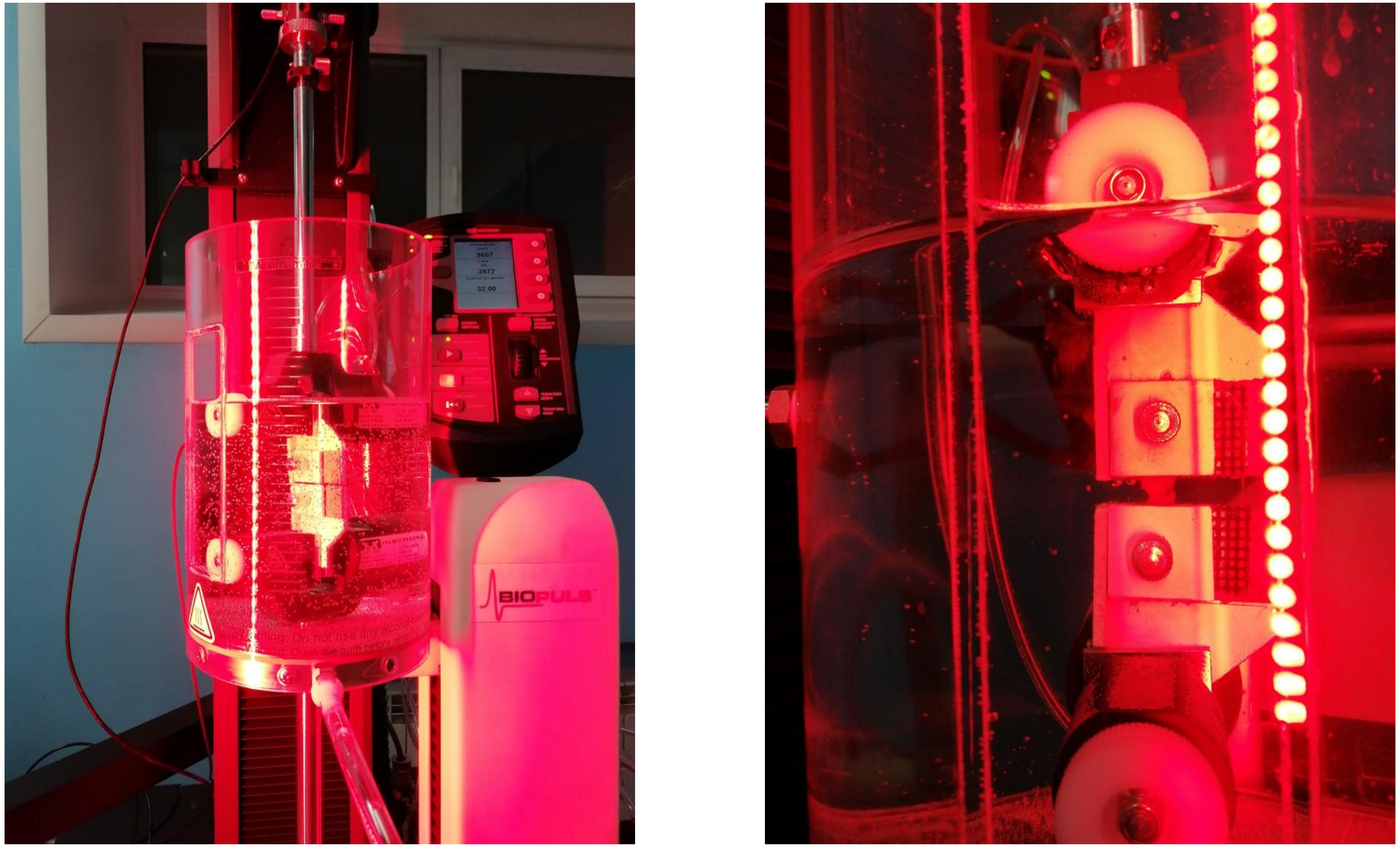

Specimen in the *Instron 5944* rupture machine

Specimen shape

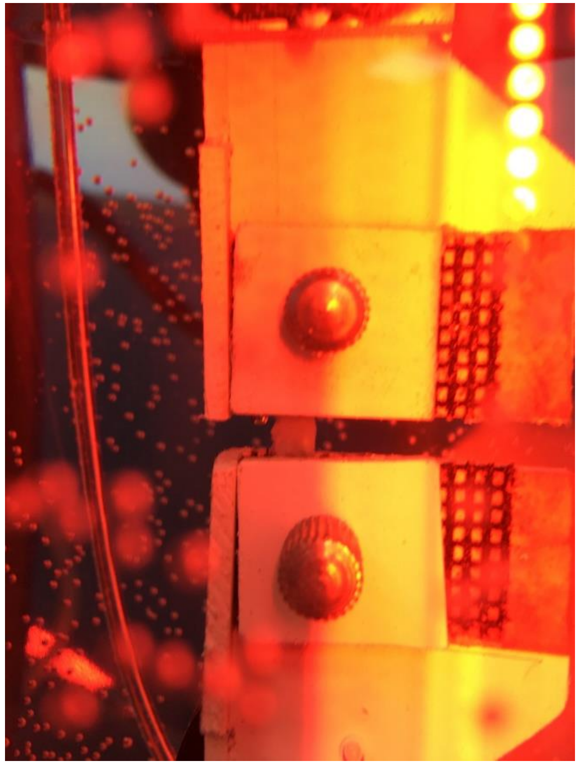

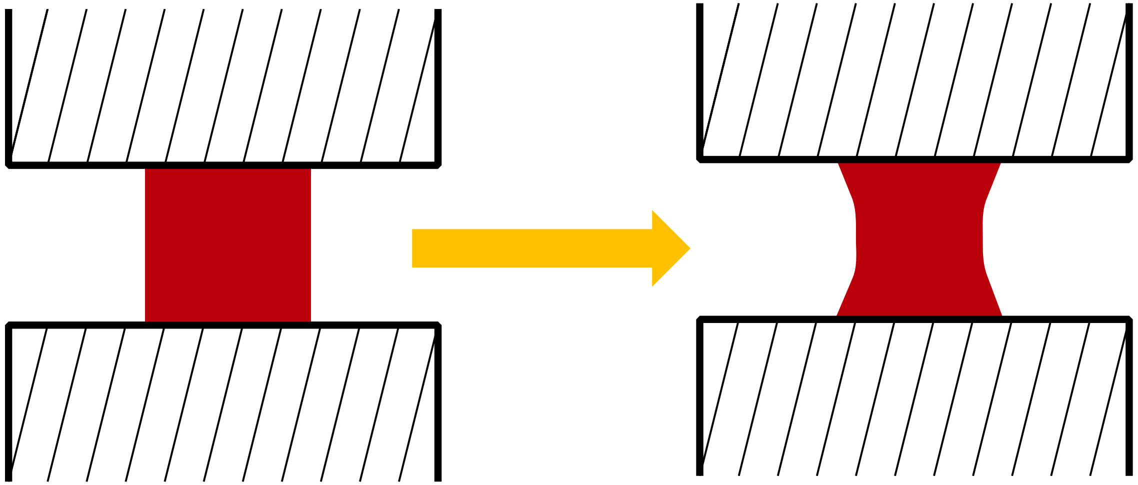

Rectangular shape

Dog-bone shape

A. Robertson. A uniaxial testing approach for consistent failure in vascular tissues. // *Journal of Biomechanical Engineering. 2018*

Methods. Stages of the loading

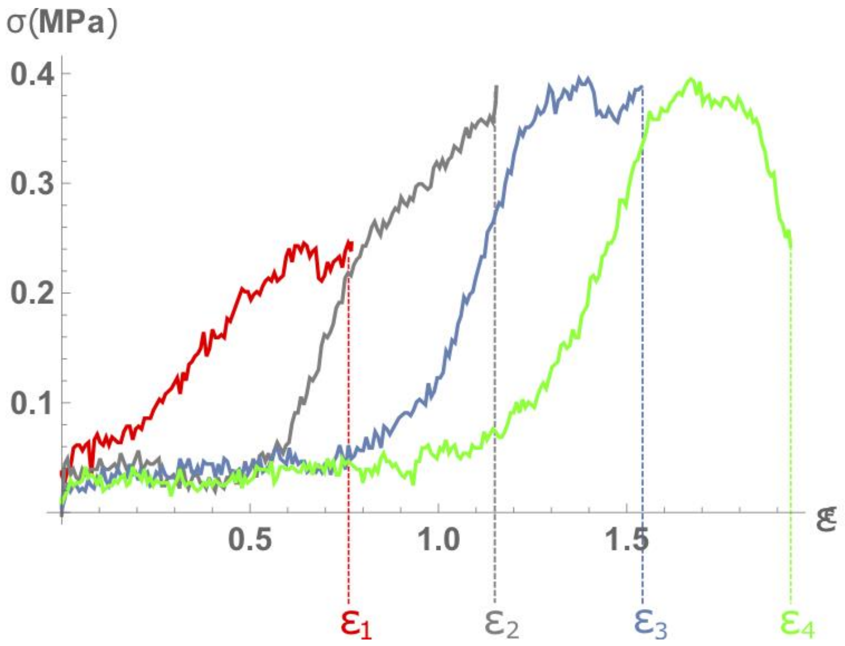

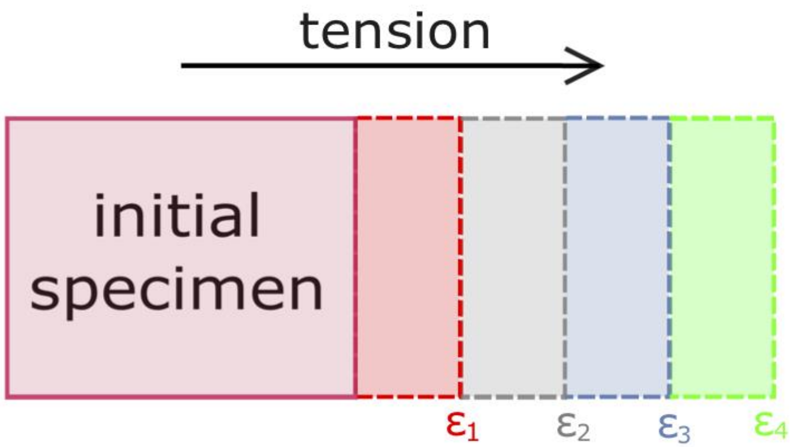

While conducting the experiment we took into account well-known phenomenon for biological tissues – **preconditioning**. The need to consider this phenomenon was due to the significant role of the matrix in the mechanics of such tissue. Taking into account its relaxation during the experiments ensures that the true stresses in the sample are correctly accounted for. This technique was used for the initial stages (stage 1-5 depending on the sample), and in the next stages the effect of this condition was not noticed.

Sommer, G., Regitnig, P., & Holzapfel, G. (2006). *Biomechanics of human carotid arteries: experimental testing and material modeling*. 5th World Congress of Biomechanics, München, Germany

Uniaxial mechanical test on part of the healthy artery

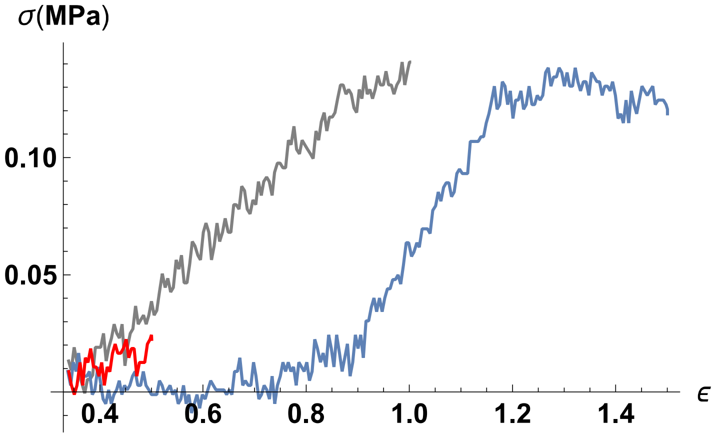

Circumferential direction

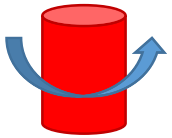

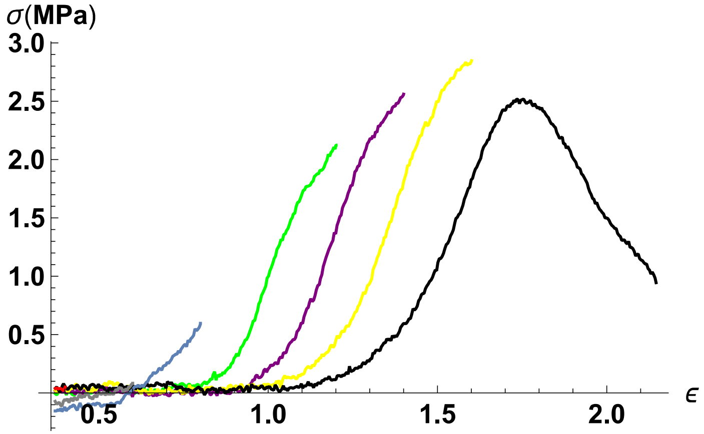

Axial direction

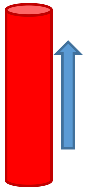

Ultimate stress and strain values

ID	Ultimate strain	Ultimate stress (MPa)
R.	1.27639	1.09936
K2.	1.5729	1.1314
V.	1.06323	1.05493
Z.	0.744889	1.00979
U.	2.85794	1.00356
K1.	4.6129	1.75217
M.	1.30277	0.382825
Ul.	3.96535	0.33317
A1	1.41559	2.4794
A2	1.37917	0.141357

Hyperelastic material models

3-parameter Mooney-Rivlin model:

$$\sigma_{3p} = \frac{F}{S_0} = 2C_1(\lambda - \frac{1}{\lambda}) + 2C_2(1 - \frac{1}{\lambda^3}) + 6C_3(\lambda^2 - \lambda - 1 + \frac{1}{\lambda^2} + \frac{1}{\lambda^3} - \frac{1}{\lambda^4})$$

5-parameter Mooney-Rivlin model:

$$\begin{aligned}\sigma_{5p} = \frac{F}{S_0} &= 2C_1(\lambda - \frac{1}{\lambda}) + 2C_2(1 - \frac{1}{\lambda^3}) + 6C_3(\lambda^2 - \lambda - 1 + \frac{1}{\lambda^2} + \frac{1}{\lambda^3} - \frac{1}{\lambda^4}) + \\ &+ 4C_4\lambda(1 - \frac{1}{\lambda^3})(\lambda^2 + \frac{2}{\lambda} - 3) + 4C_5(2\lambda + \frac{1}{\lambda^2} - 3)(1 - \frac{1}{\lambda^3})\end{aligned}$$

Yeoh model:

$$\sigma = \frac{F}{S_0} = 2(\lambda - \lambda^{-2})(C_1 + 2C_2(\lambda^2 + 2\lambda^{-1} - 3))$$

Neo-Hookean model:

$$\sigma = \frac{F}{S_0} = 2C_1(\lambda - \frac{1}{\lambda^2})$$

The quality of approximation achieved with different models

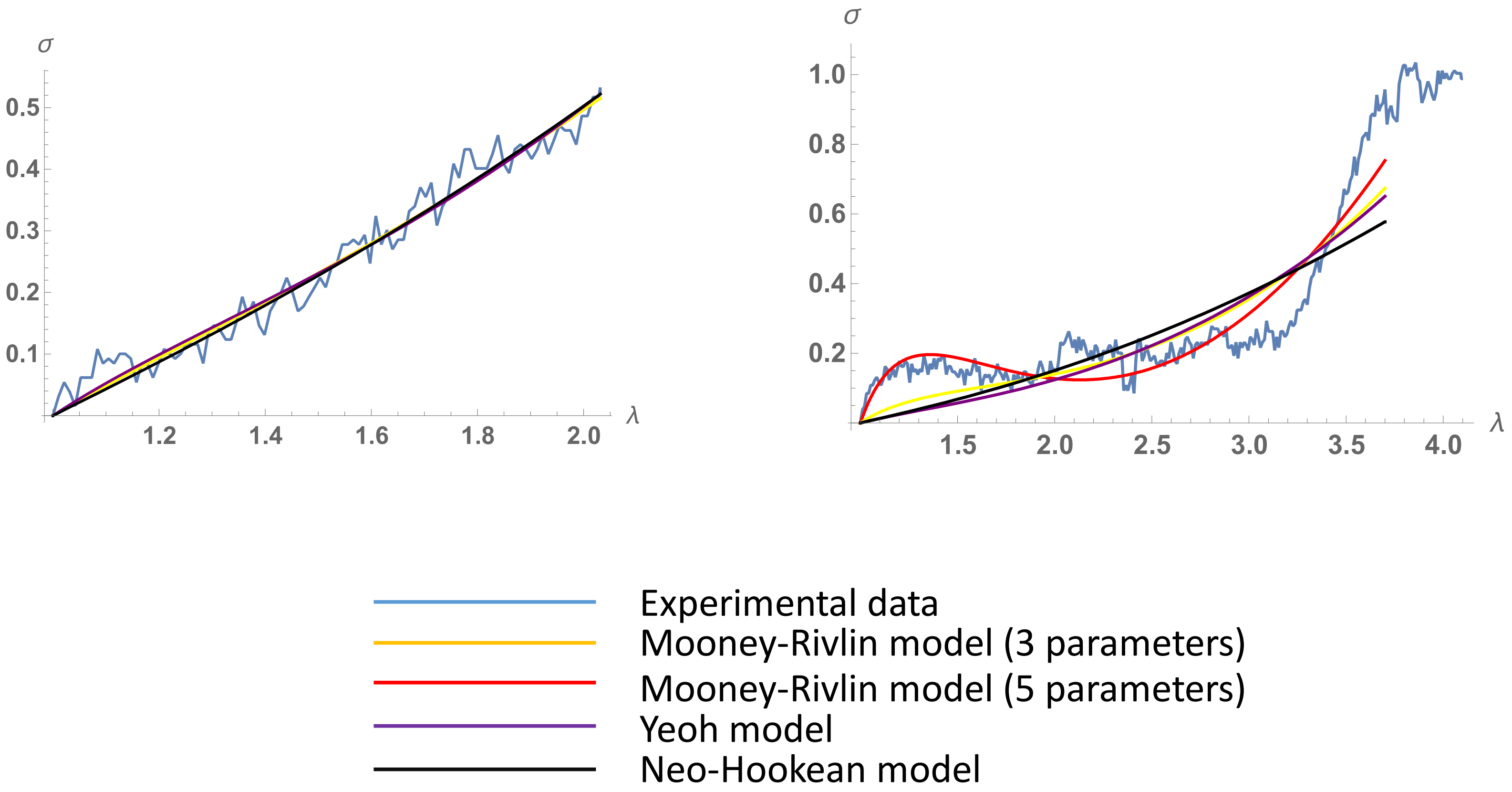

Hierarchy of models

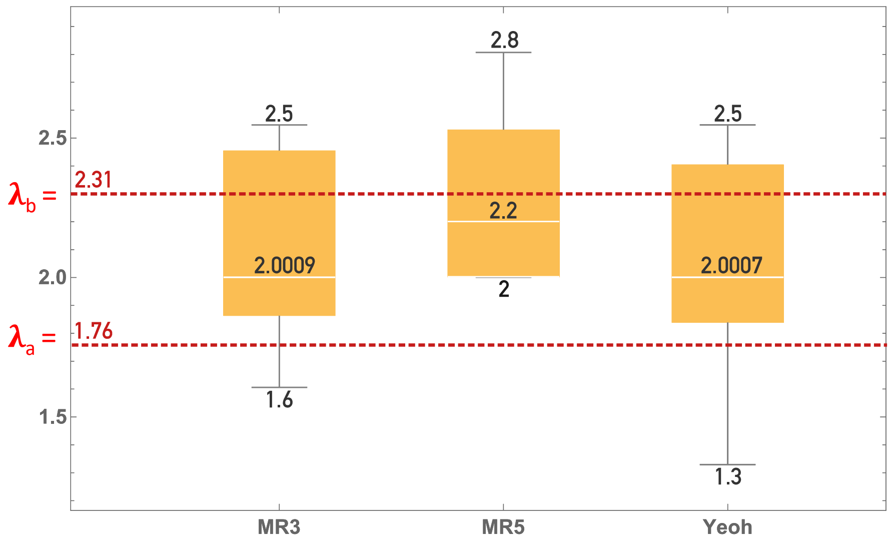

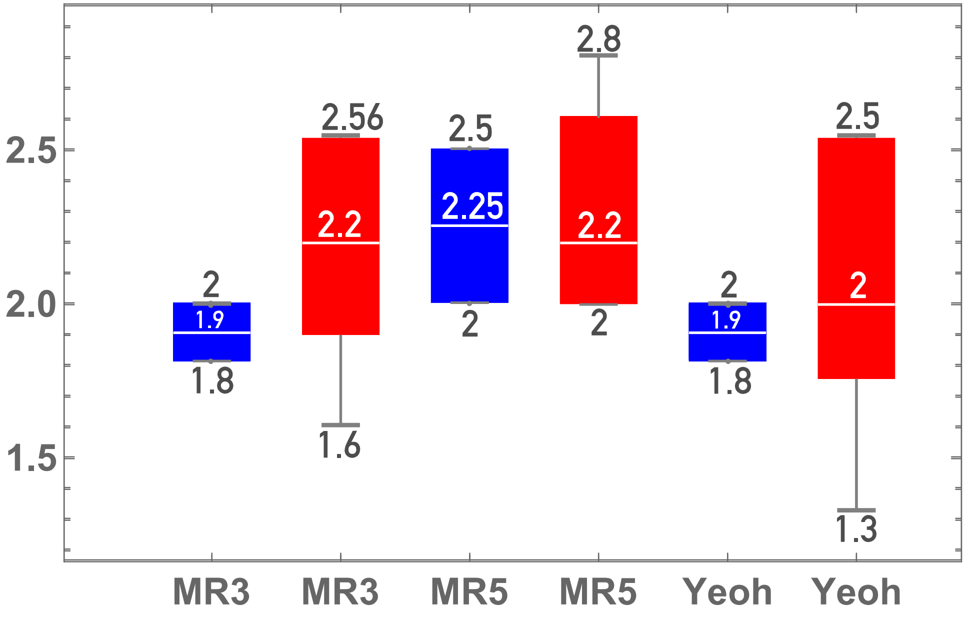

Yellow – all samples
Blue – unruptured aneurysms
Red – ruptured aneurysms

MR3 – 3-parameter Mooney-Rivlin model

MR5 – 5-parameter Mooney-Rivlin model

YEOH – Yeoh model;

λ_a – elastin and collagen bear loading

λ_b – elastin ruptures, only collagen bears loading

Hierarchy of models

Aneurysm status / Degree of deformation	**Ruptured aneurysms**	**Unruptured aneurysms**
Small relative elongation	Neo-Hookean model	Neo-Hookean model
Medium elongation	Yeoh model	Neo-Hookean model
Large relative elongation	5-parameter Mooney-Rivlin model	5-parameter Mooney-Rivlin model

Parshin et al. On the optimal choice of a hyperelastic model of ruptured and unruptured cerebral aneurysm // Scientific reports. 2019

The jumps on the strain-stress diagramms

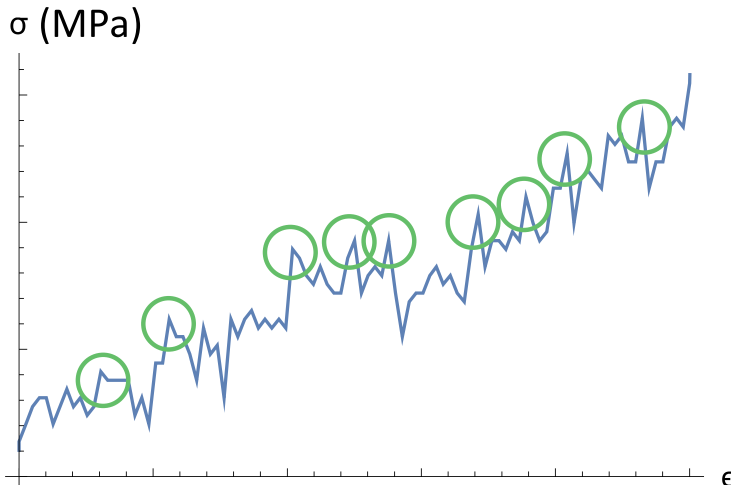

Zwick&Roell Z10
Maximum load force:
10 kN

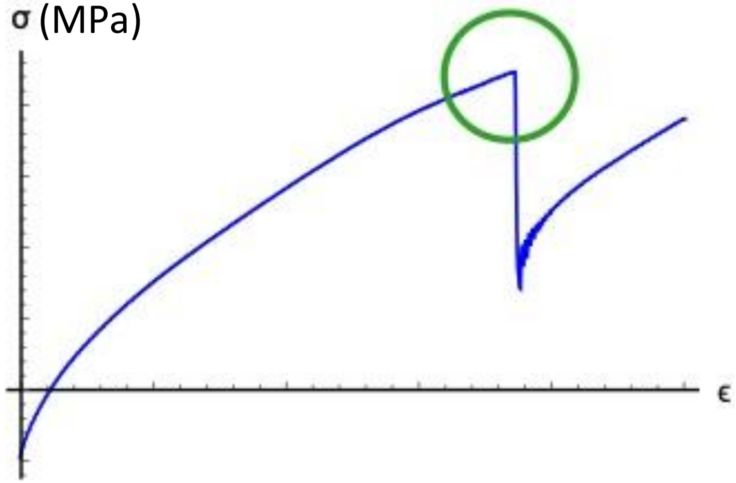

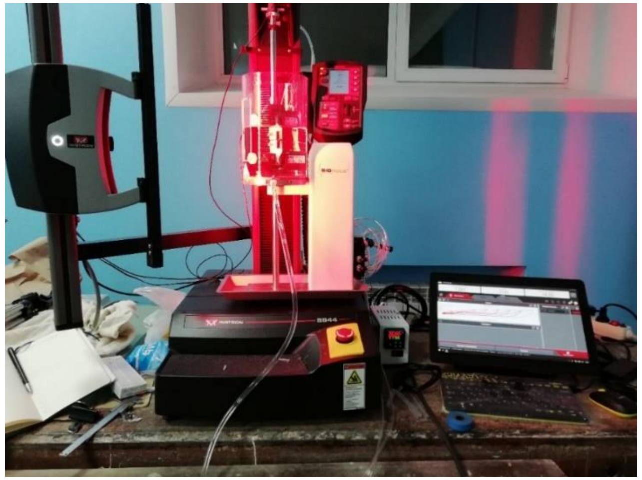

Instron 5944
Maximum load force:
10 N

Elastin layer rupture

I. Ruptured

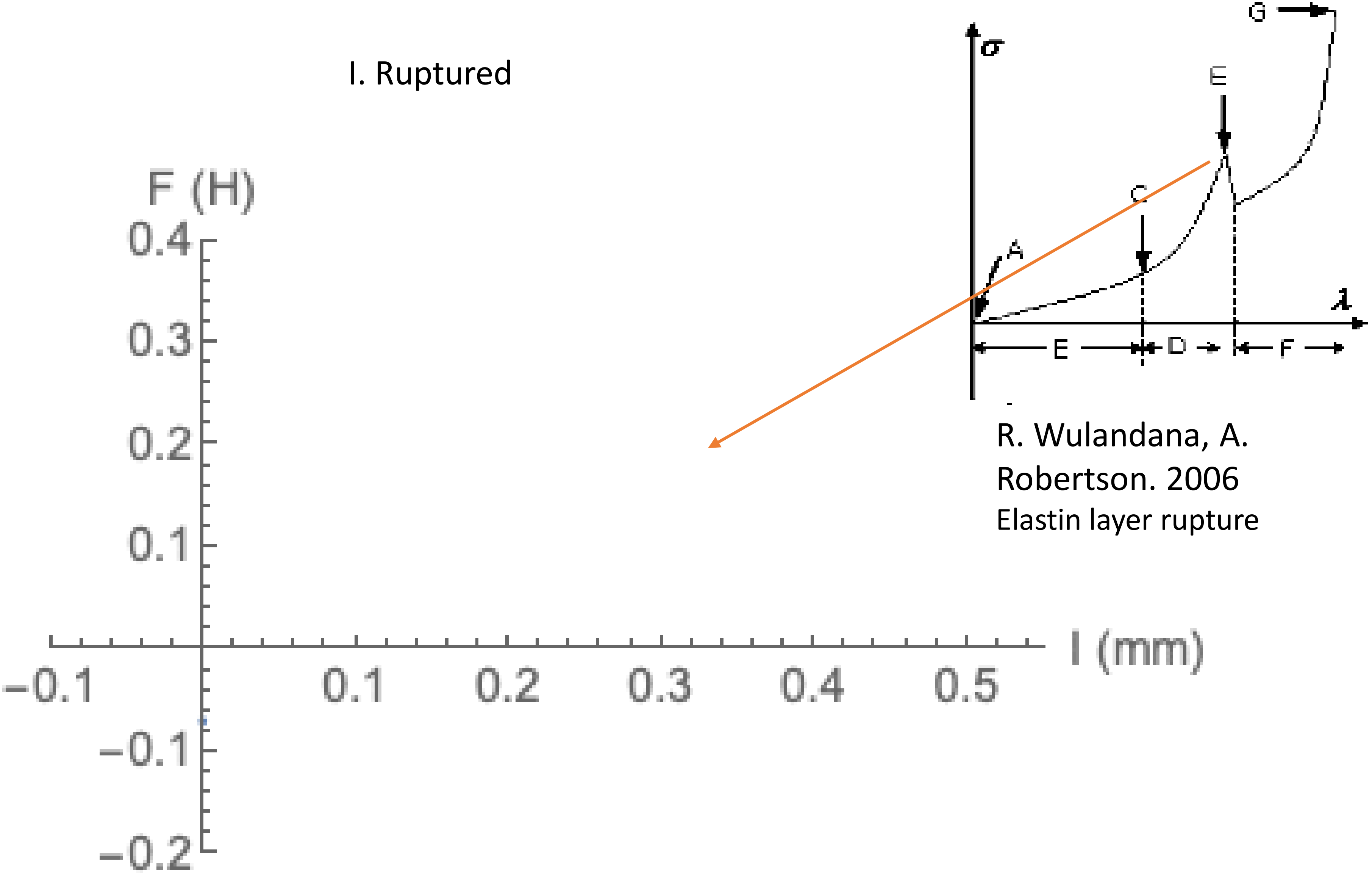

R. Wulandana, A. Robertson. 2006
Elastin layer rupture

Analyzing the jumps magnitude

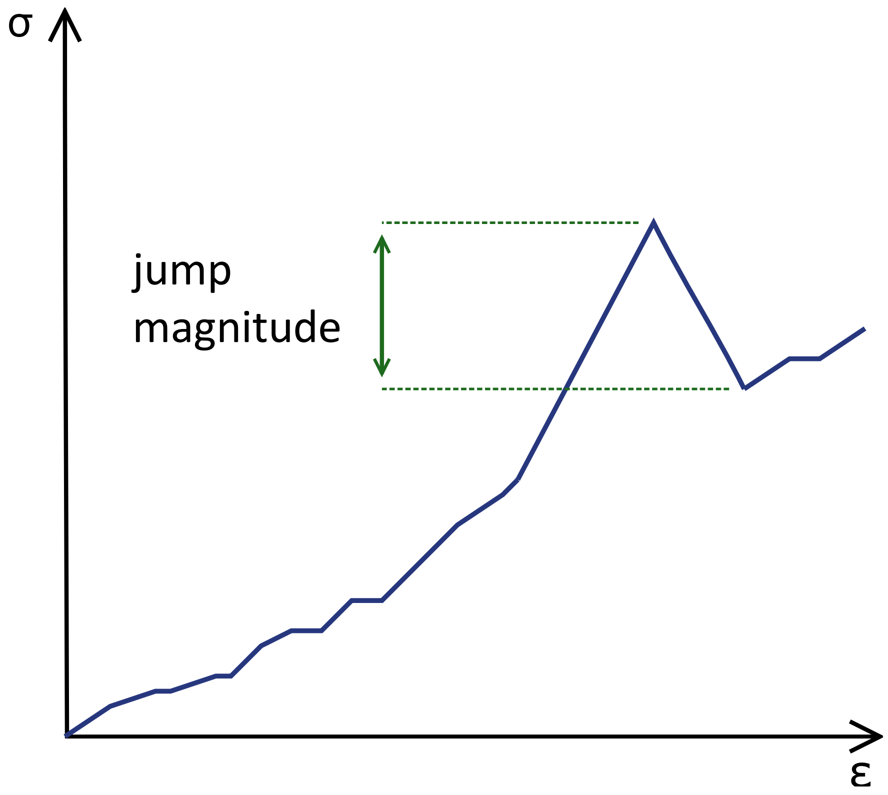

Patient ID	Aneurysm status
K1	Unruptured
K2	Unruptured
V.	Ruptured
U.	Ruptured
A.	Healthy

The distribution of jumps magnitude

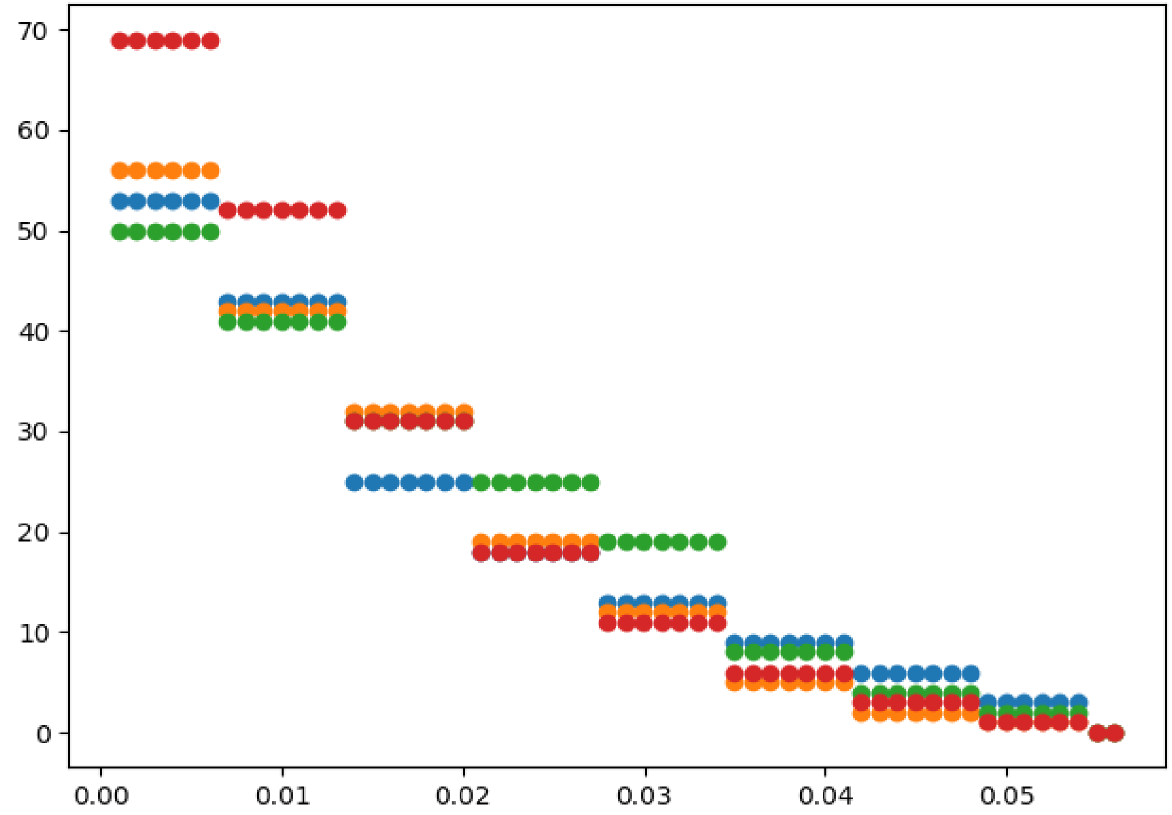

By horizontal axis – threshold of the jump's magnitude, by vertical – the number of the jumps that fit into the threshold's range.

Comparing the ruptured and unruptured cases

● ruptured ● unruptured

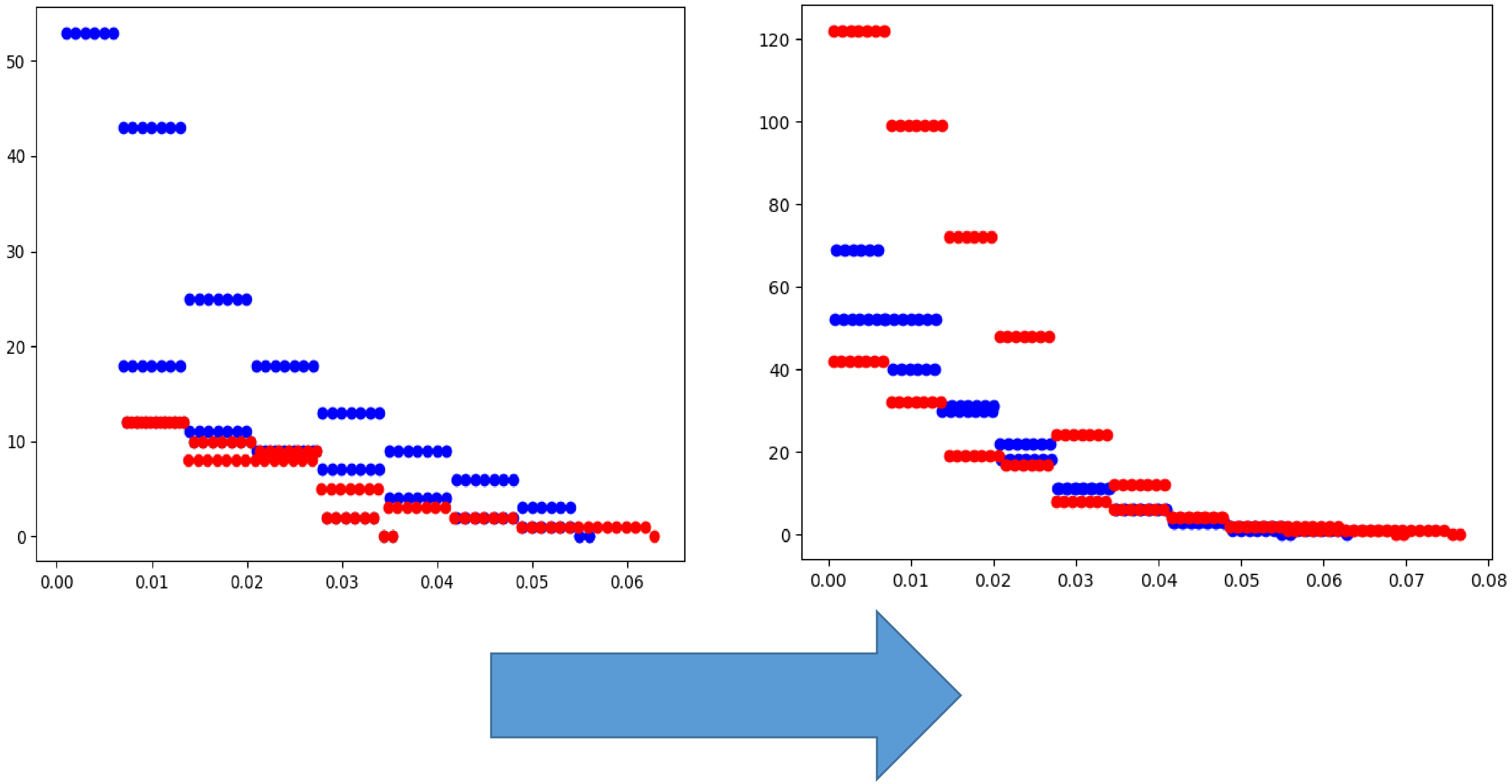

The differences in the morphology of ruptured and unruptured aneurysms

Ruptured

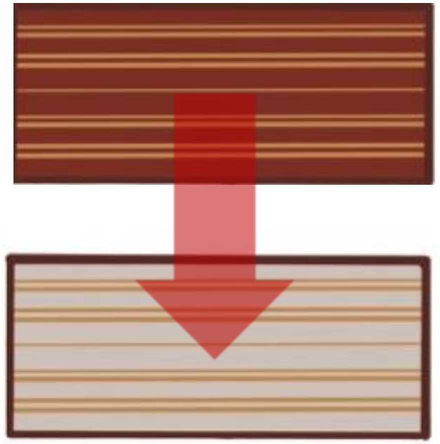

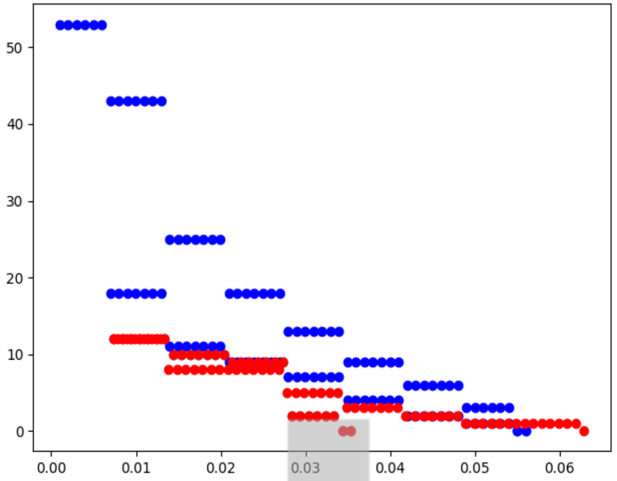

Before tension

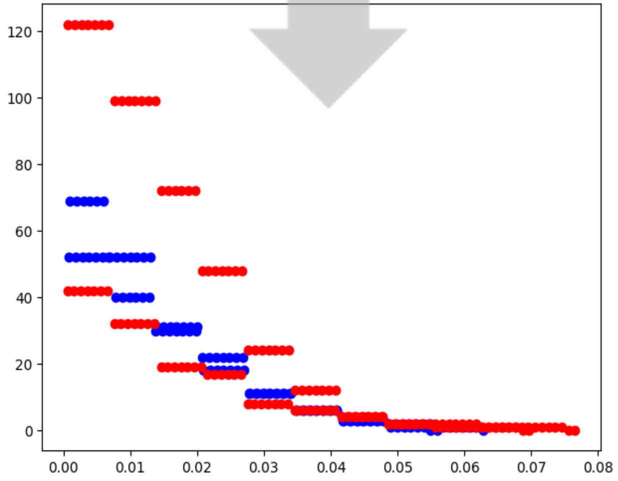

After tension

Unruptured

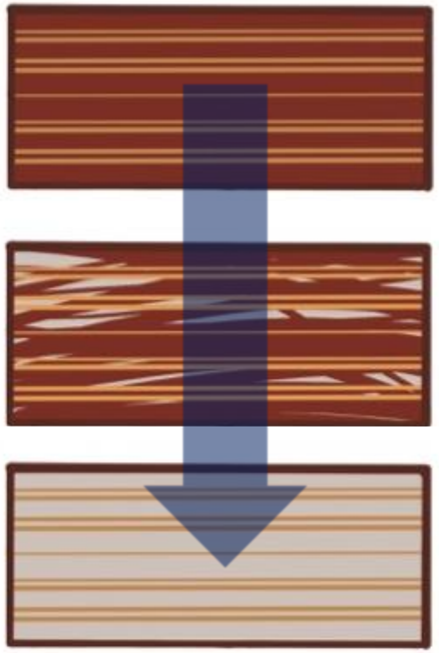

Comparing the unruptured, ruptured and healthy cases

● ruptured ● unruptured

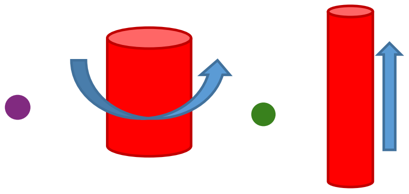

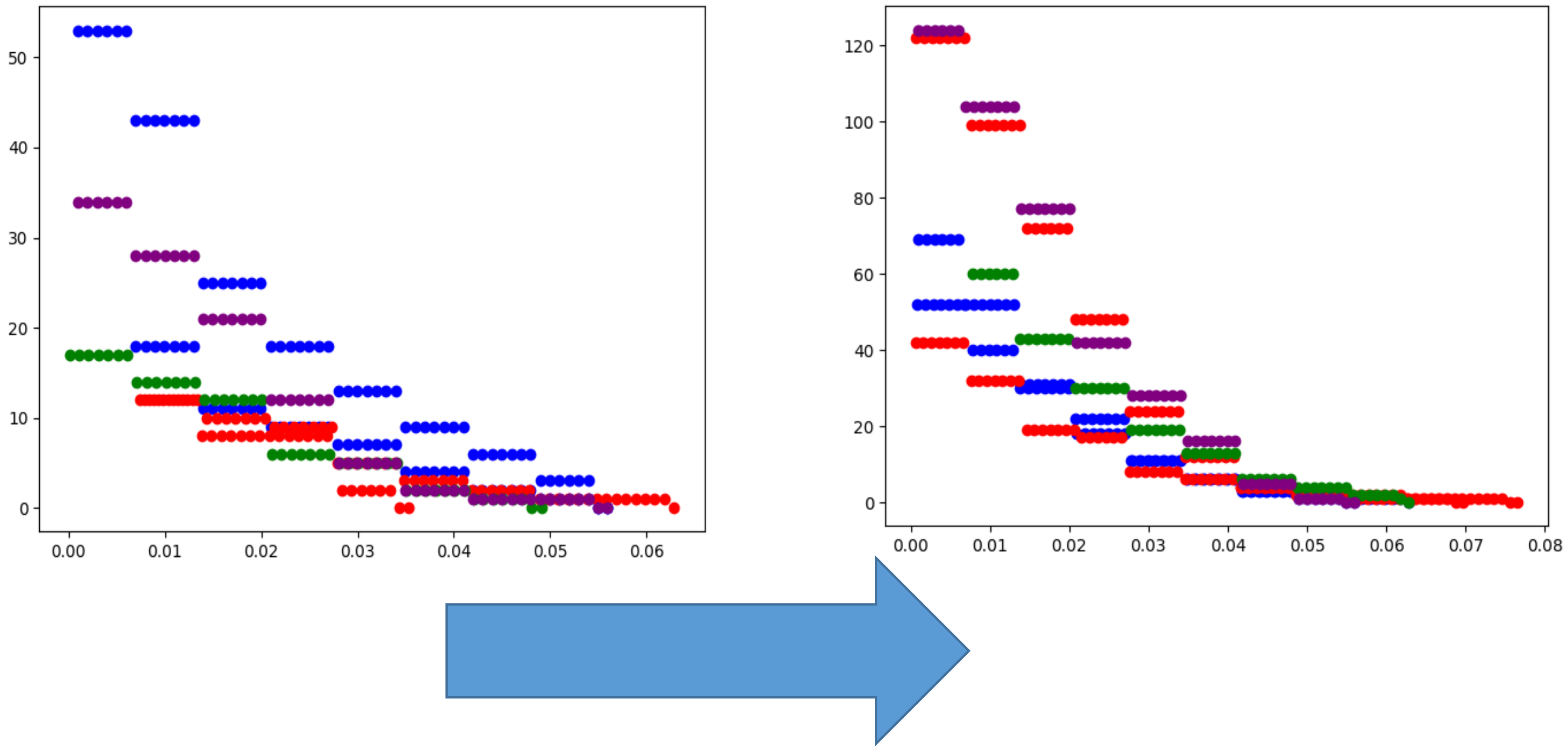

The distribution of collagen fibers in the vessel tissue

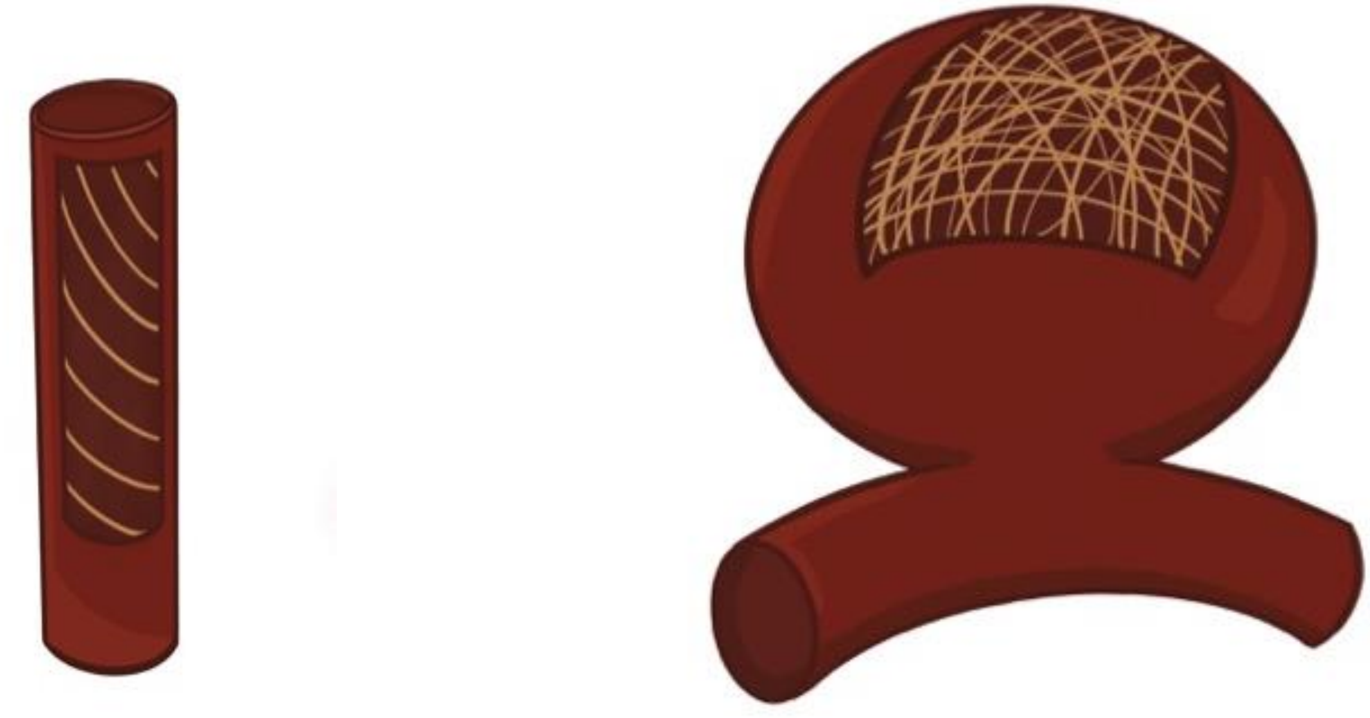

Collagen fibers in the tissues of a healthy vessel is directed at an angle of 30-50 degrees to the axis of the vessel. Due to the random destruction of layers in the dome of the aneurysm and the growth of connective tissue, the aneurysmal tissue does not have a similarly ordered structure.

A.Ye. Medvedev, V.I. Samsonov, V.M. Fomin. On the rational structure of blood vessels // PMiTPh. 2016

The distribution of collagen fibers in the vessel tissue

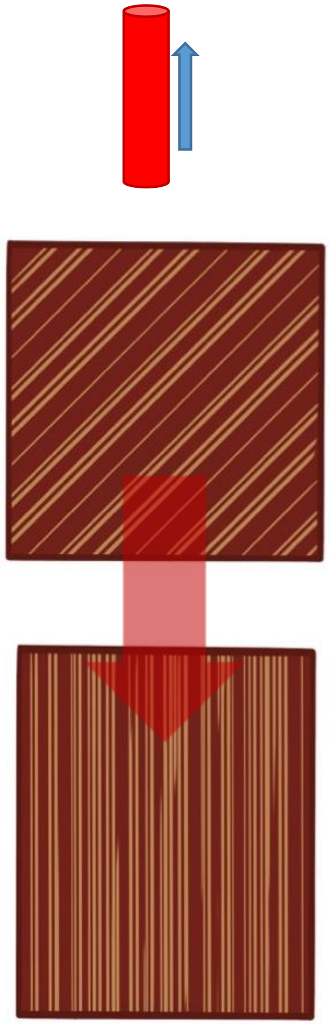

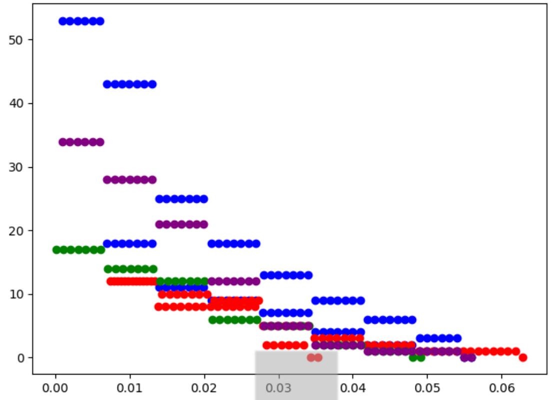

Before tension

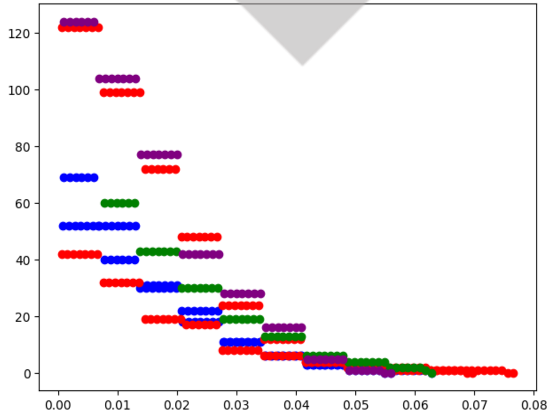

After tension

Connection with the histology data?
(Perspectives for future studies)

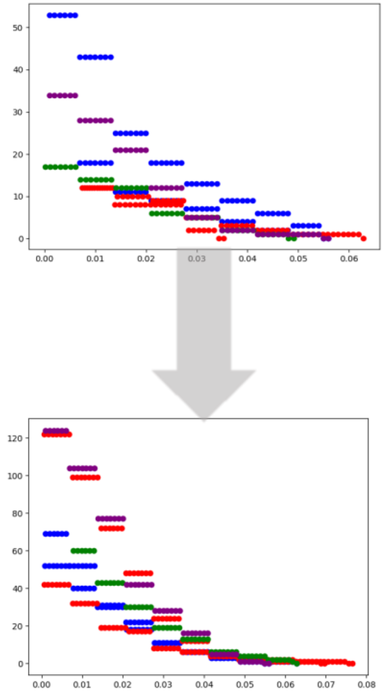

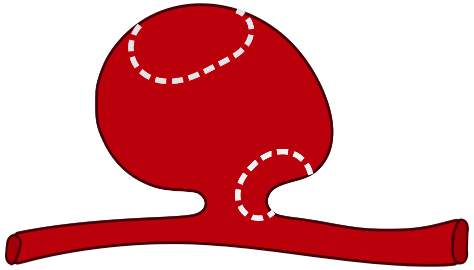

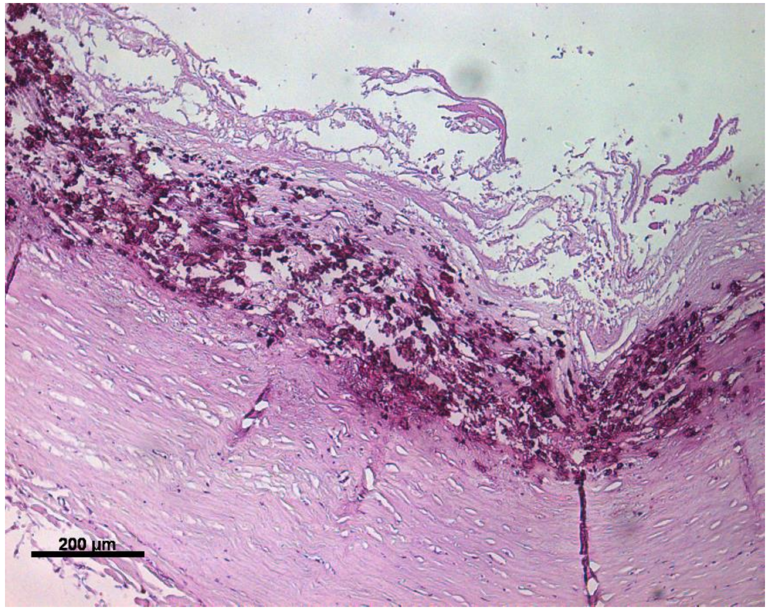

Parameter/Location	Dome	Neck
Ultimate deformation	1.50007	0.500467
Ultimate stress	0.279878	0.247911
interfiber swelling	+	+
Neovasculogenesis	+	+
Calcification	Large foci	The initial stages of calcification

Parshin, Daniil, et al. "Different stages of the evolution of cerebral aneurysms: joint analysis of mechanical test data and histological analysis of aneurysm tissue." *EPJ Web of Conferences*. Vol. 221. EDP Sciences, 2019.

Conclusions

- The result of a mechanical test of 12 aneurysm samples and one artery is given;
- Mooney-Rivlin, Yeoh and Neo-Hookean models for each test are built;
- The hierarchy of hyperelastic models is created based on the results of the approximation;
- The jumps on stress-strain diagrams analyzed.

Part V. Laser induced fluorescence as a method of classification of cerebral aneurysm tissue

Fluorescence

The 210-350 nm laser is used with the size of spot approximately 5x14 мм. Fluorescence spectra of resected vessels' fragments were measured. During the spectrometer's exposure time (1 sec.) the emitting pulses were accumulated. The linearity of fluorescence was monitored. Pulse energy did not exceed 200 mkJ per pulse. The measurements in laser wavelength diapason 210-290 nm were performed using a special filter (short-wave boundary at 300 nm), in 300-350 nm – using BC-8 filter. Each spectrum was normalized with total energy of laser irradiation during the exposure time and relative spectral sensitivity of the spectrometer.

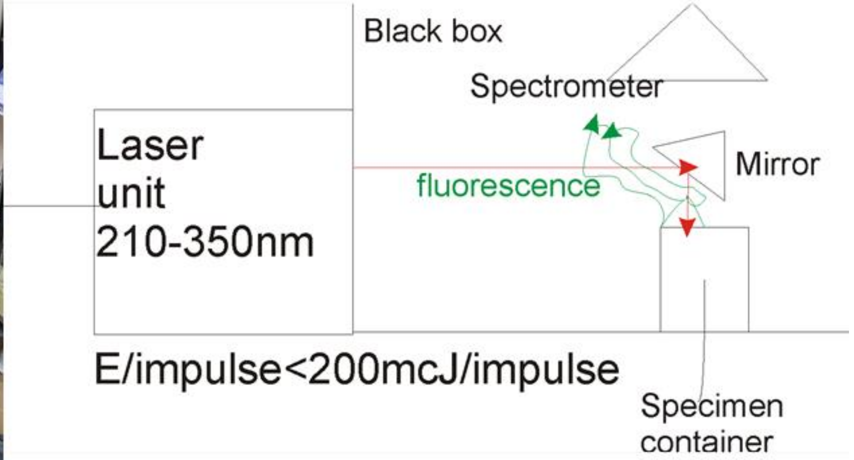

Fluorescence

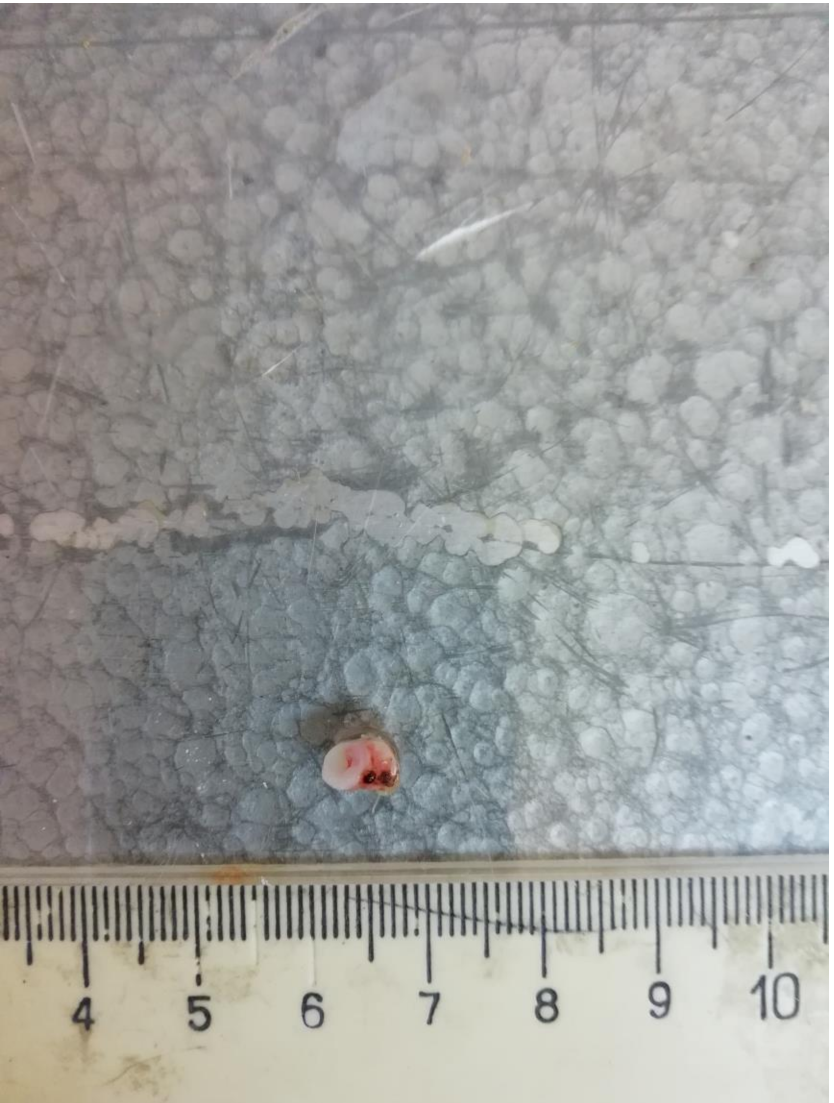

Before the start of the experiment we clean blood pieces from the specimen and prepare a rectangular shape specimen. For each laser wavelength we perform 20 acquisitions.

Fluorescence

Spectra were analyzed with the principal component method. All spectra are well described by the sum of three components, presented in the picture below. As the components are alternating, spectra of real fluorophores are their linear combinations. By selection method we obtained spectra of narrow peaks.

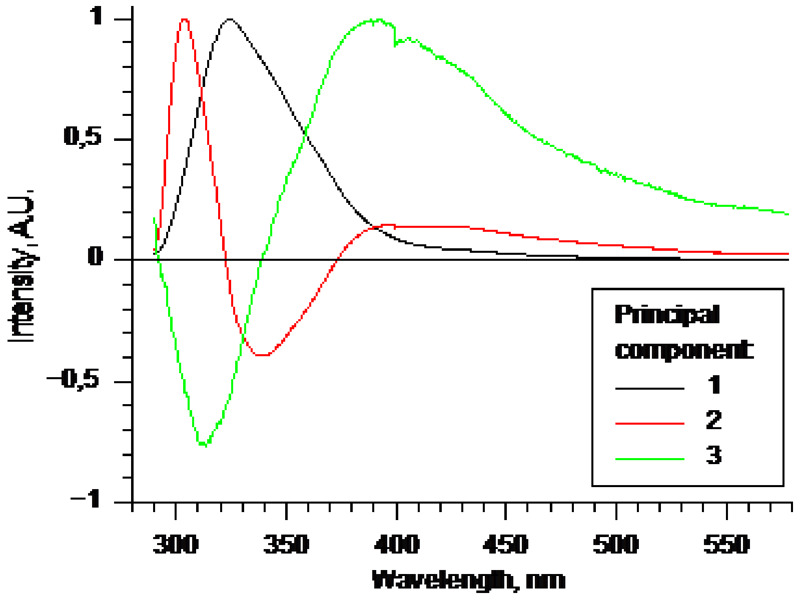

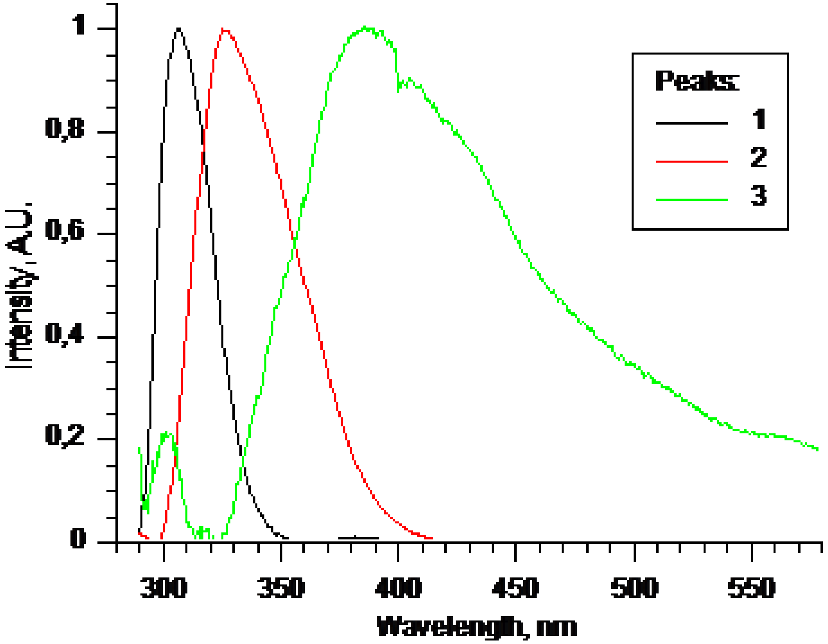

Fluorescence

Peak 1 has maximum at 308 nm and it corresponds well with the fluorescence spectrum of tyrosine amino acid, peak 2 has maximum at 326 nm and is conditioned by amino acid tryptophan (depending on the surroundings fluorescence peak can occur in 320-360 nm diapason), peak 3 at 382 nm and matches the maximum in fluorescence spectrum of cross-links in collagen (but probably wider in the long-wave part, as collagen contains another fluorophore in an amount proportional to collagen).

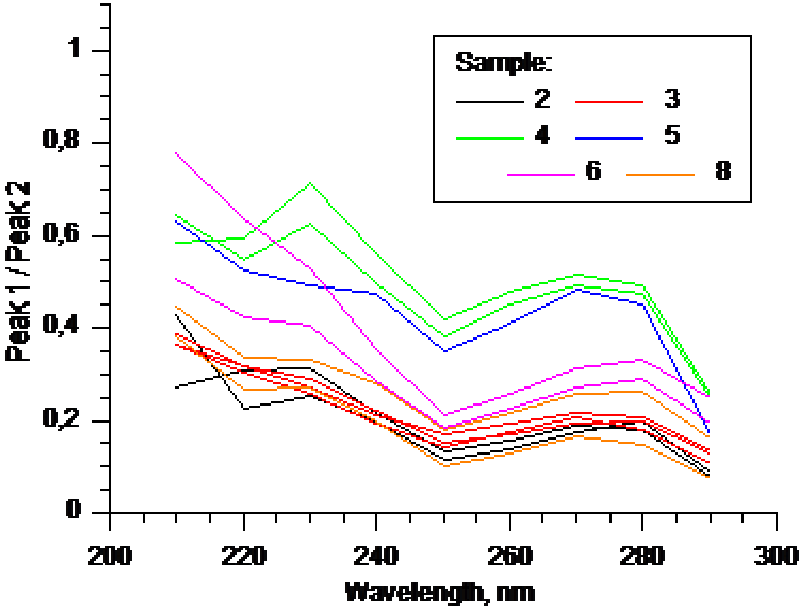

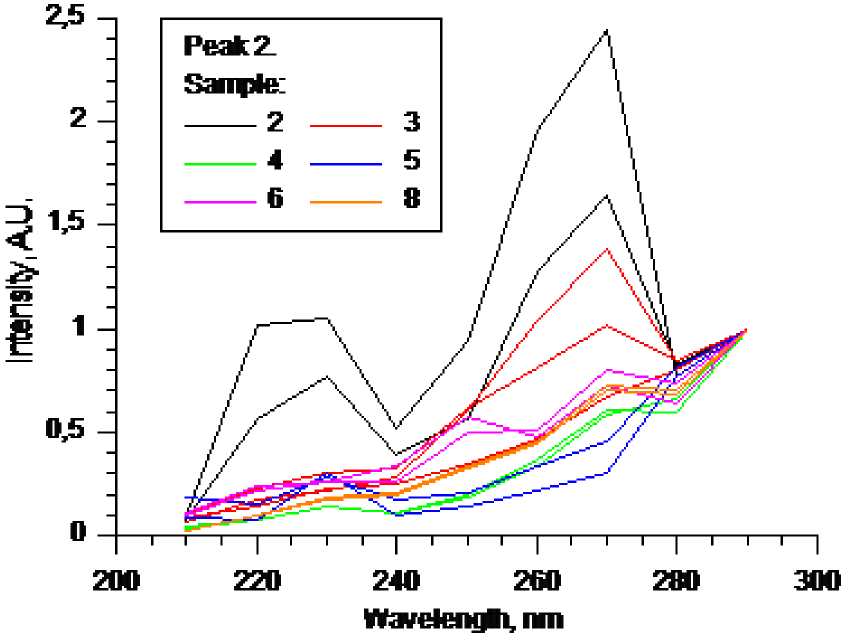

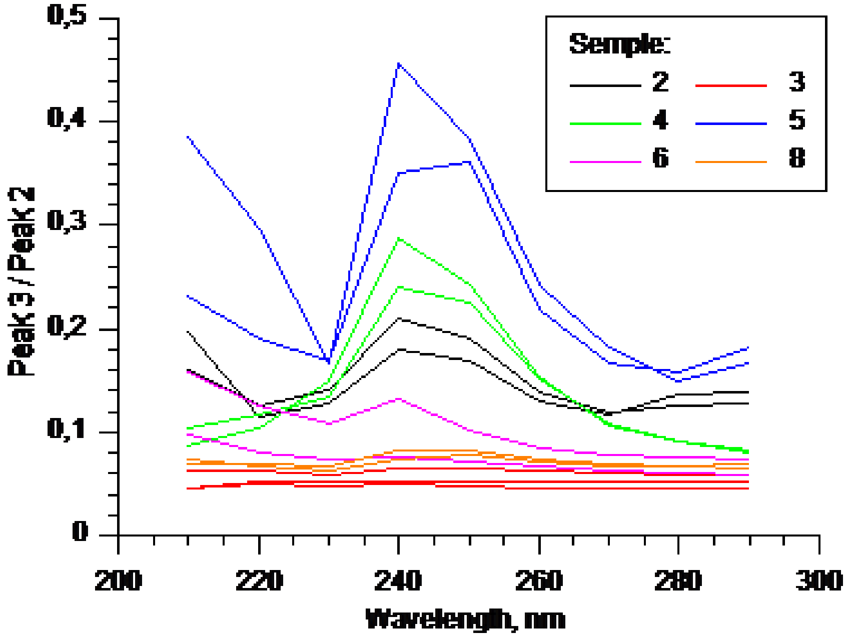

Fluorescence

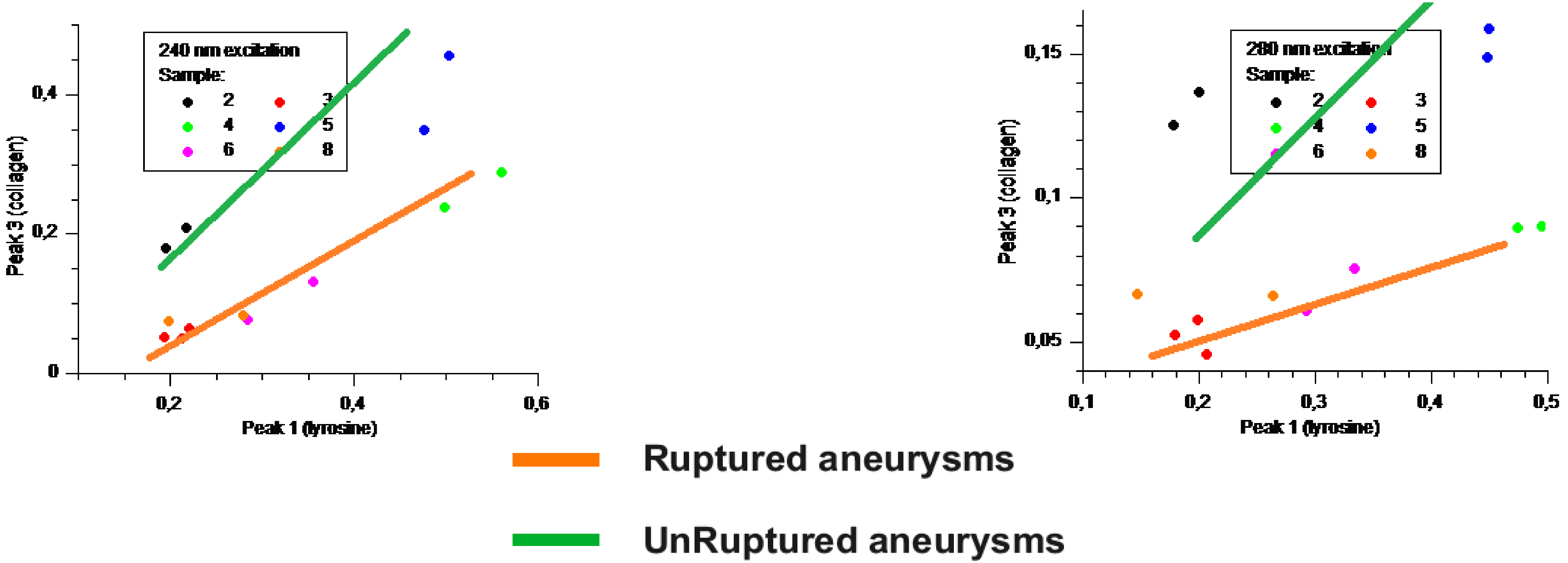

Inhere contributions to the spectrum of peaks 1 and 3 are shown normalized with the contribution of peak 2, for excitation wavelength 290 nm.

D. V. Parshin, E. O. Tsibulskaya, A. V. Dubovoy, A. P. Chupakhin, and N. A. Maslov, **Application of laser-induced fluorescence method to the study of the cerebral aneurysm wall: First results and perspectives,** AIP Conference Proceedings **2125**, 020007 (2019); https://doi.org/10.1063/1.5117367

Part VI. Boundary conditions problem: patient specific vs phantom, rigid vs FSI, steady vs transient

The pathway

- The experimental research (mechanical test and investigation of protein consist).
- Numerical simulation of a blood flow with the aneurysm-dangerous behavior detecting.
- Statistical analysis of shapes.
- Mathematical modelling of the vessel wall.
- Mechanical-chemical model of the aneurysm growth and rupture.

Preoperative prediction model of the growth and rupture of a real aneurysm.

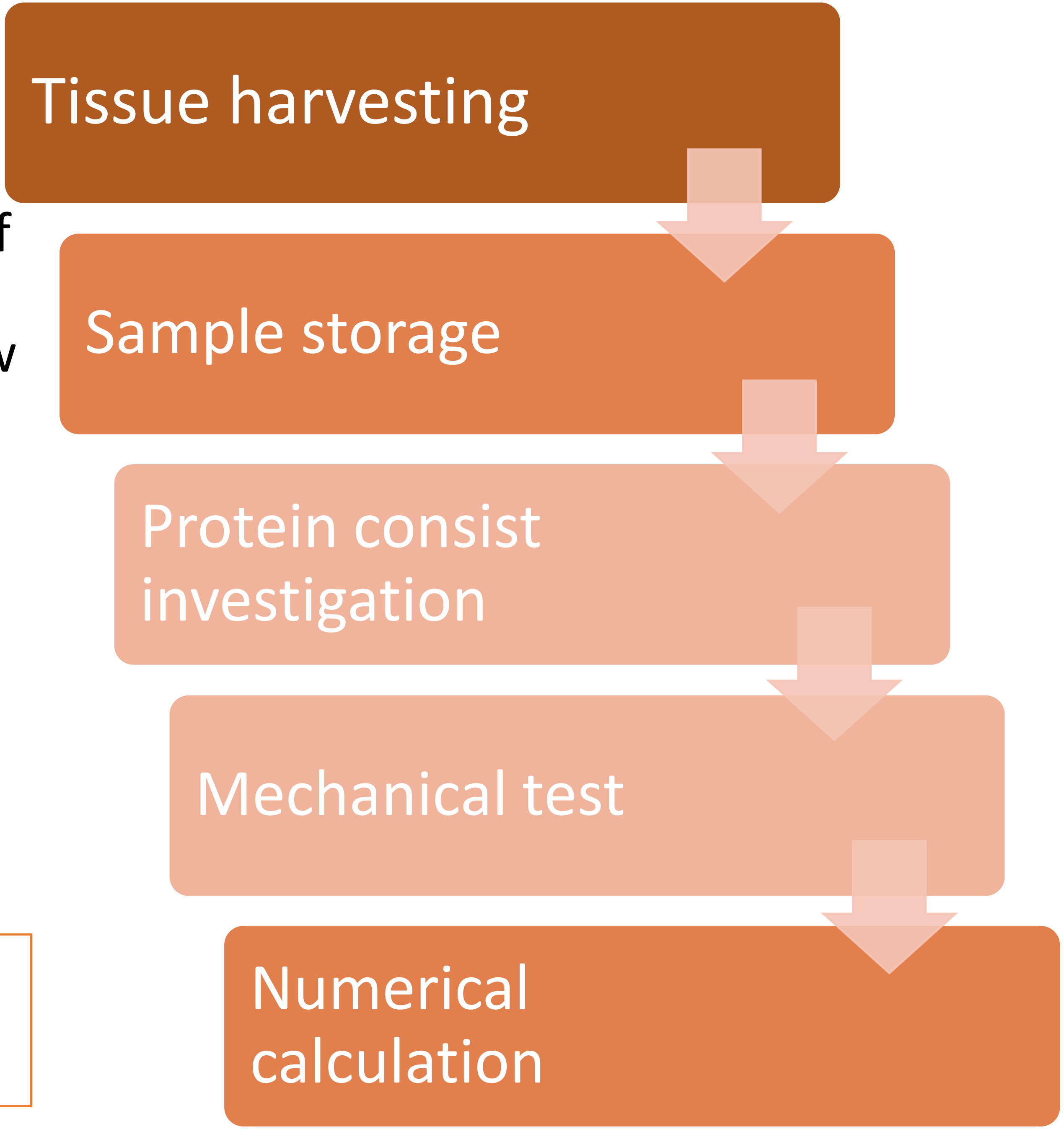
Tissue harvesting

Sample storage

Protein consist investigation

Mechanical test

Numerical calculation

Intraoperative velocity measurement

- A Doppler Transonic ultrasound sensor was used to measure the flow rate value distally to the aneurysm, both before and following treatment. The data was digitised using the open software WebPlotDigitizer (version 3.12) and the result obtained was used for the setup of the patient-specific FSI problem.
- Flow rate measurements: a-before treatment, b-following treatment and digitised waveform before treatment (on the right).

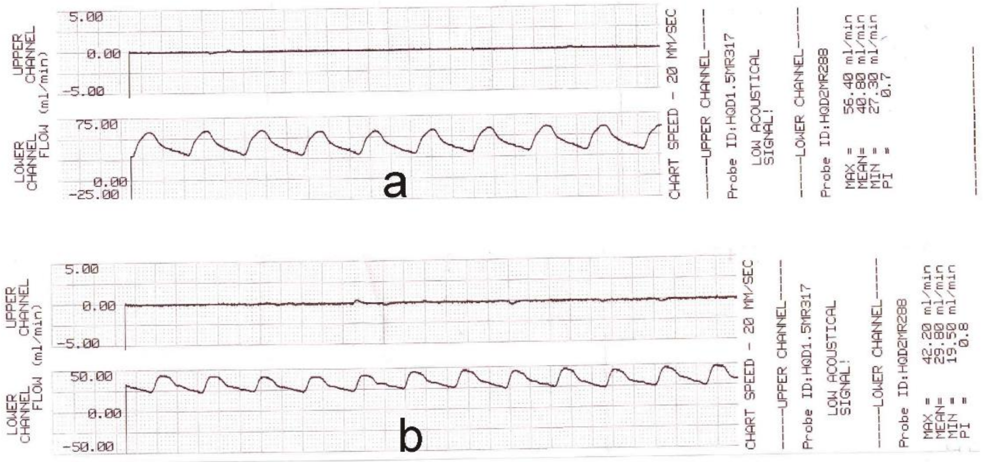

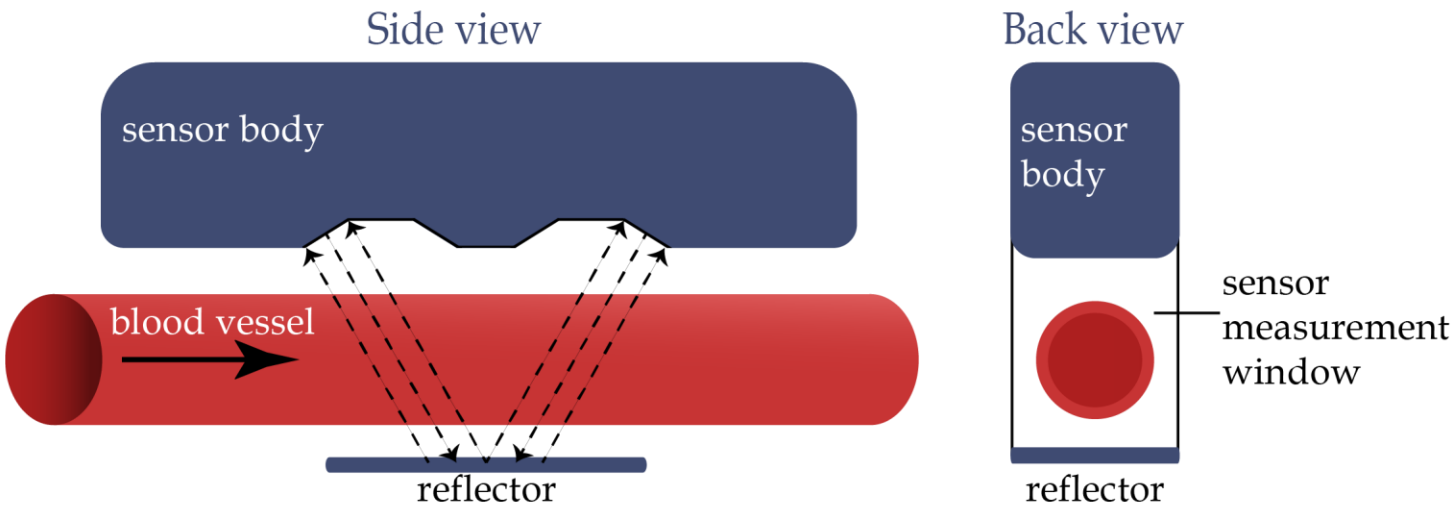

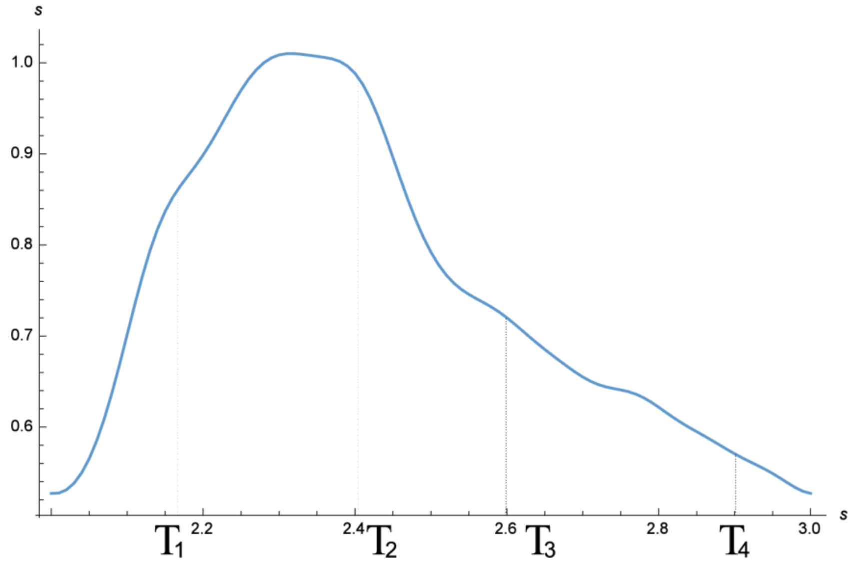

Mechanical test

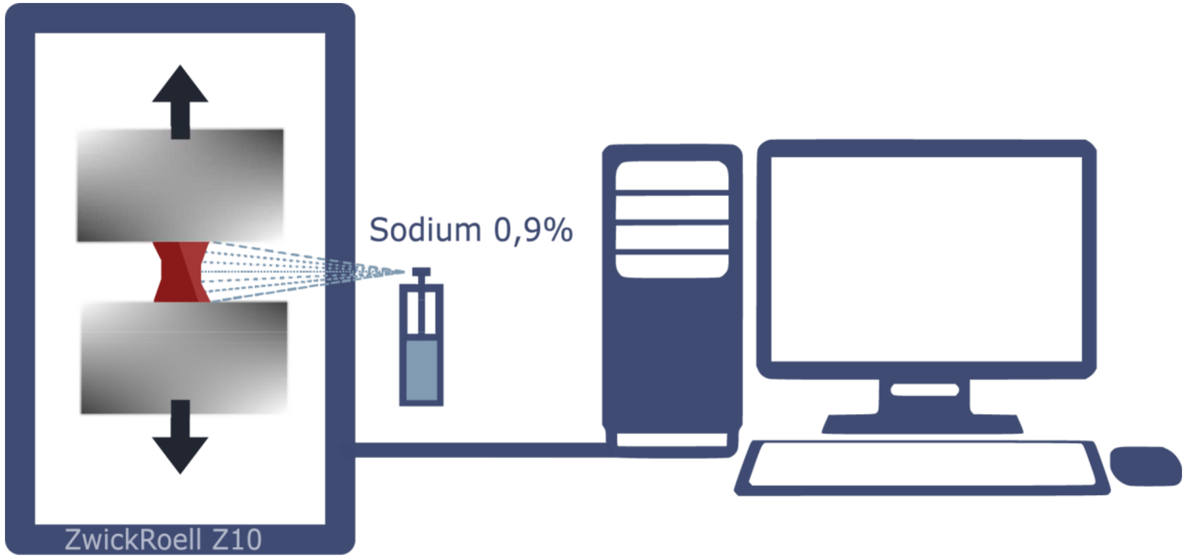

Experiment on the rupture machine Zwick/Roell Z100, Germany (LIH SB RAS)

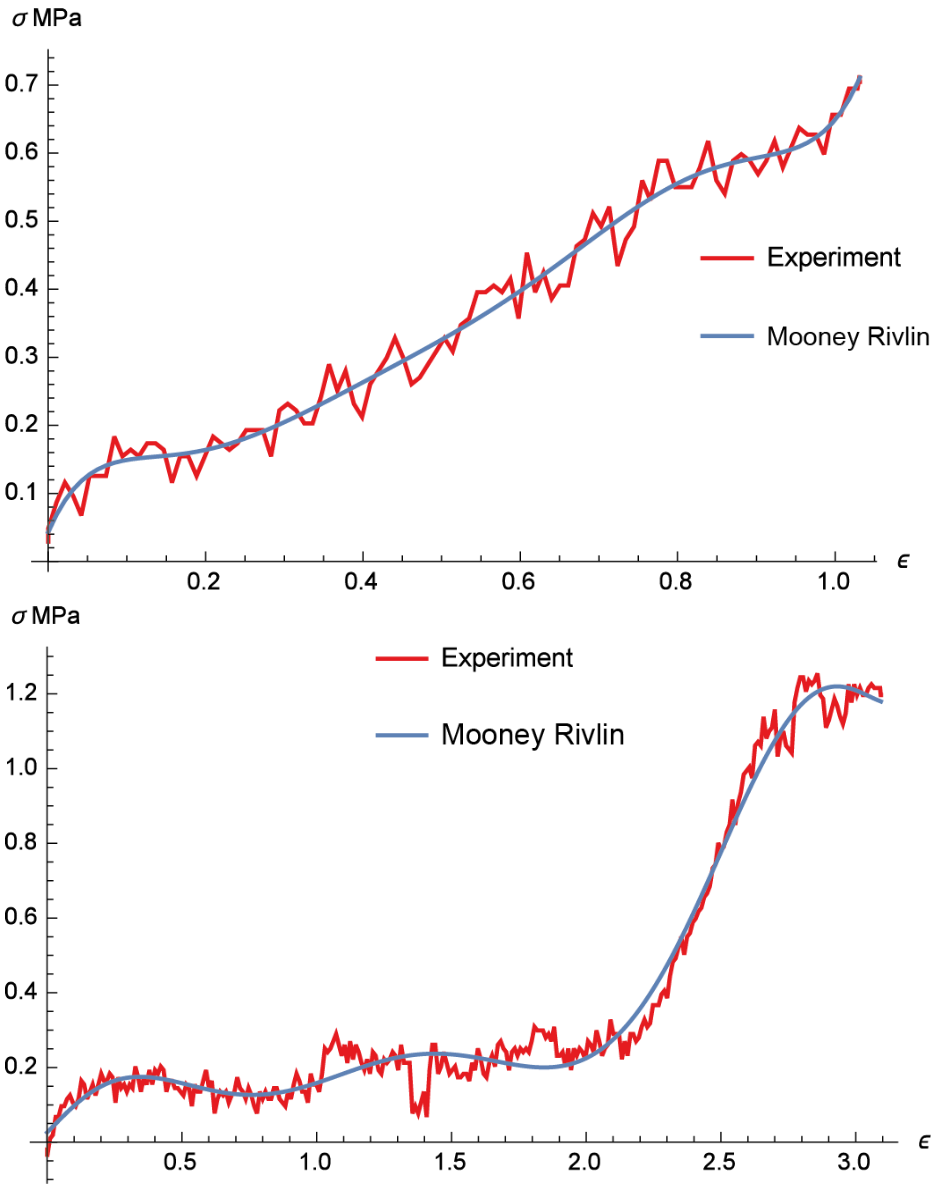

- Experimental data (red line) and Mooney-Rivlin (blue line) approximation.

Numerical simulations in ANSYS. Setup

- <u>Experimental setup:</u>
- Unsteady flow
- Inlet condition: Time dependent velocity (flowrate) profile
- Outlet condition: Pressure
- Boundary surface condition (vessel wall): no slip condition (rigid walls)
- Finite volume method for Navier-Stokes equations.
- Incompressible viscous Newtonian fluid.

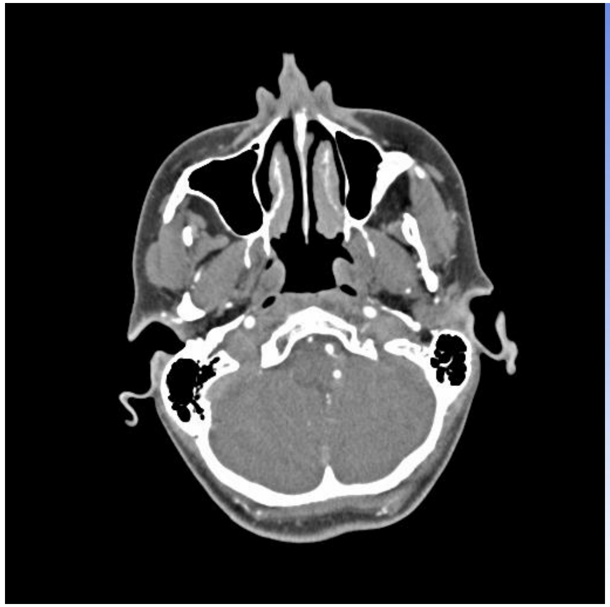

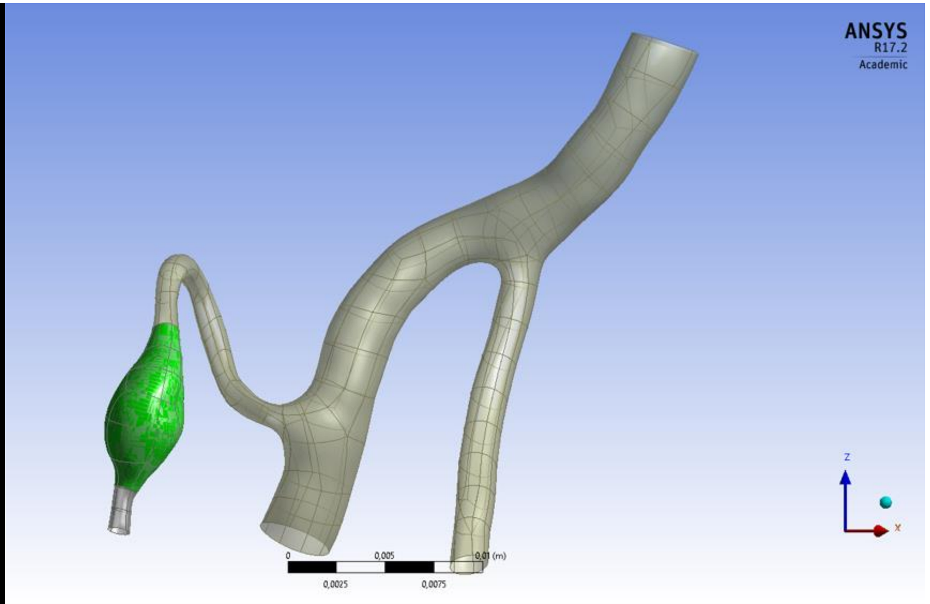

Conditions x Scenarios	Rigid walls	FSI scenarion A	FSI scenarion B	FSI scenarion C	FSI scenarion D
Inlet	flow rate	flow rate	flow rate	$V_0 + V_a \sin 2\pi t$	$V_0 + V_a \sin 2\pi t$
Outlet	Pressure	Pressure	Pressure	Pressure	Pressure
Surface type	Rigid	Elastic	Elastic	Elastic	Elastic
Surface condition	No slip	No slip +displacement	No slip +displacement	No slip +displacement	No slip +displacement
Blood vessel wall	-	Non-homogeneous	Homogeneous	Non-homogeneous	Homogeneous
Fluid - structure coupling	-	Pressure	Pressure	Pressure	Pressure

Results. streamlines

- Streamlines for Scenario A corresponding to different times, for rigid approach (on the left) and for FSI approach (on the right).

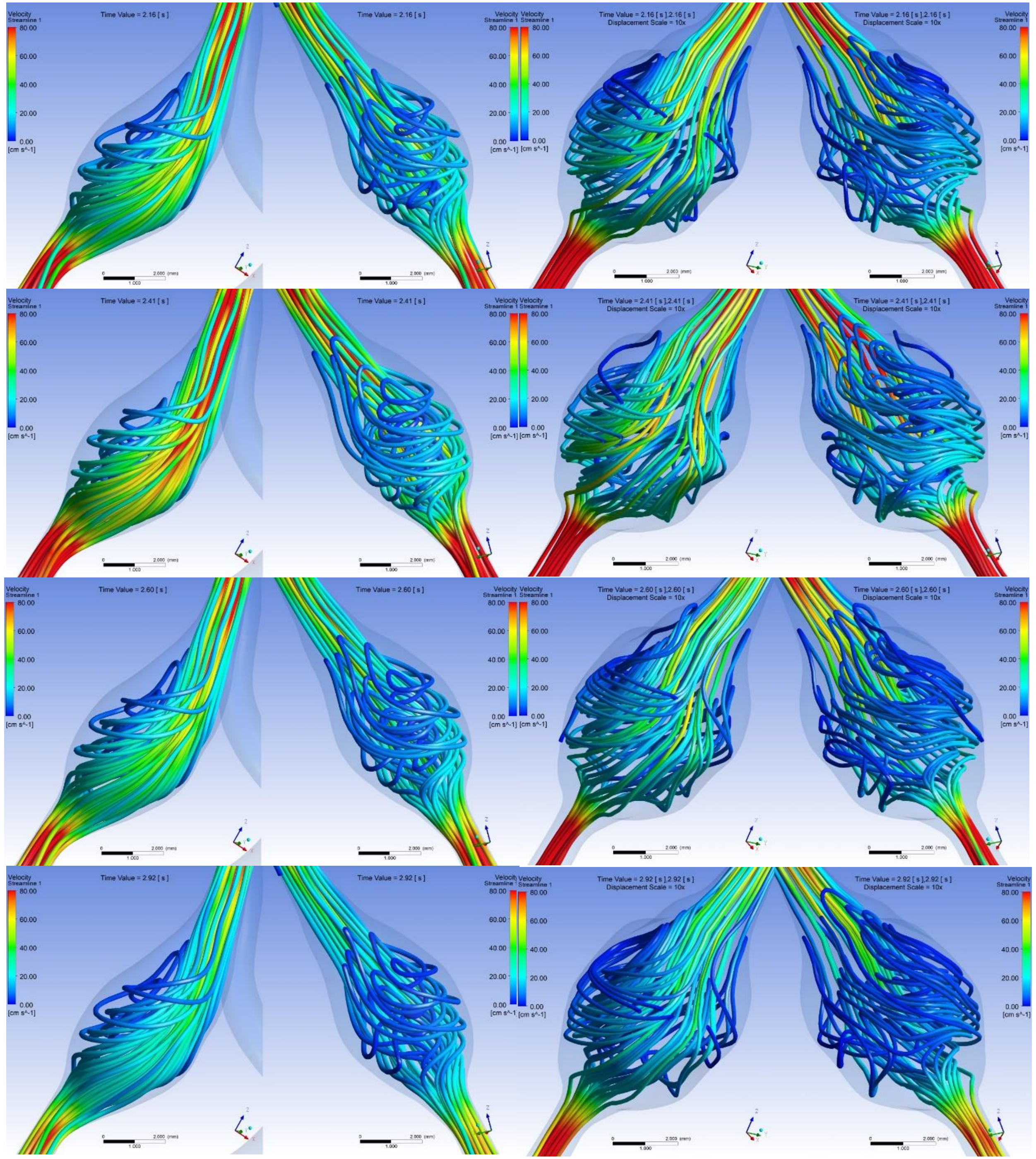

Results. High wss PATHWAY TO FIND RUPTURE SITE

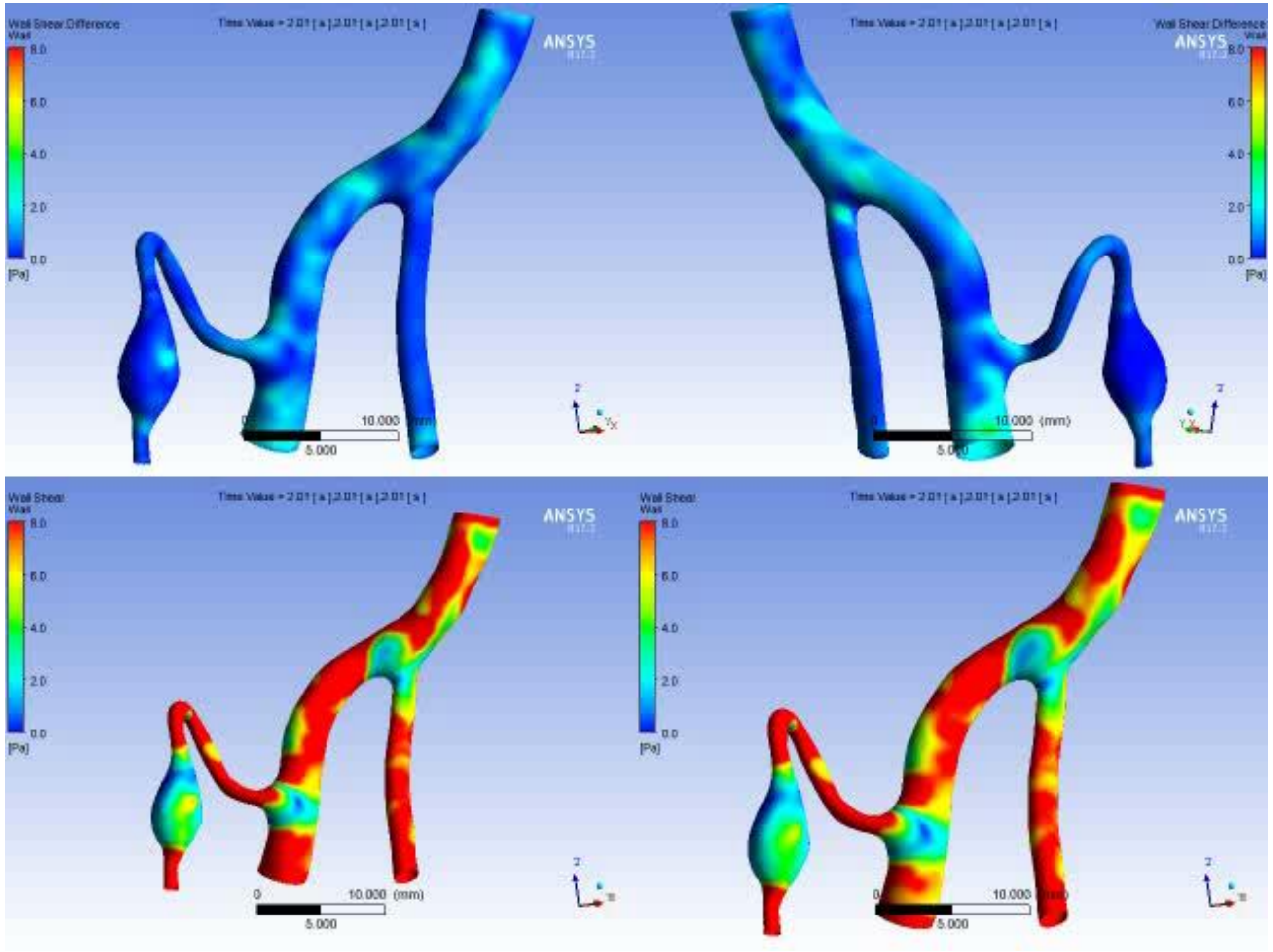

There is a maximum difference in the value of WSS for the 2 previous approaches and this place exactly coincides with the place of rupture of the aneurysm.

Results

The diagrams of the minimums and maximums of the velocities and WSS or scenarios A-D and the rigid wall for each time moment T1-T4.

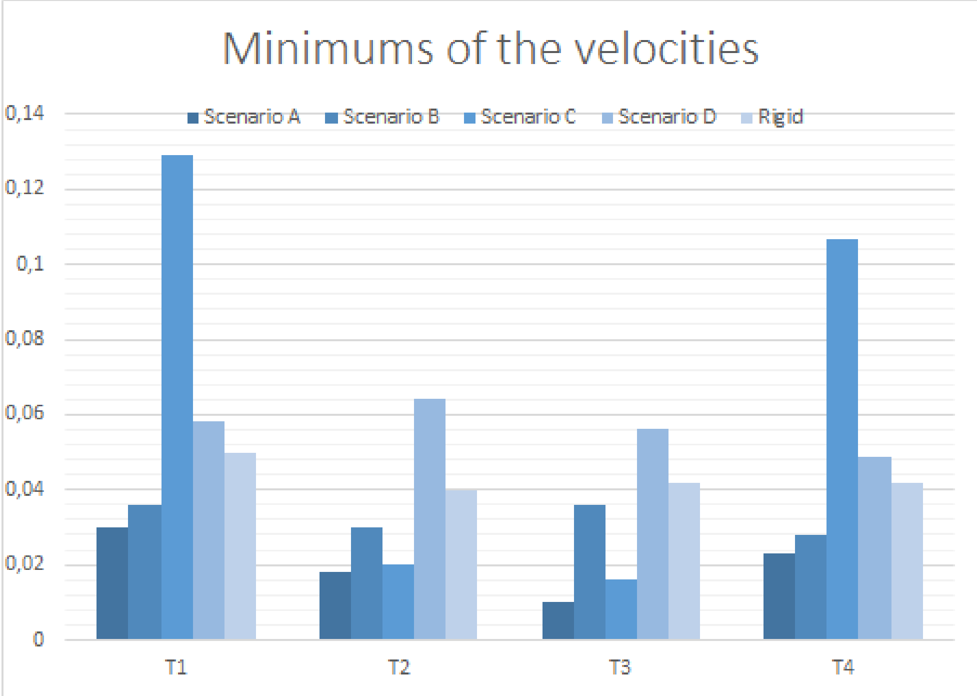
Minimums of the velocities

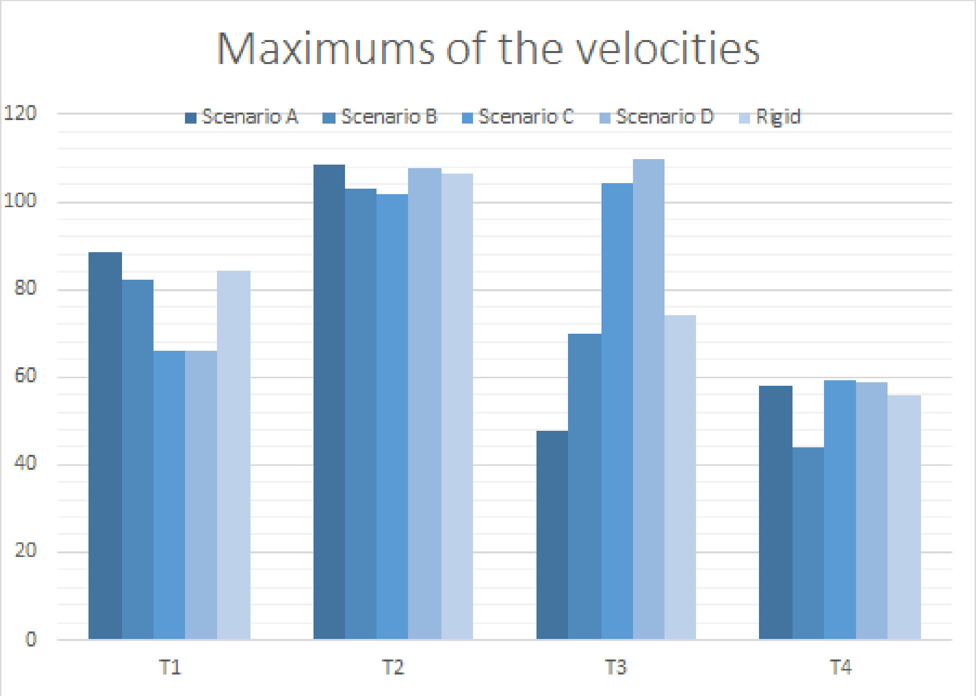
Maximums of the velocities

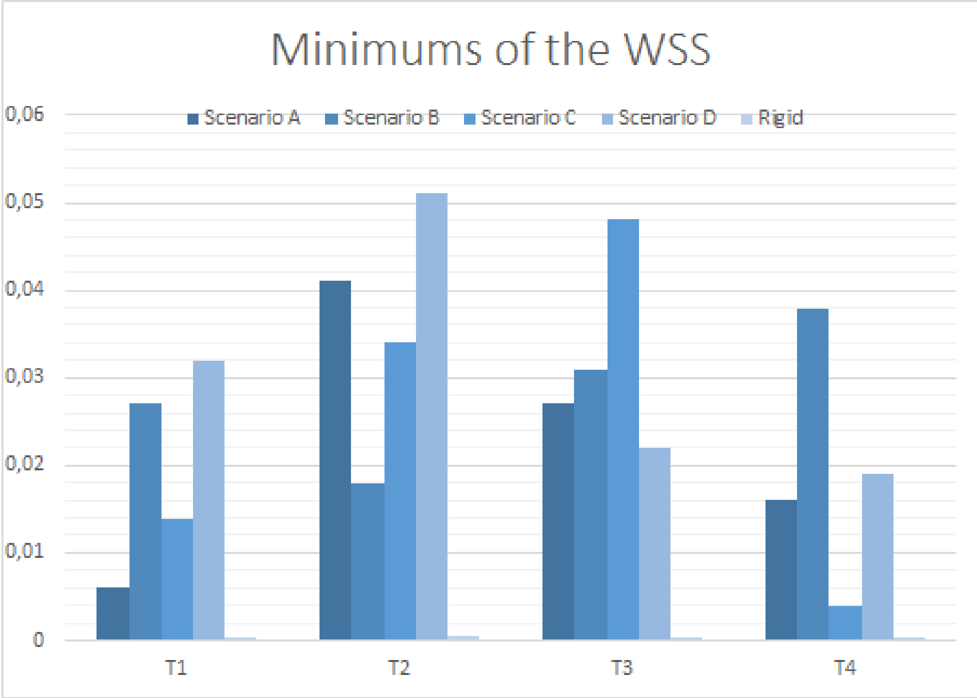
Minimums of the WSS

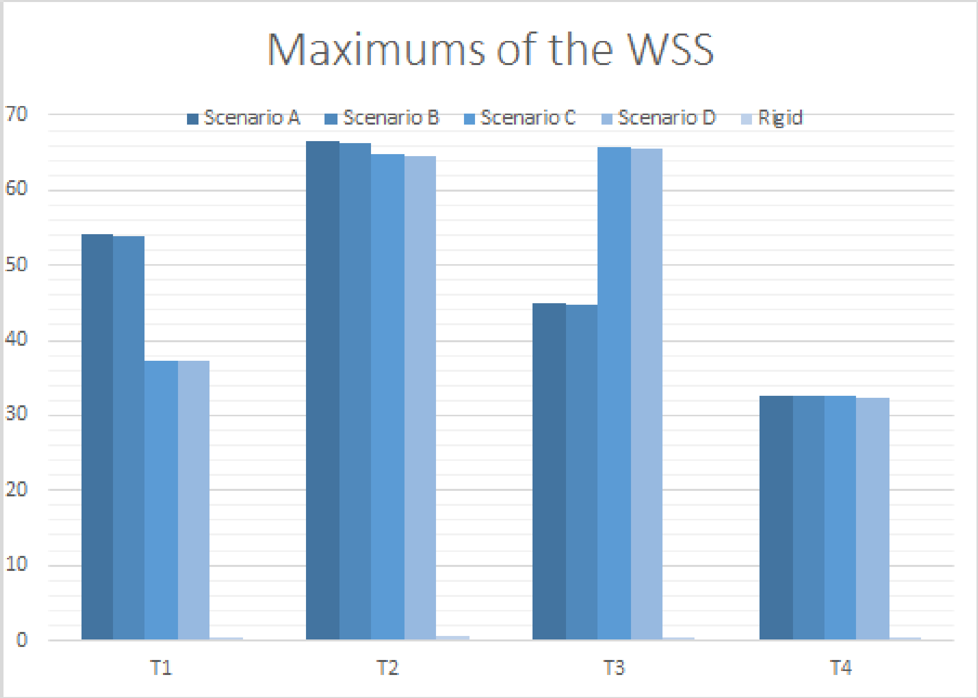
Maximums of the WSS

Results. Inflow concentration index

The IC index, which measures the degree of concentration of the flow stream entering the aneurysm, was also calculated:

$$ICI = \frac{Q_{in}/Q_v}{A_{in}/A_o}$$

Where Q_{in} is the flow rate into the aneurysm (inflow), Q_v is the flow rate in the parent artery, A_{in} is the area of the inflow region, and A_o is the area of the ostium surface.

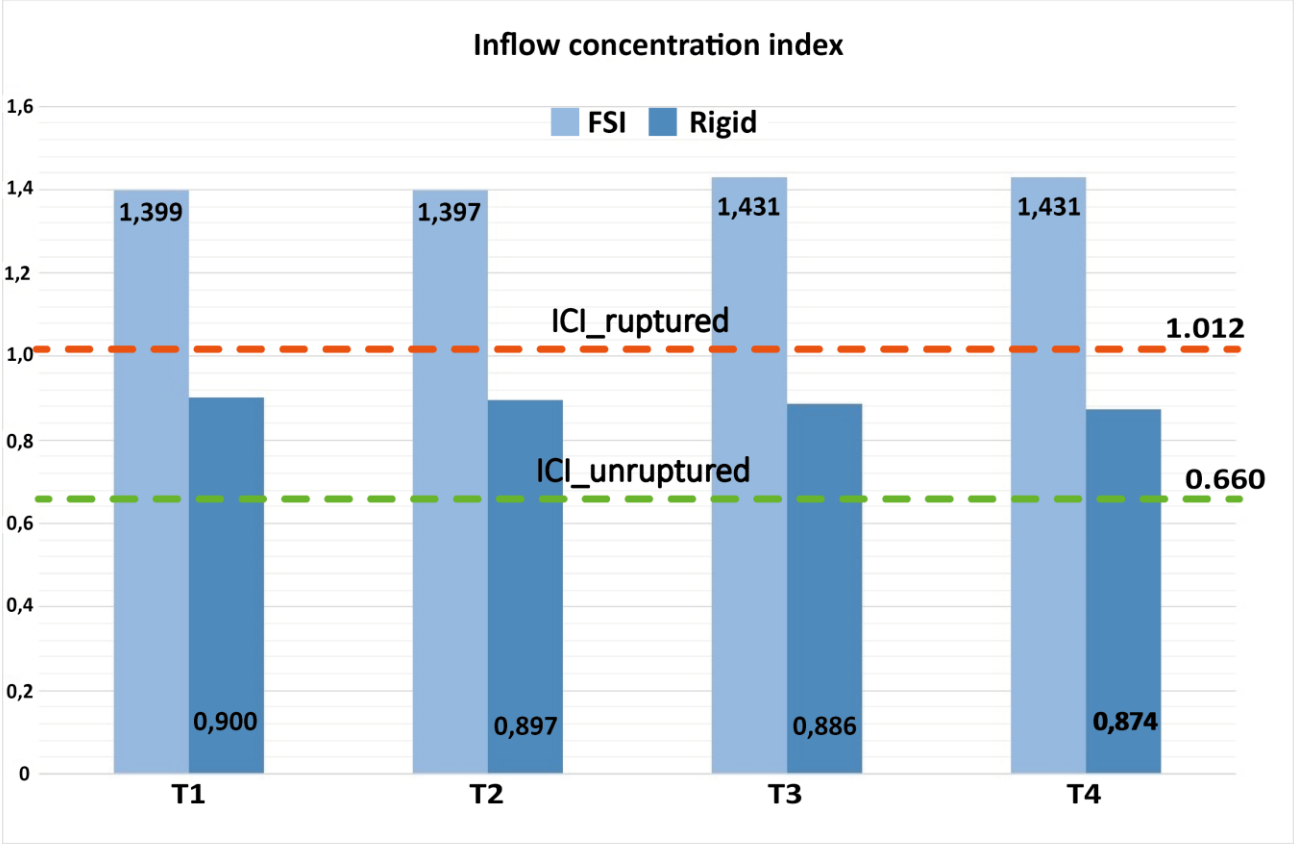

Parshin et al. In preparation for submitting

Conclusions

- The calculations were performed in 4 scenarios with boundary conditions from both literature and patient-specific ones.
- The best localization of the rupture site is performed using the FSI approach and with the substitution of the velocity profile for a particular patient. In the case of a linear model of wall elasticity, the Young's modulus does not play a large role in localizing the rupture site.
- Verification of the aneurysm status was performed with using ICI- criterion. FSI – approach gave more plausible result of a such verification.

Part VII. Signs of cerebrovascular disease in terms of various components of the energy of the circulatory system

Chapter 1. Efficiency of vascular bypass: model study

Bypass surgery

➢Cerebral bypass is a junction of cerebr
or cerebral-extracranial vessels to suppl
necessary volume of blood flow rate.

➢**Applications:**

- Cerebral aneurysms
- Intracranial stenosis
- Tumors
- Moya-moya disease

➢Types of main bypass techniques:

1. Side-to-side
2. End-to-end
3. End-to-side

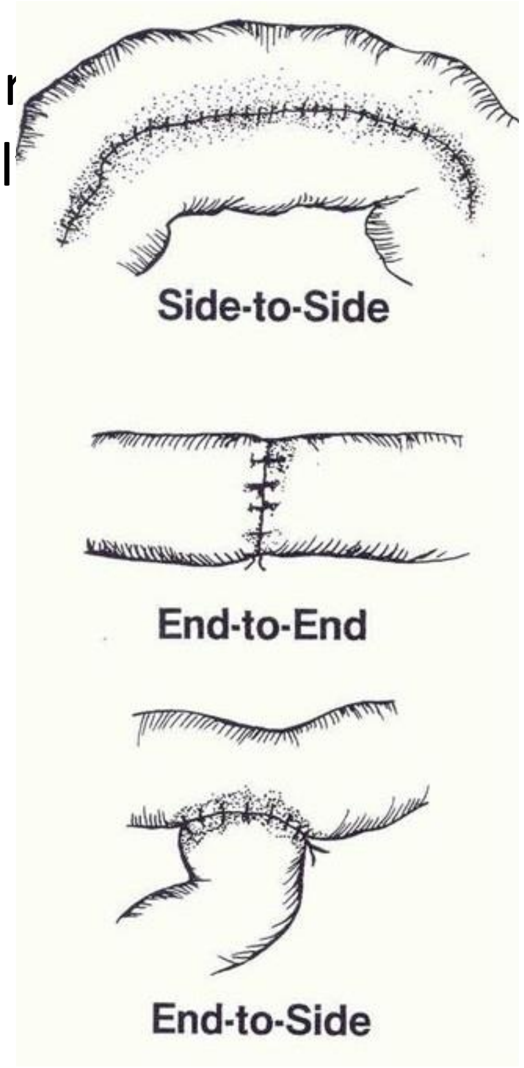

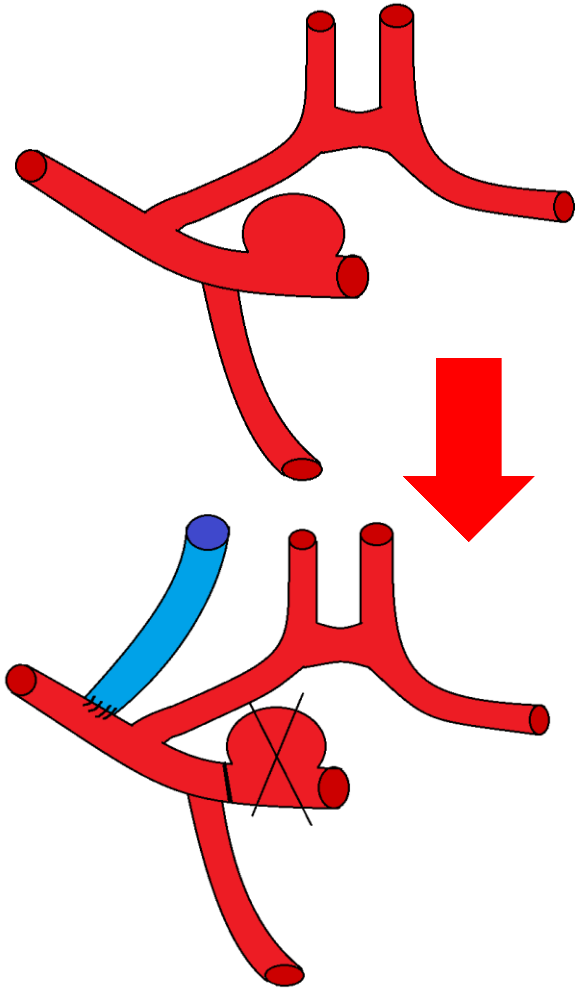

The technique of Bypass surgery

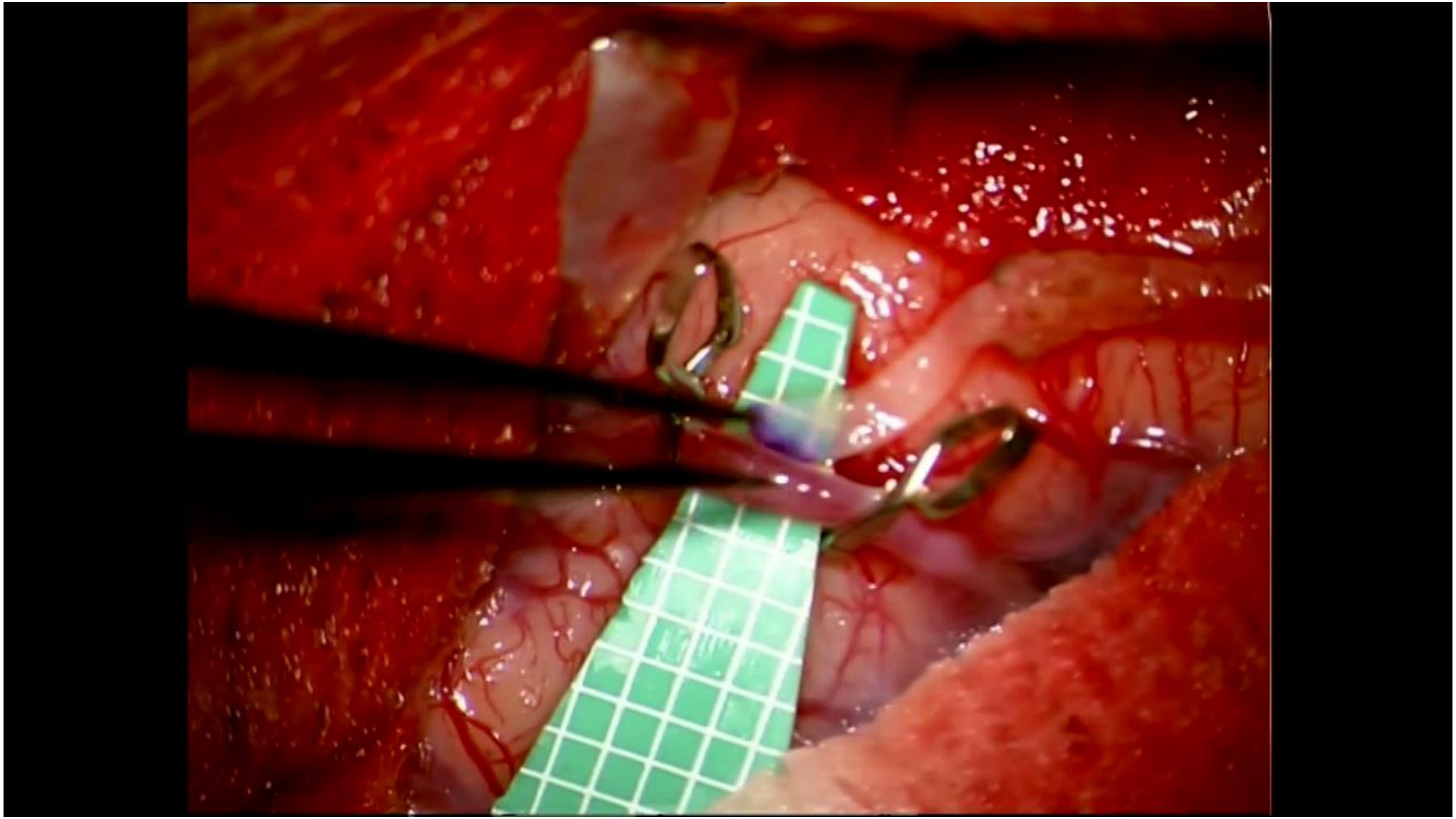

The ZOO of THE PROBLEMS!!!

- The necessity of bypass surgery

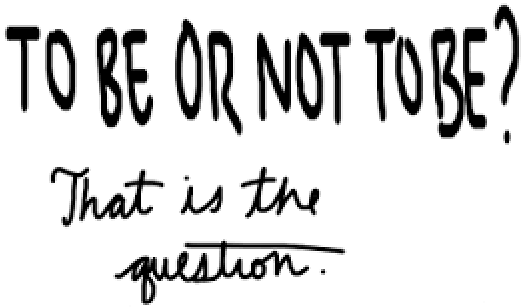

TO BE OR NOT TO BE?

That is the question.

W. Shakespire

- Optimal placement of bypass graft

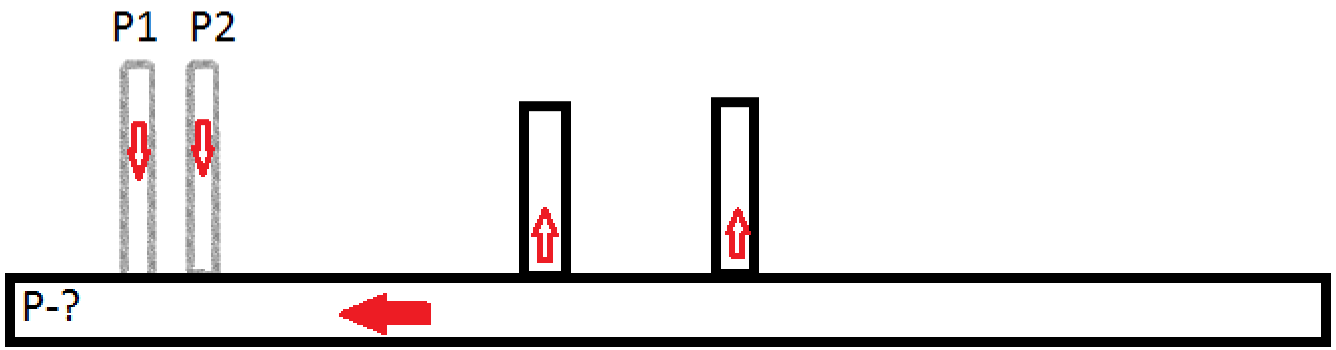

The ZOO of THE PROBLEMS!!!

- Optimal bypass angle and the

Shape of an ‘arteriometric window’

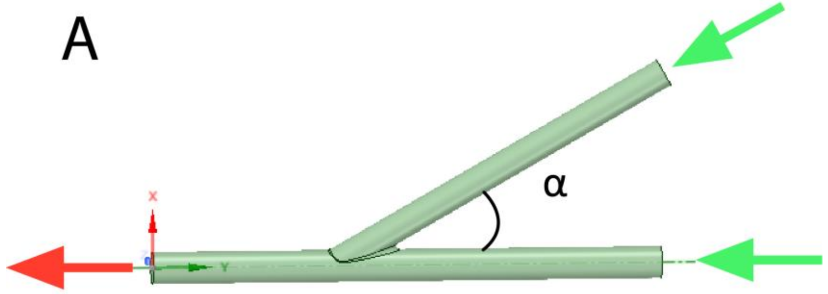

- ARTERIAL vs VIENUS graft

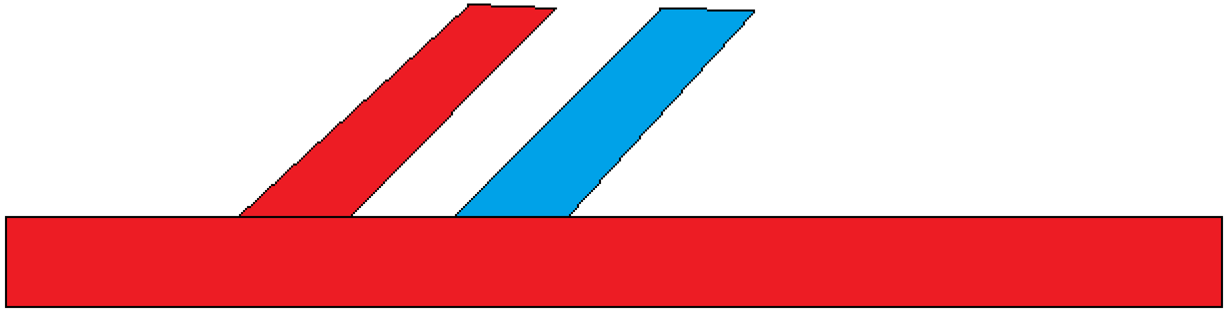

Optimal bypass angle

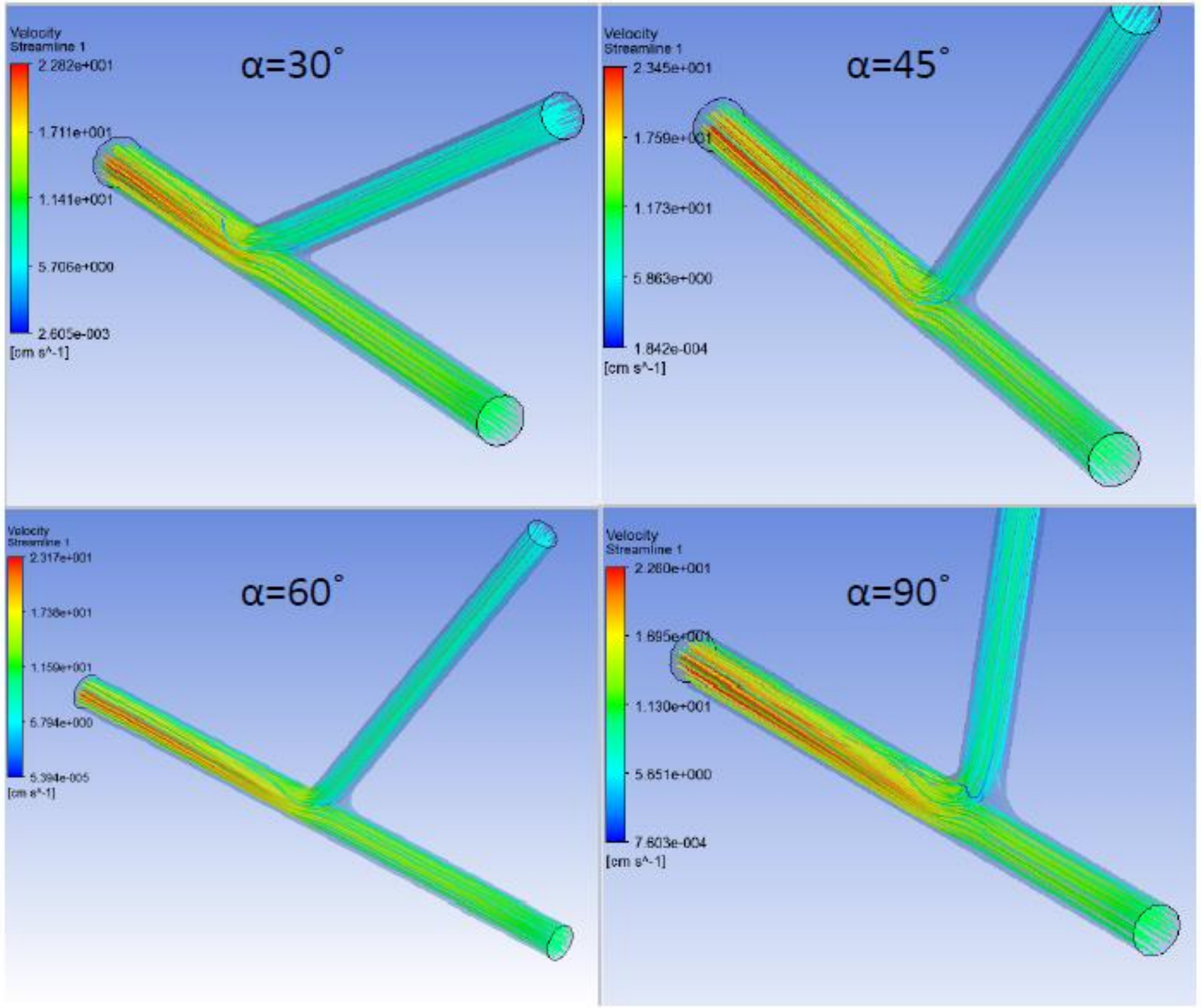

What is going on?

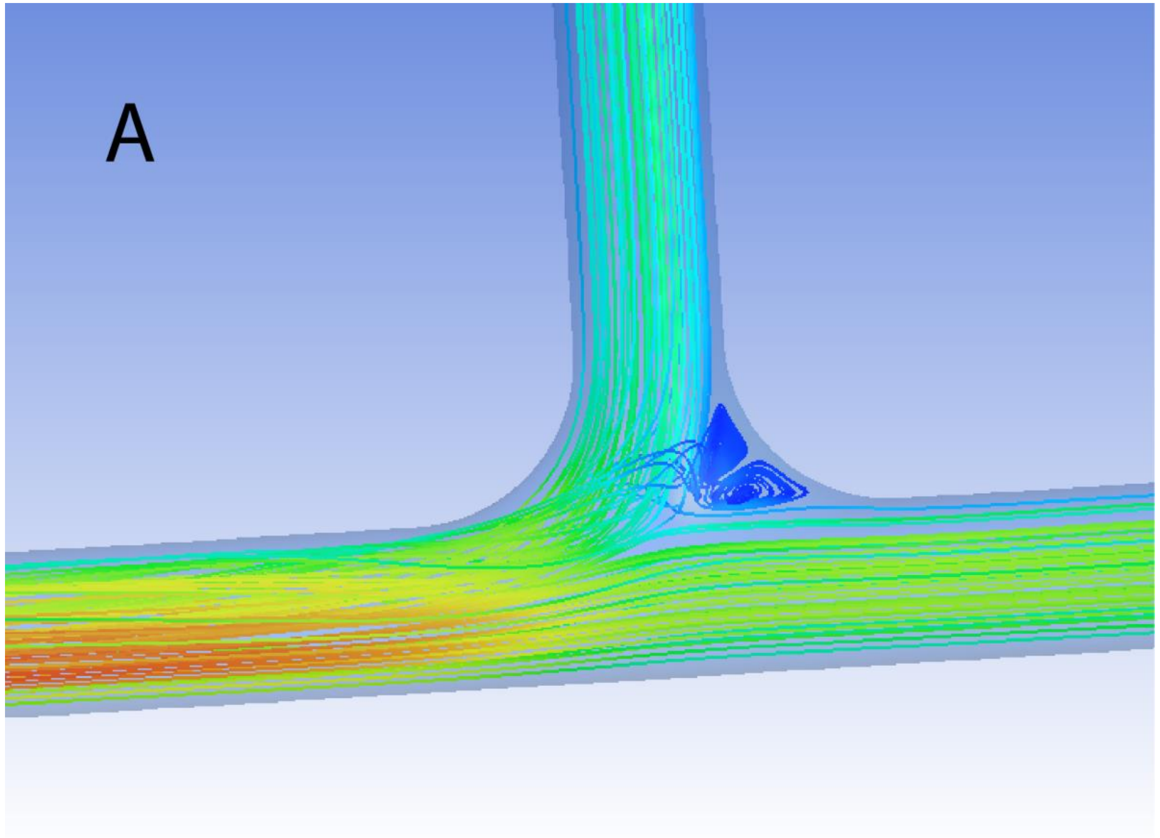

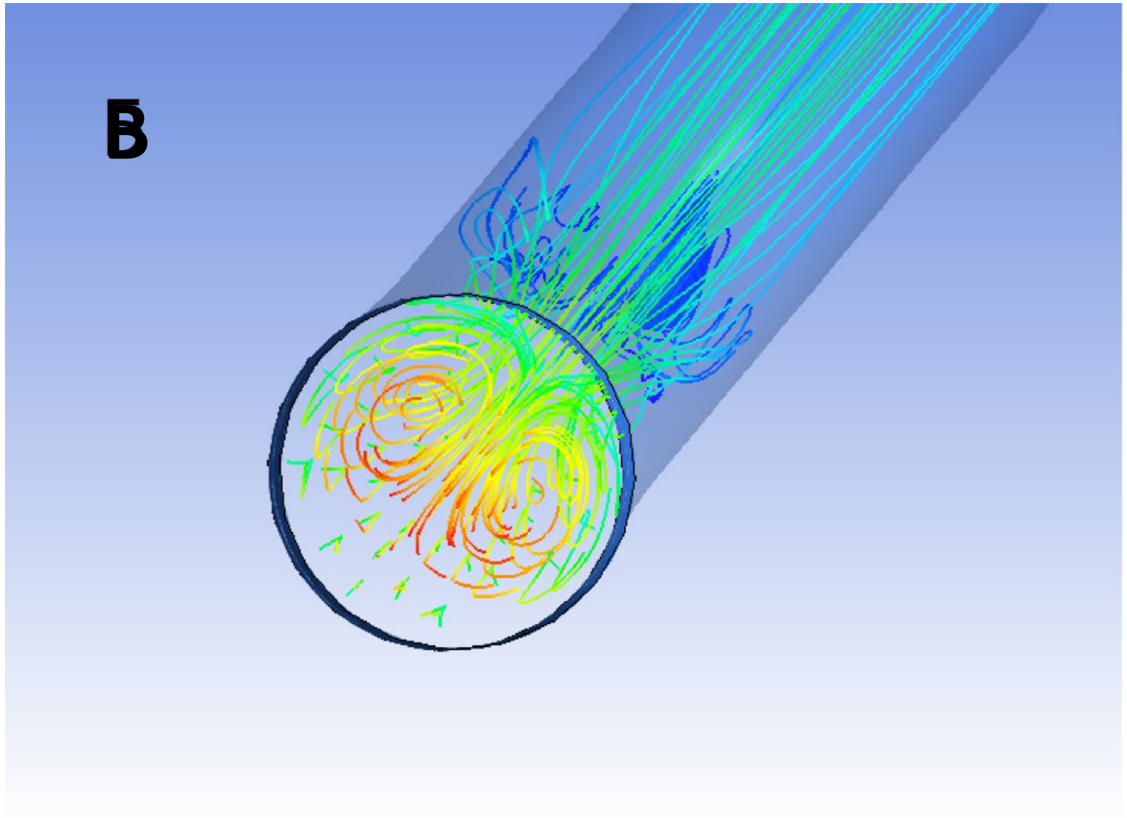

Viscous dissipation energy

We are about to analyze:

$$D = 4\mu \int_{\Omega} |\omega|^2 \, d\Omega,$$

The energy which dissipate in the volume Omega. It’s of sense to consider unit value, when you are going to compare different volumes.

Hemodynamic problem

- Steady blood flow for viscous inviscid fluid, Navier-Stokes equations:
- $$\begin{cases} \rho(u\nabla u - \mu\Delta u) = -\nabla p \\ div\, u = 0 \end{cases}$$
- u – velocity
- ρ – density
- p – pressure

For the simulations we used unstructured tetrahedral mesh with 5 inflation layers.

Comparing of the mesh quality

flowrate difference (g/s)	M1-M2	M2-M3	M3-M4
LACA	0,0058	-0,0109	-0,0115
RACA	-0,0181	0,0071	0,0163
LPComA	0,0122	0,0053	0,0036
RPComA	-0,0091	-0,0045	-0,0028
LMCA	-0,0163	-0,019	-0,015
RMCA	0,0257	0,0221	0,0093
AComA	-0,0089	-0,028	-0,0263

M1 – mesh with 1 million of elements
M2 – mesh with 2 million of elements
M3 – mesh with 3 million of elements
M4 – mesh with 4 million of elements

	M1	M2	M3	M4
Time of convergence (min)	12	16	21	30

What could we change?

Clinically we can change:

- graft diameter
- Blood flow rate (by choosing corresponding donor-artery)
- Angle of bypass graft installation

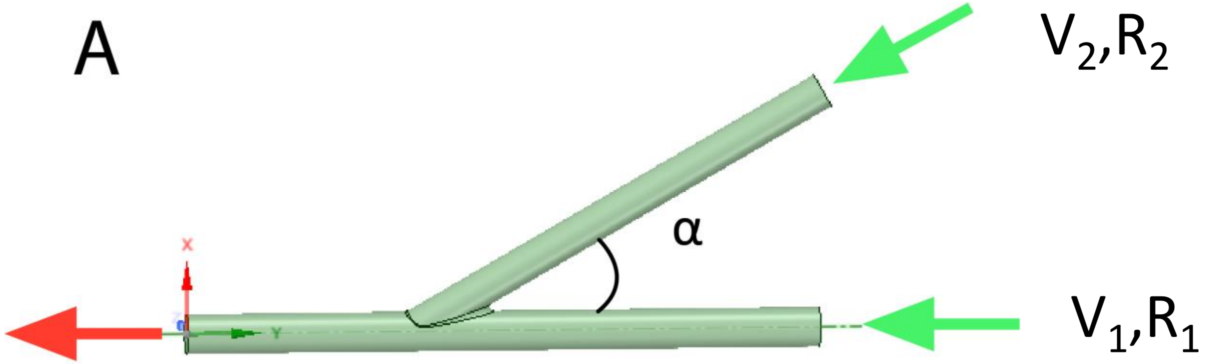

4 angles * 9 points for diameter ration * 9 points for the velocity ratio = 324 simulations

Value of Dissipative energy integral

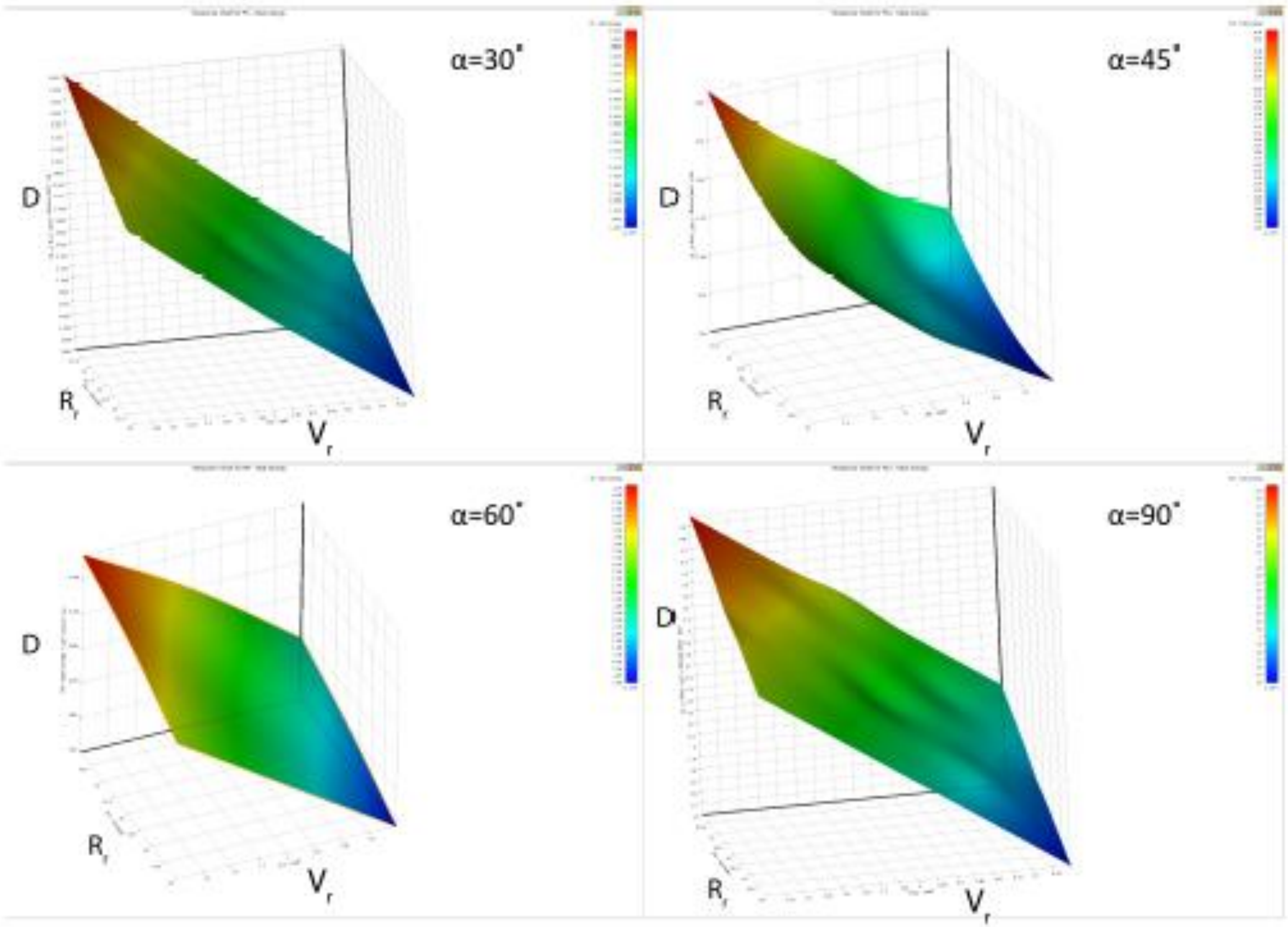

Ratio of diameters

Ratio of the velocities

Optimal bypass placement angle analysis

Wall shear stress values (Max), Pa

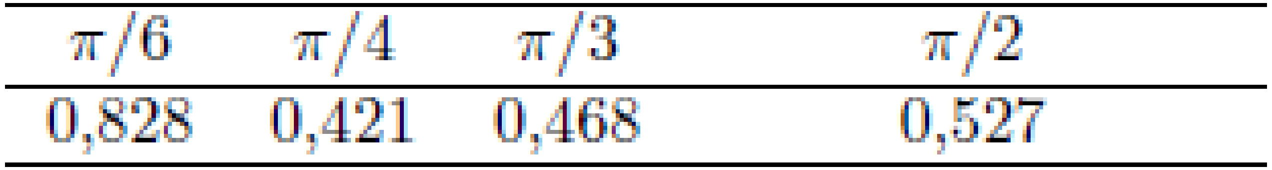

$\pi/6$	$\pi/4$	$\pi/3$	$\pi/2$
0,828	0,421	0,468	0,527

V(cm/s),R(mm)	π/6	π/4	π/3	π/2
Minimal values of D integral, J/s $*10^{-7}$				
V_1=6, R_1=14	**13523**	17192	**13365**	**13892**
V_1=6 ,R_1=13.896	14799	**16387**	16246	15736
Maximal values of D integral, J/s $*10^{-7}$				
V_1=14 ,R_1=10,1	**36734**	**48062**	**42211**	**39886**

CONCLUSIONS

We demonstrated that π/3 angle is the best pathway of treatment in terms of bifurcation energy loss and π/4 is the worst one.

WSS doesn’t play any role in this problem if we study on RIGID case. The investigation of FSI case is now in progress!

Chapter 2. Energy criteria

Multiple cerebral aneurysms

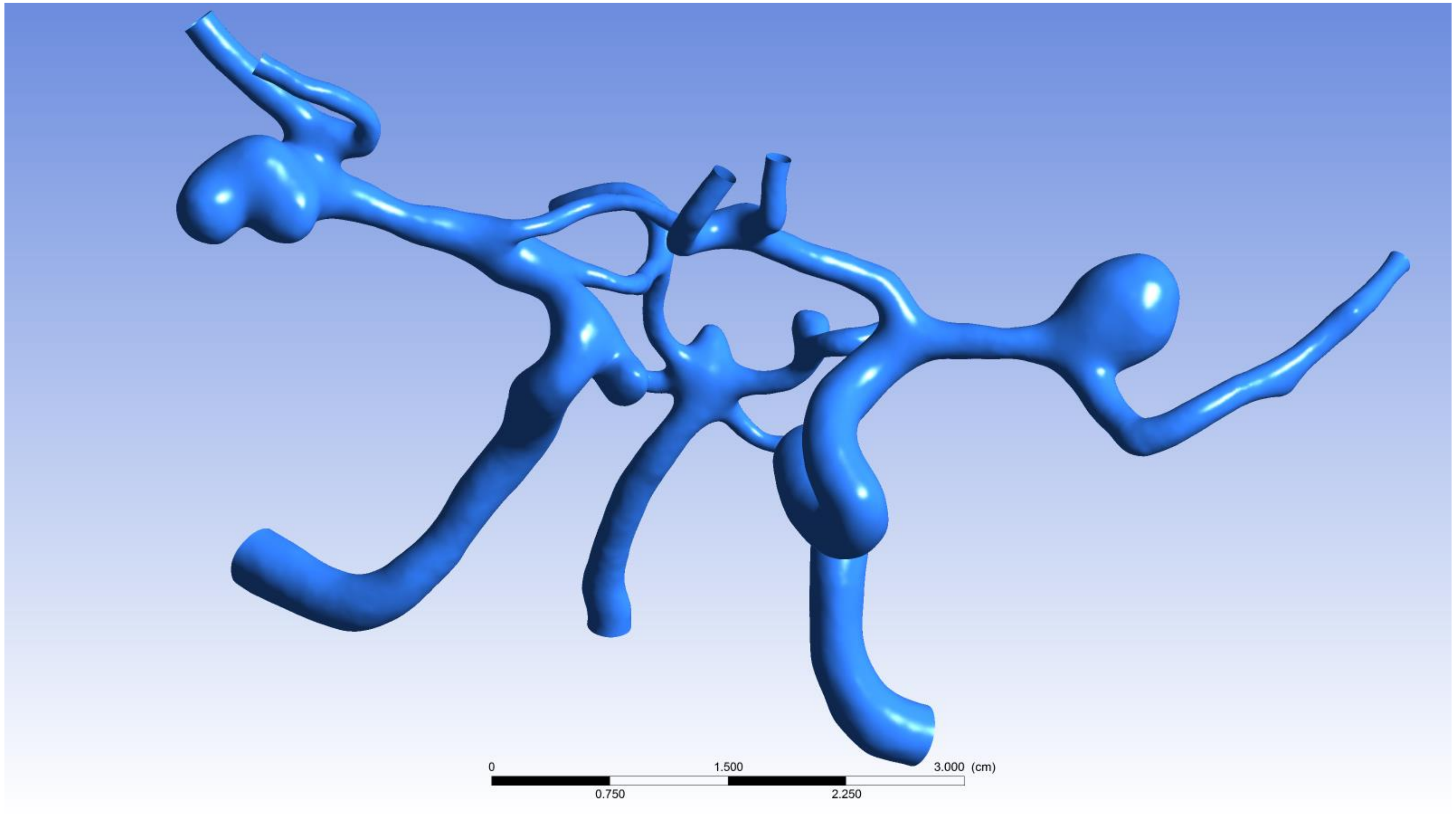

Khe, A. K., Chupakhin, A. P., Cherevko, A. A., Eliava, S. Sh., & Pilipenko, Y. V. (2015). Viscous dissipation energy as a risk factor in multiple cerebral aneurysms. *Russian Journal of Numerical Analysis and Mathematical Modelling*, *30*(5), 277–287. https://doi.org/10.1515/rnam-2015-0025

Multiple aneurysms. Cases studied

Burdenko National Medical Research Center of Neurosurgery

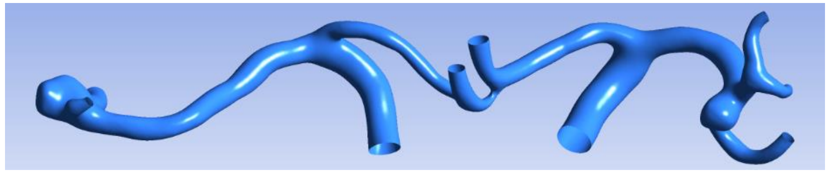

ANB, F, 54, **2** aneurysms:
left MCA*, right MCA

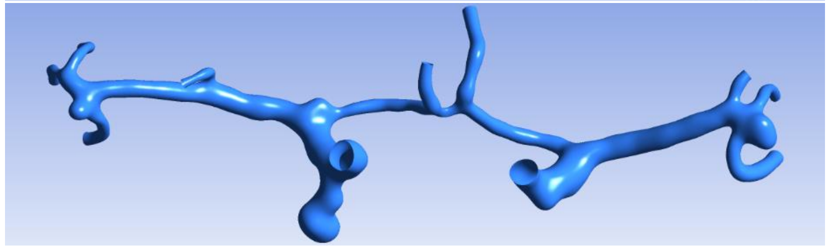

SLS, F, 56, **3** aneurysms:
right ICA*, right MCA, left MCA

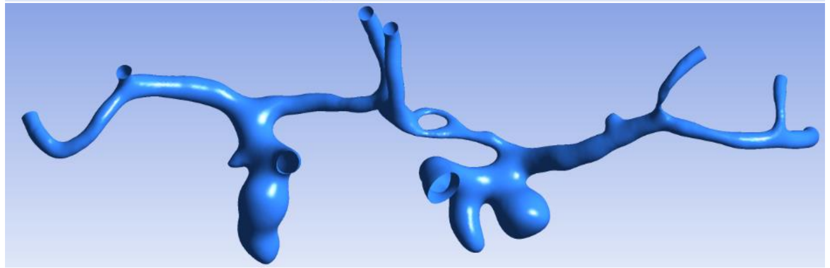

BEP, F, 53, **4** aneurysms:
2 right ICA* and 2 left ICA

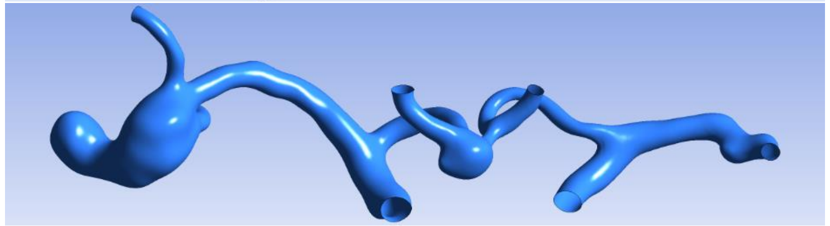

LYE, M, 55, **2** aneurysms:
right MCA*, right ACA-ACommA

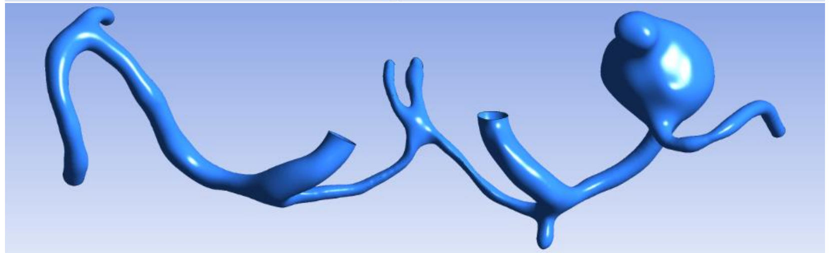

DRZ, M, 54, **2** aneurysms:
left MCA, left ICA*

* Ruptured aneurysm

Main hydrodynamic characteristics

Computation and comparison of the essential hydrodynamic parameters (pressure, velocity, wall shear stress) did not reveal any parameter correlating with the aneurysm rupture.

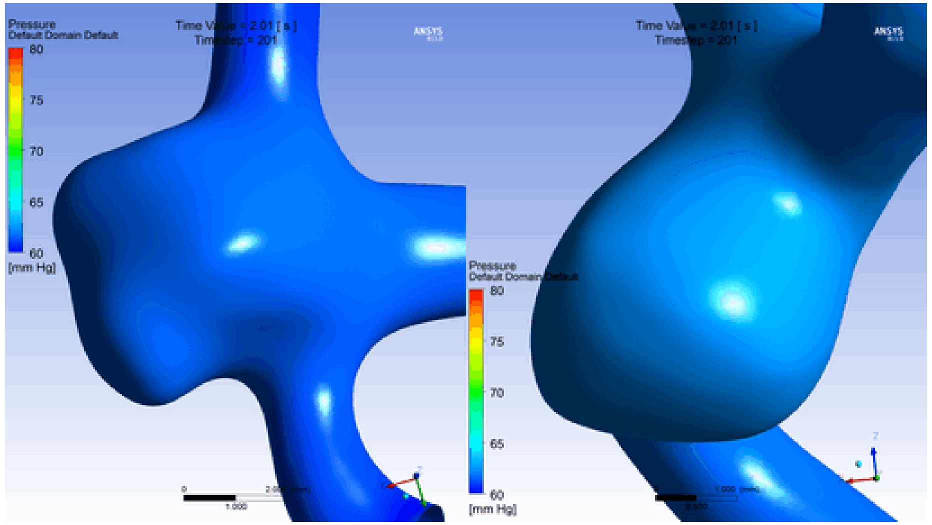

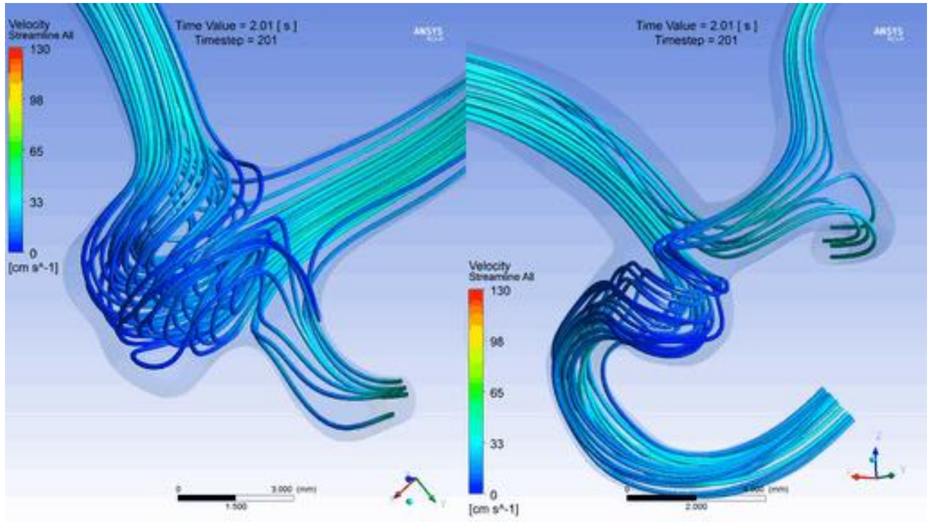

Viscous dissipation energy

Total mechanical energy dissipating in a unit time interval:

$$W = 4\mu \int_{\Omega} |\omega|^2 d\Omega$$

μ – is the dynamic viscosity, $\omega = \nabla \times \boldsymbol{v}$ – is the vortex vector.

Additional quantities:

- Total dissipation energy per one period:

$$E = \int_0^T W dt$$

- Average dissipation energy per unit volume:

$$\bar{E} = E/V$$

- Dissipation energy rate per unit surface area:

$$W_s = W/S$$

- Total dissipation energy per unit surface area:

$$E_s = E/S$$

Results

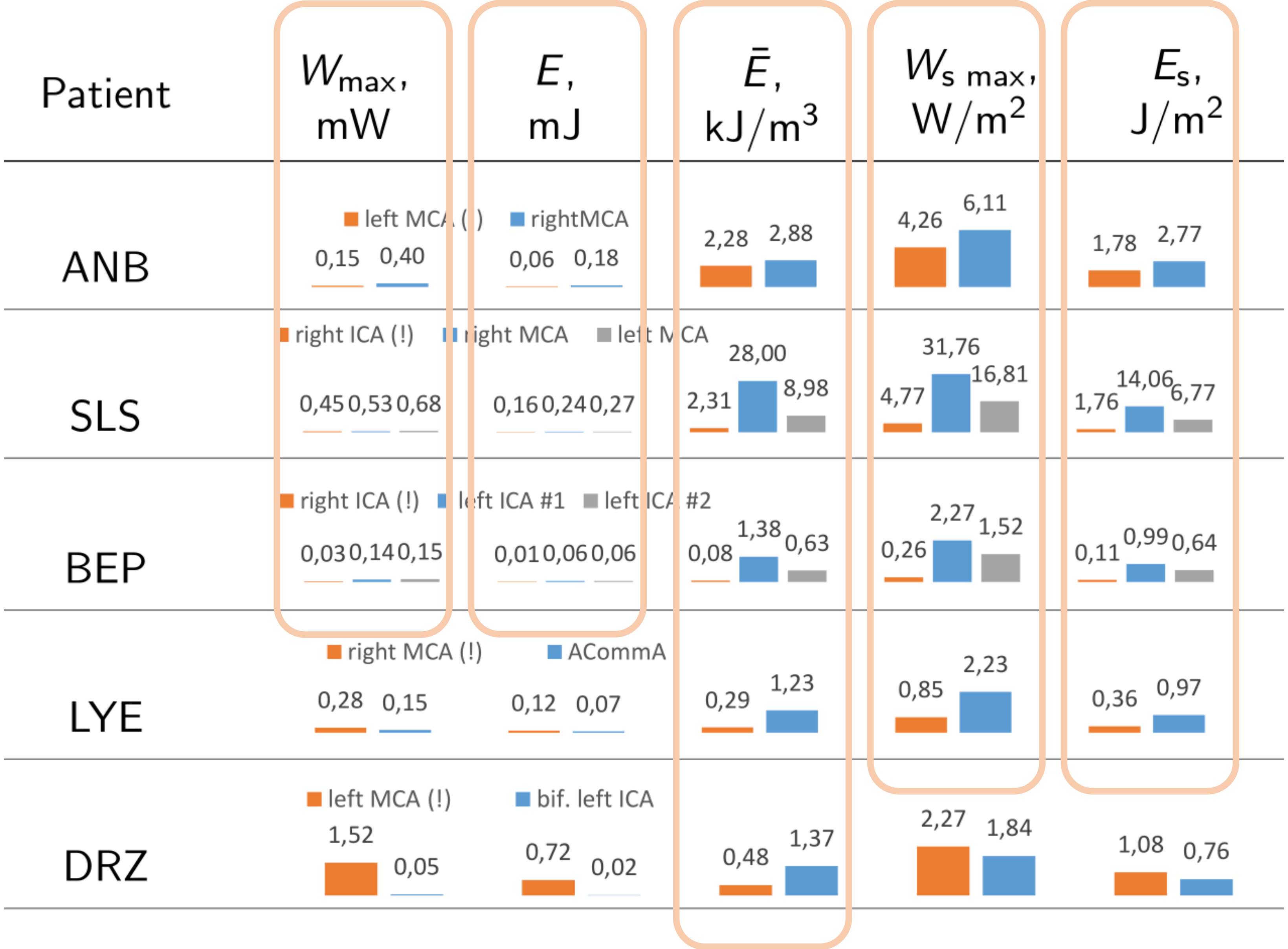

Patient	W_{max}, mW	E, mJ	$\bar{E}$, kJ/m^3	$W_{s\ max}$, W/m^2	E_s, J/m^2
ANB ■ left MCA ( ) ■ rightMCA	0,15 0,40	0,06 0,18	2,28 2,88	4,26 6,11	1,78 2,77
SLS ■ right ICA (!) ■ right MCA ■ left MCA	0,45 0,53 0,68	0,16 0,24 0,27	2,31 28,00 8,98	4,77 31,76 16,81	1,76 14,06 6,77
BEP ■ right ICA (!) ■ left ICA #1 ■ left ICA #2	0,03 0,14 0,15	0,01 0,06 0,06	0,08 1,38 0,63	0,26 2,27 1,52	0,11 0,99 0,64
LYE ■ right MCA (!) ■ ACommA	0,28 0,15	0,12 0,07	0,29 1,23	0,85 2,23	0,36 0,97
DRZ ■ left MCA (!) ■ bif. left ICA	1,52 0,05	0,72 0,02	0,48 1,37	2,27 1,84	1,08 0,76

- To assess a risk of the aneurysm rupture in case of multiple aneurysms, it is proposed to use viscous dissipation energy, which is the lowest for a ruptured aneurysm.

Energy of the system

- Energy of the hydroelastic system: $E = E_{\mathrm{e}} + E_{\mathrm{k}} + E_{\mathrm{b}}$
- Elastic energy: $E_{\mathrm{e}} = \frac{Ed}{2(1-\nu^2)} \int_S \mathrm{d}S$
- Kinetic energy: $E_{\mathrm{k}} = \frac{1}{2} \int_V \rho |\mathbf{v}|^2 \mathrm{d}V$
- Willmore bending energy: $E_{\mathrm{b}} = \frac{E\, d^3}{24(1-\nu^2)} \int_S H^2 \, \mathrm{d}S$
  - where E is Young’s modulus, ν is Poisson’s ratio, d is the wall thickness, H is the mean curvature
- Energy dissipated due to viscosity: $E_{\mathrm{v}} = 4\mu \int_V |\boldsymbol{\omega}|^2 \, \mathrm{d}V$

Aim

- The aim of this work is to assess different energy components in the hydroelastic system such as arterial aneurysms with diverticula.

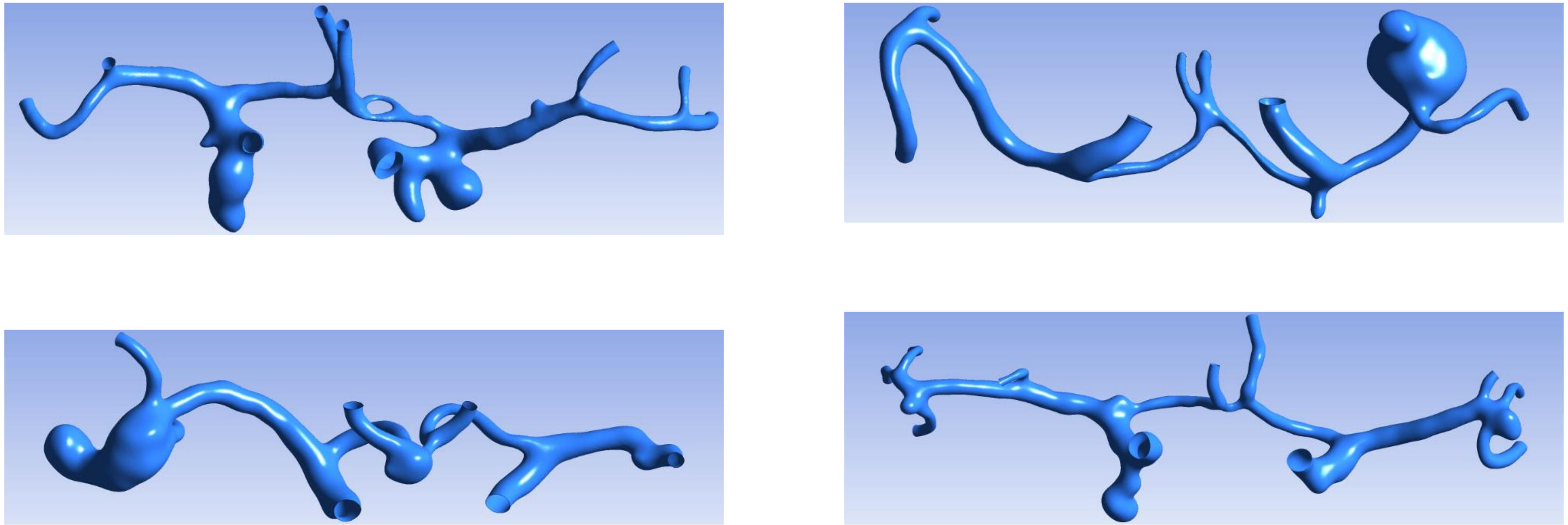

Numerical simulations: configurations

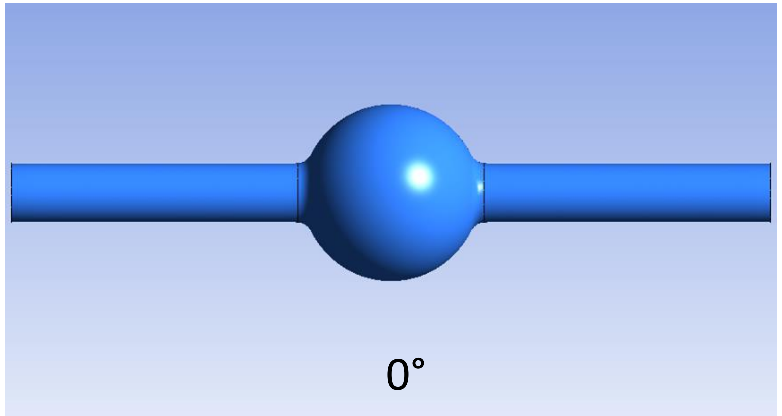
0°

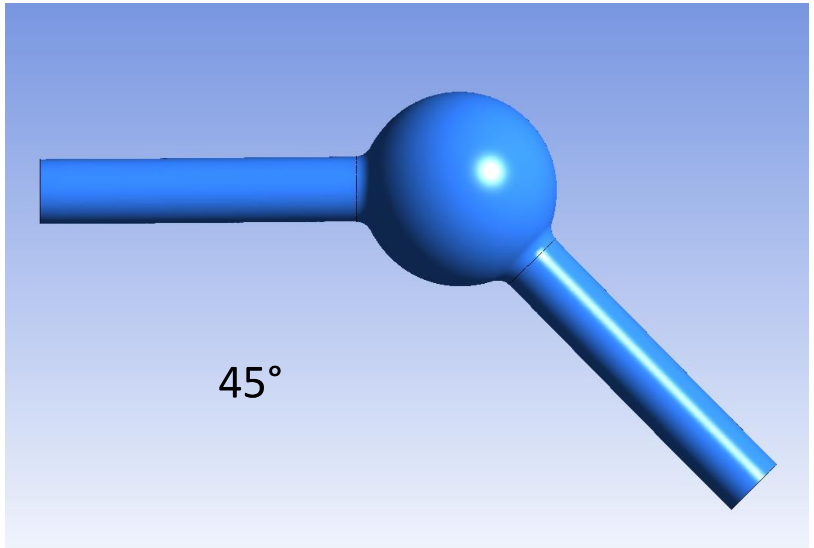
45°

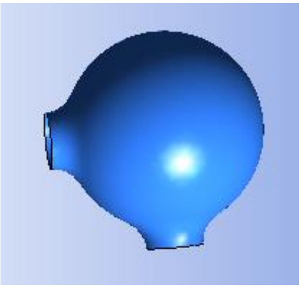
90°

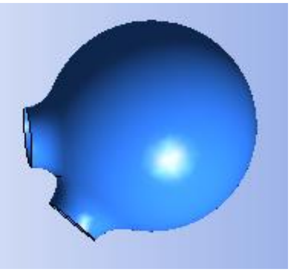
135°

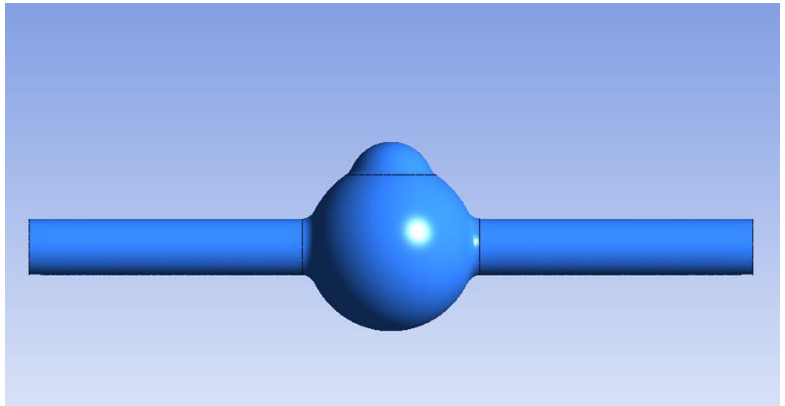
H = ¼ D

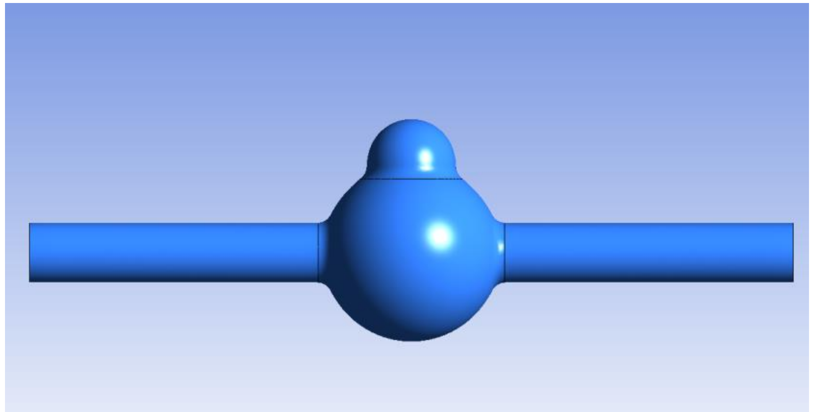
H = ½ D

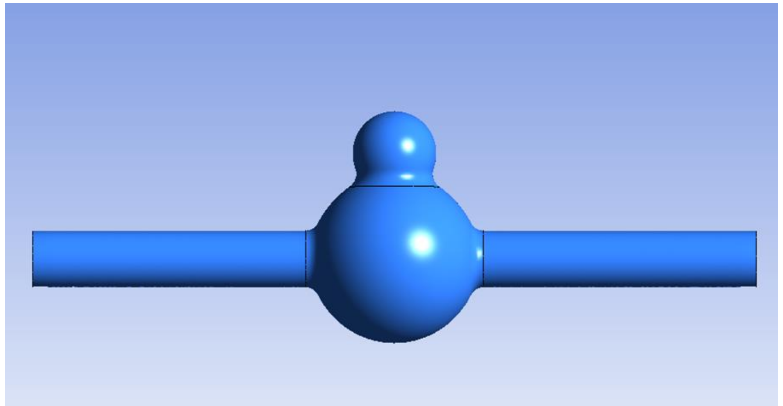
H = ¾ D

Mamatyukov, M. Yu., Khe, A. K., Parshin, D. V., Plotnikov, P. I., & Chupakhin, A. P. (2019). On the energy of a hydroelastic system: Blood flow in an artery with a cerebral aneurysm. *Journal of Applied Mechanics and Technical Physics*, *60*(6), 977–988. DOI: 10.1134/S0021894419060014

Computational framework

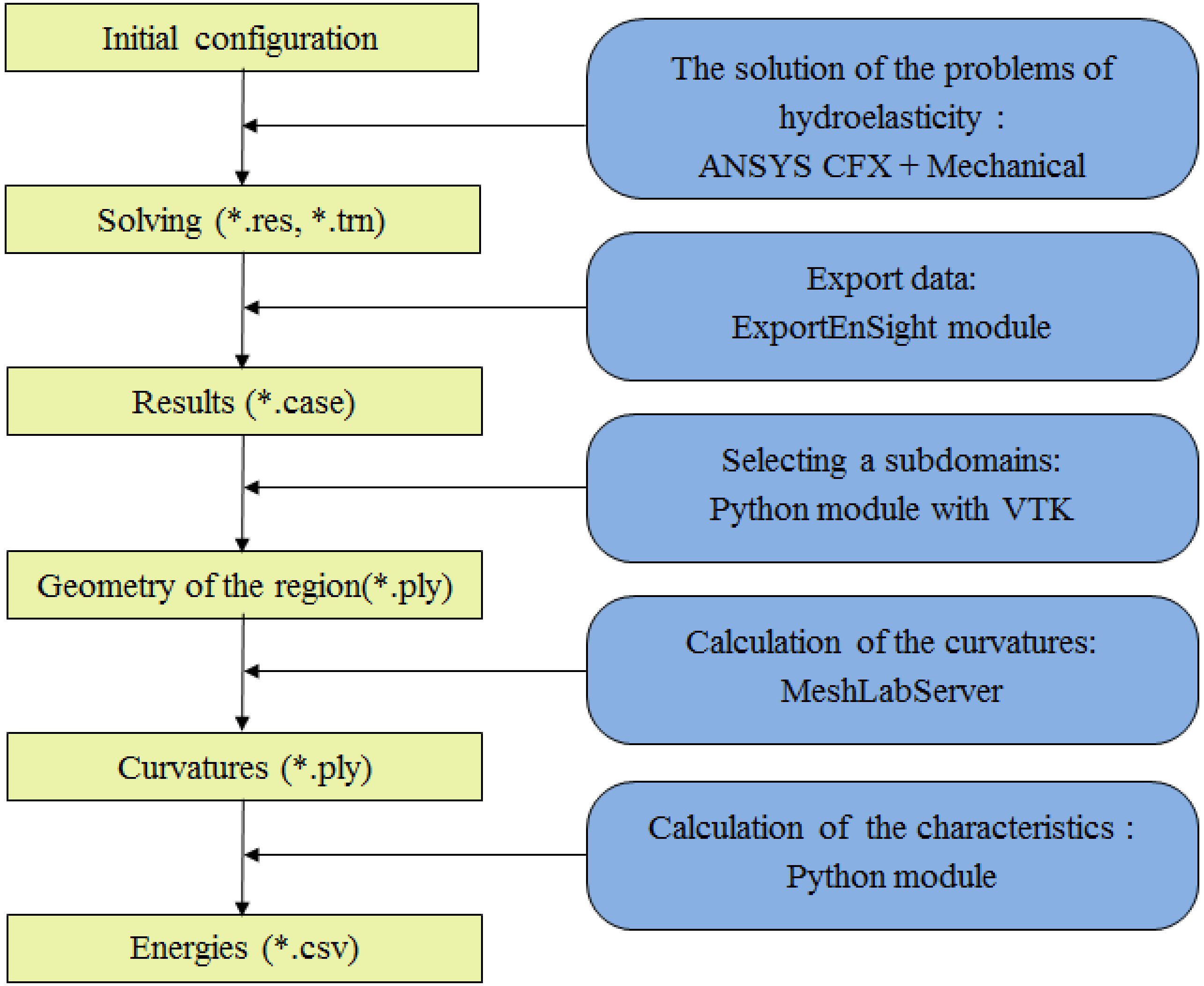

Initial configuration

The solution of the problems of hydroelasticity : ANSYS CFX + Mechanical

Solving (*.res, *.trn)

Export data: ExportEnSight module

Results (*.case)

Selecting a subdomains: Python module with VTK

Geometry of the region(*.ply)

Calculation of the curvatures: MeshLabServer

Curvatures (*.ply)

Calculation of the characteristics : Python module

Energies (*.csv)

Streamlines and WSS

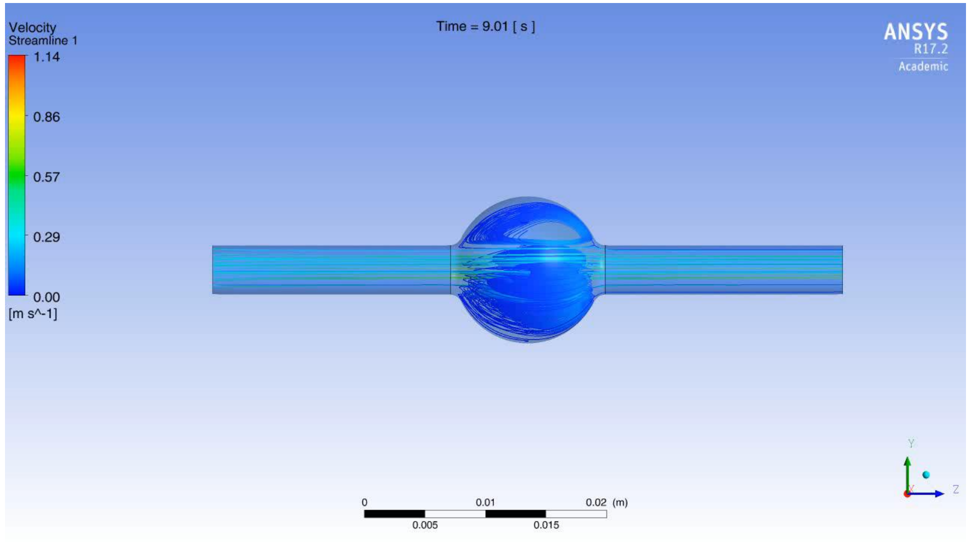

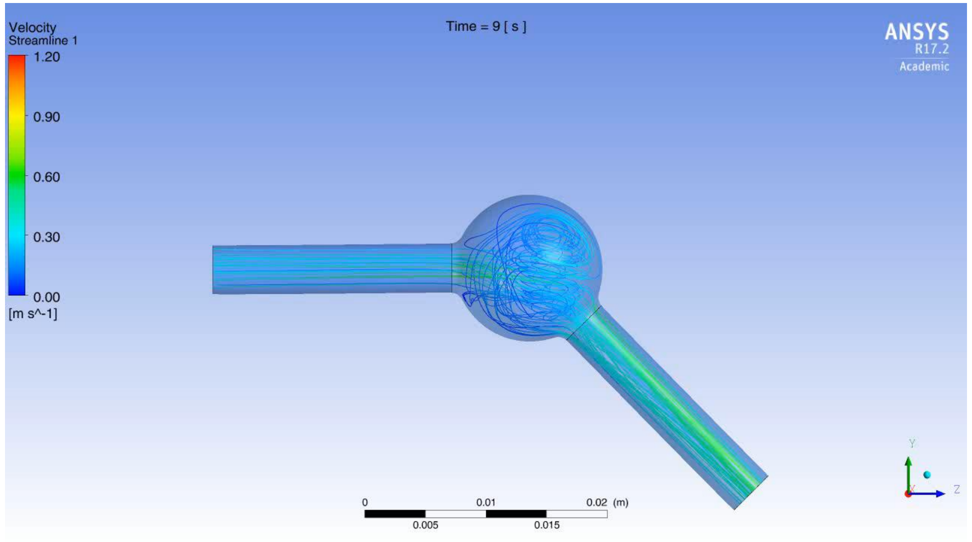

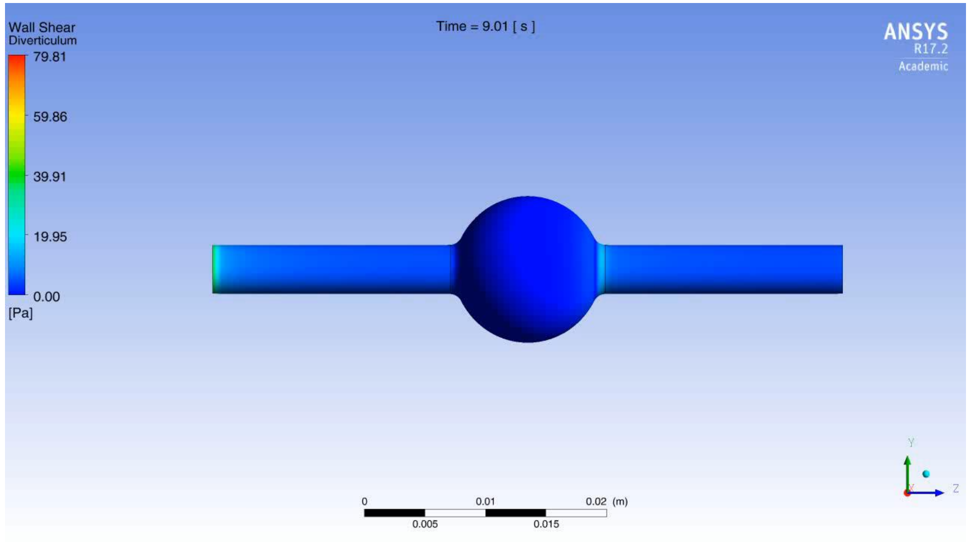

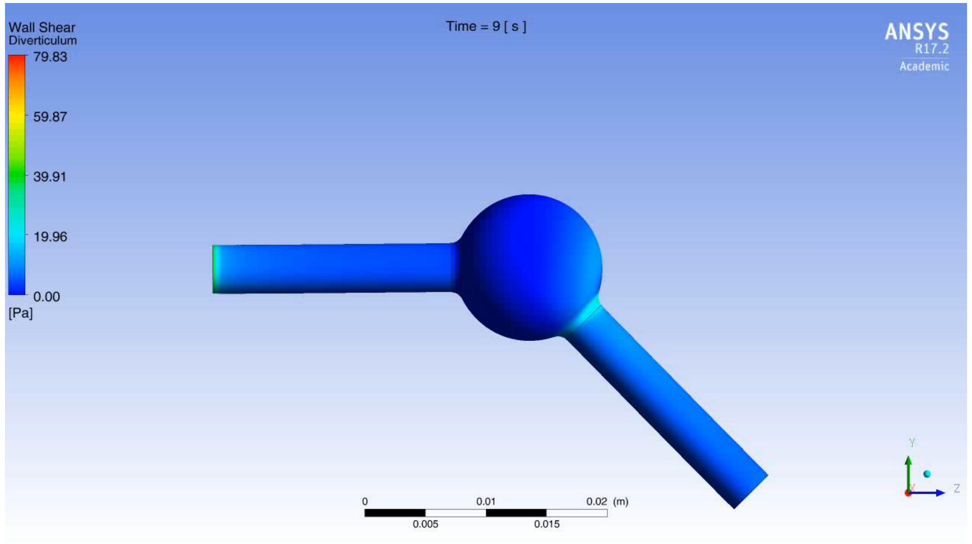

Streamlines: 0°

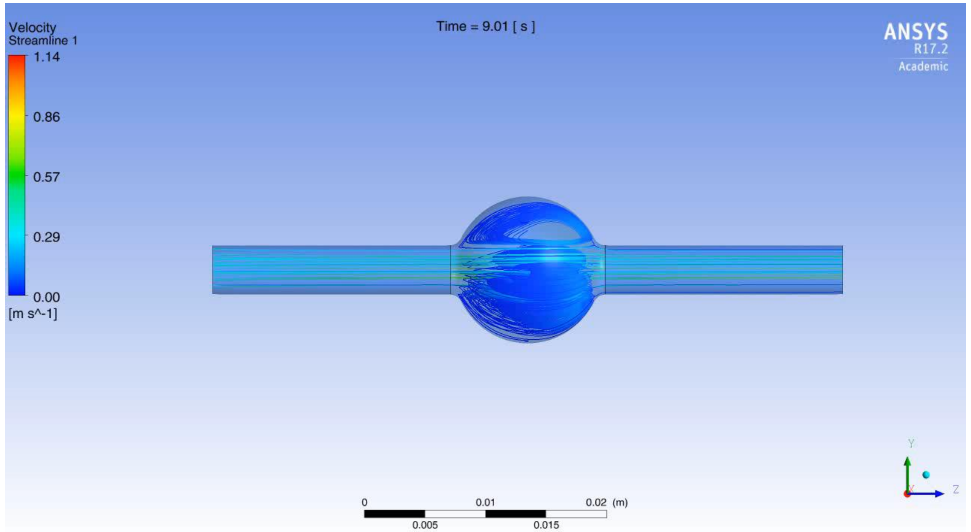

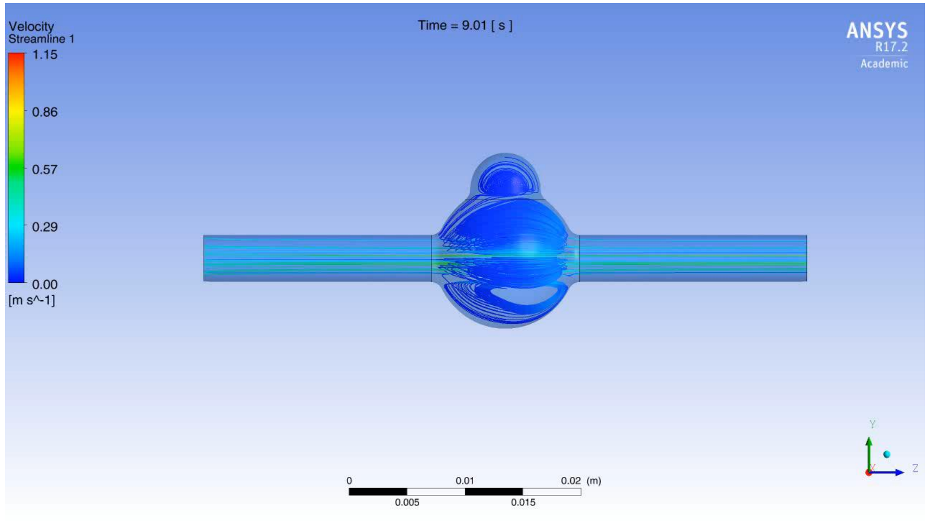

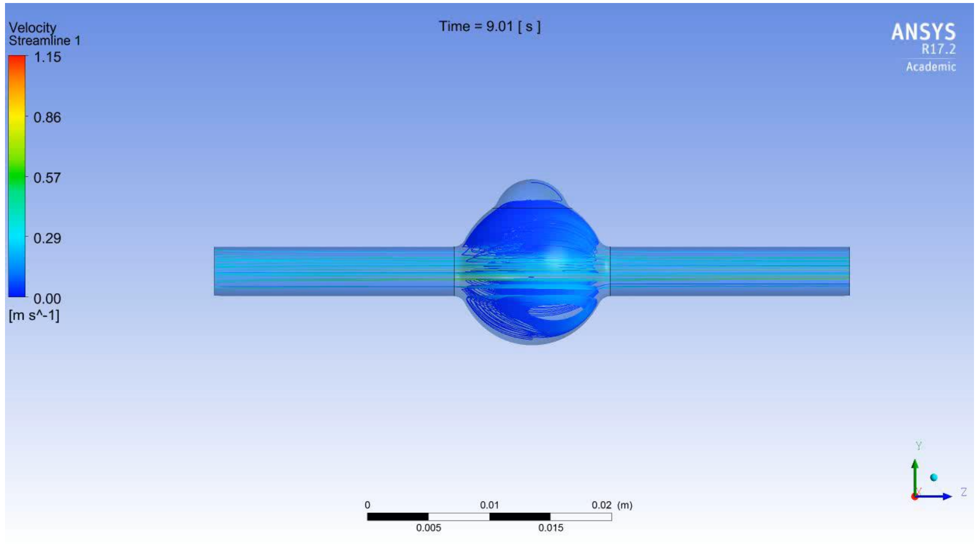

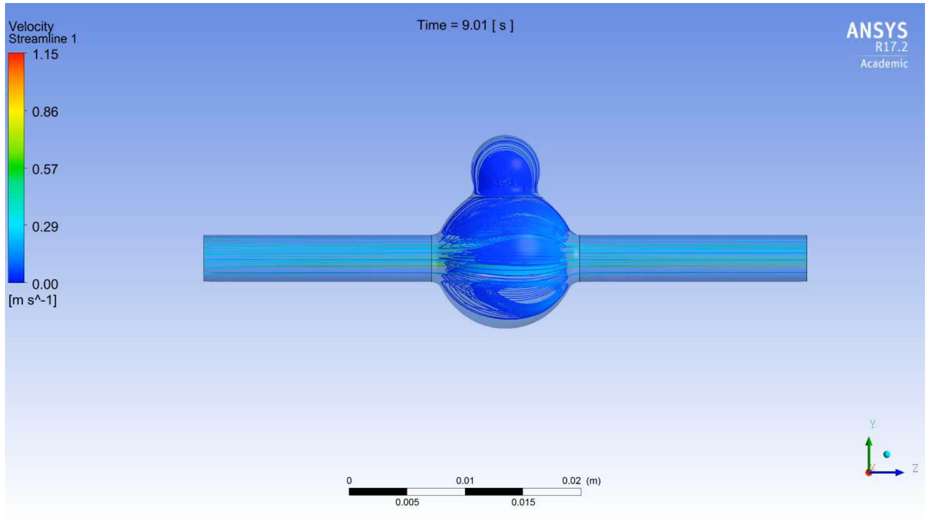

Streamlines: 45°

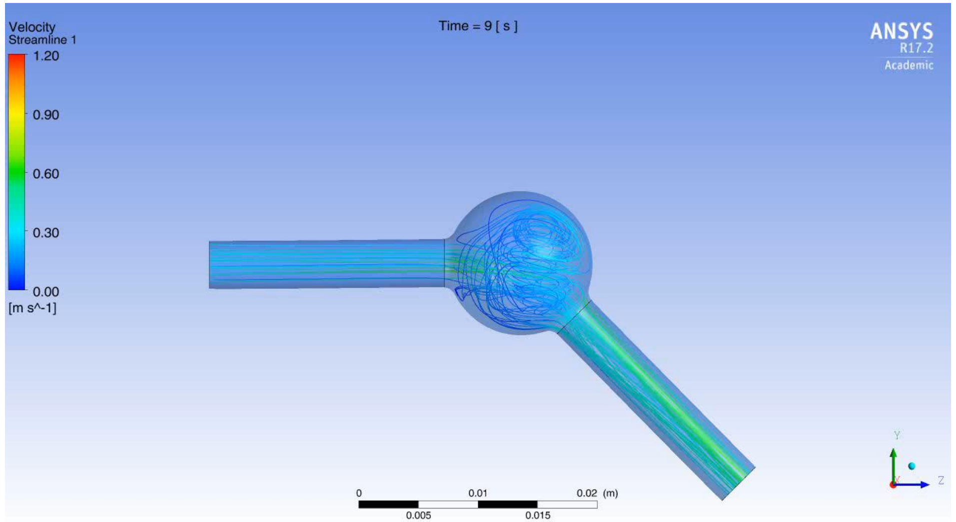

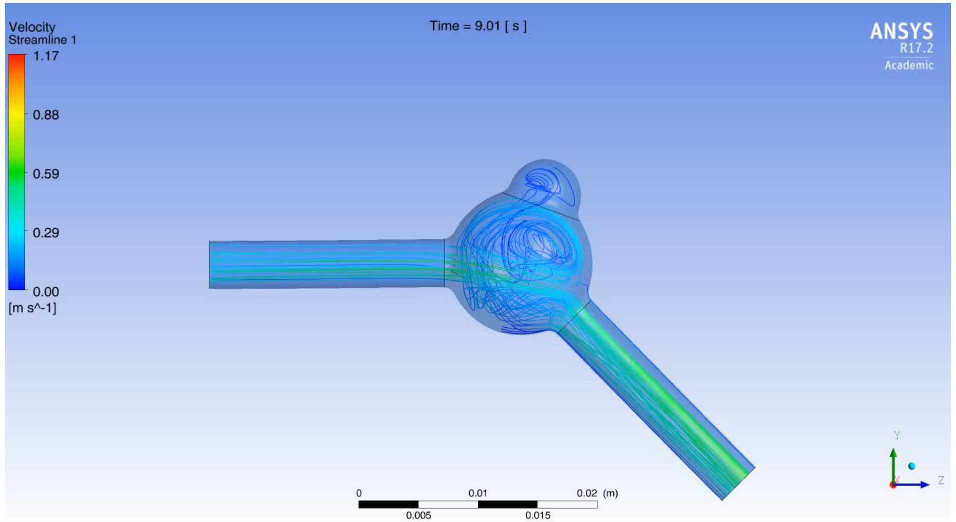

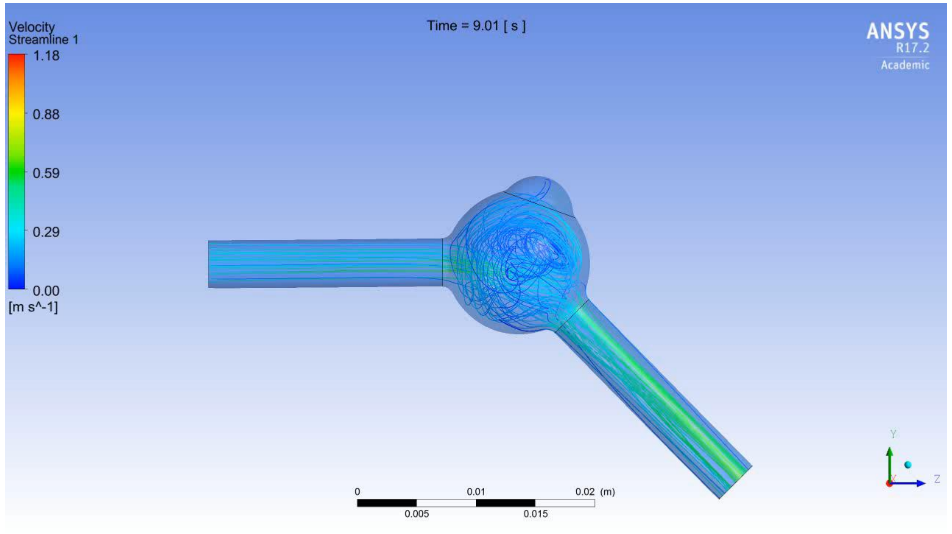

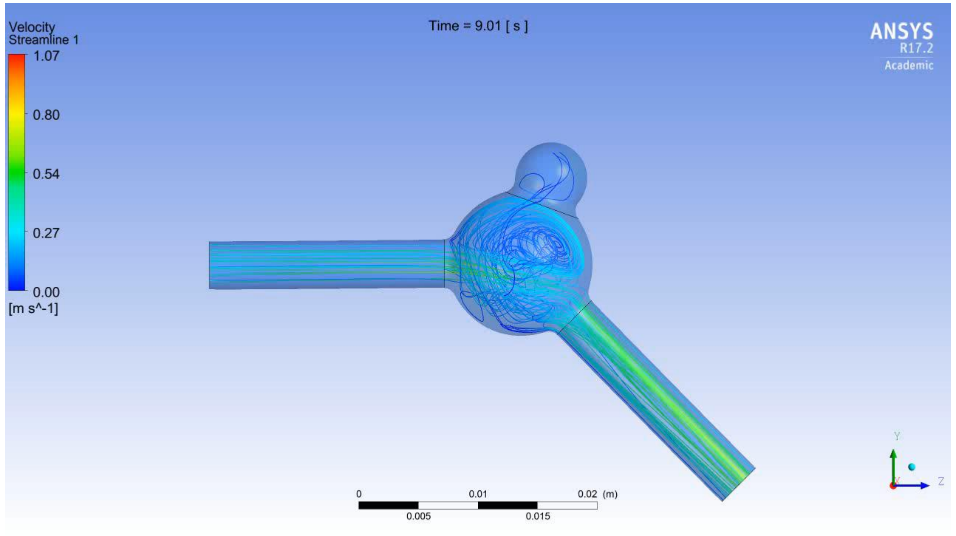

Does WSS indicator really indicate something?

High WSS

Sforza et al. (2011) suggest that aneurysm growth occurs on high WSS regions

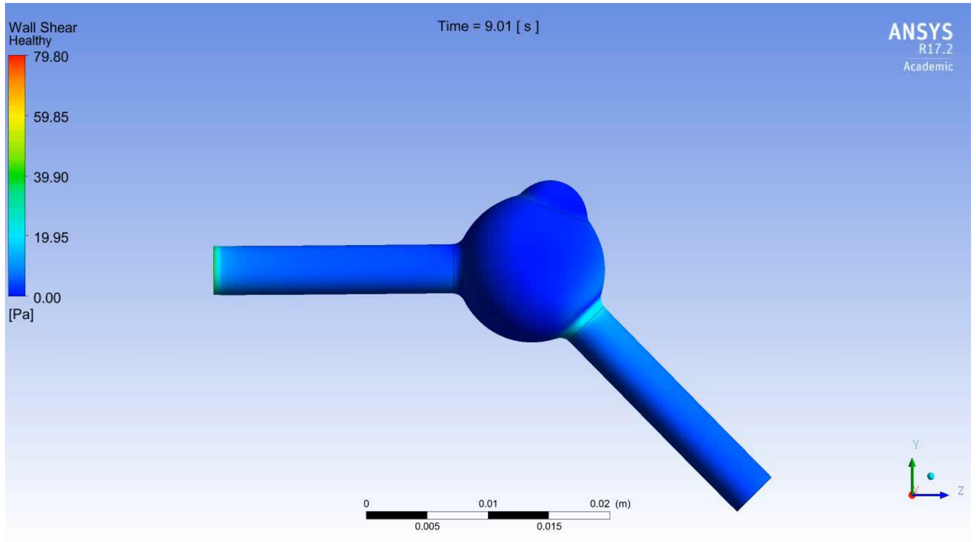

Low WSS

Boussel et al. (2008) suggest that aneurysm growth occurs on abnormally low WSS regions

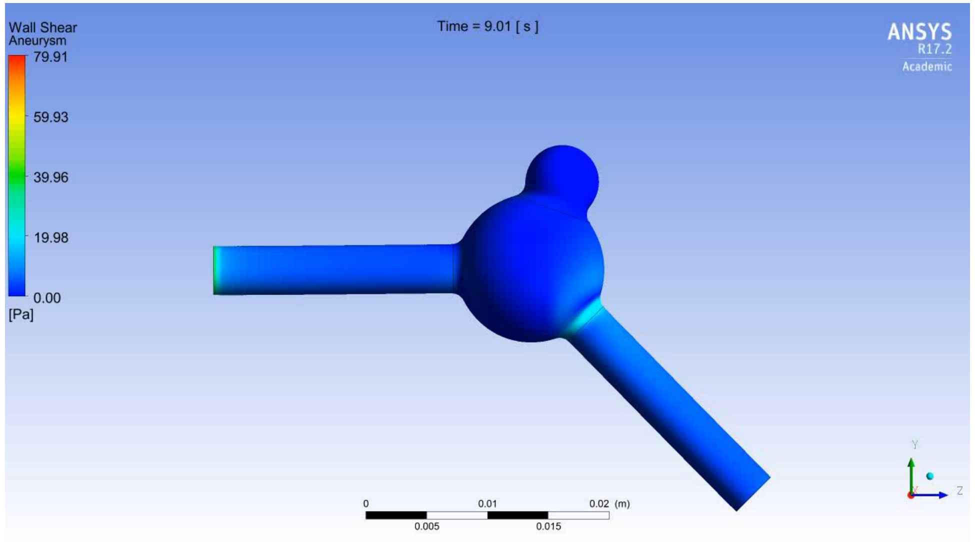

Simulation results: Elastic energy

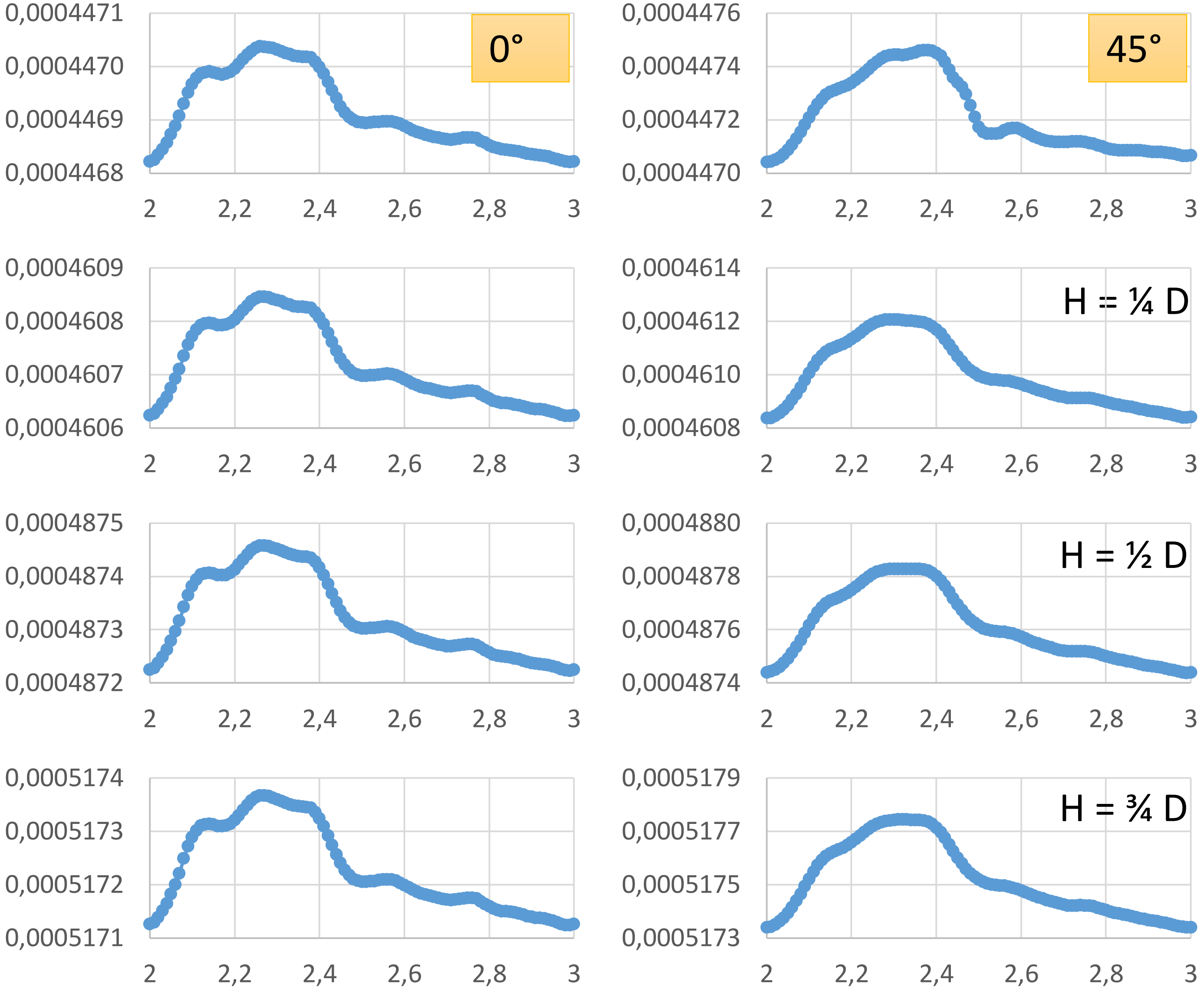

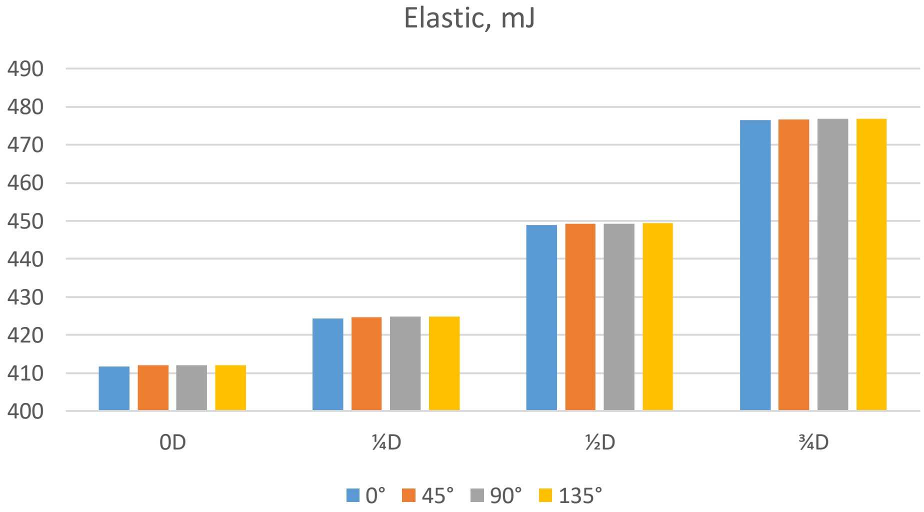

Increases with angle

Simulation results: Bending energy

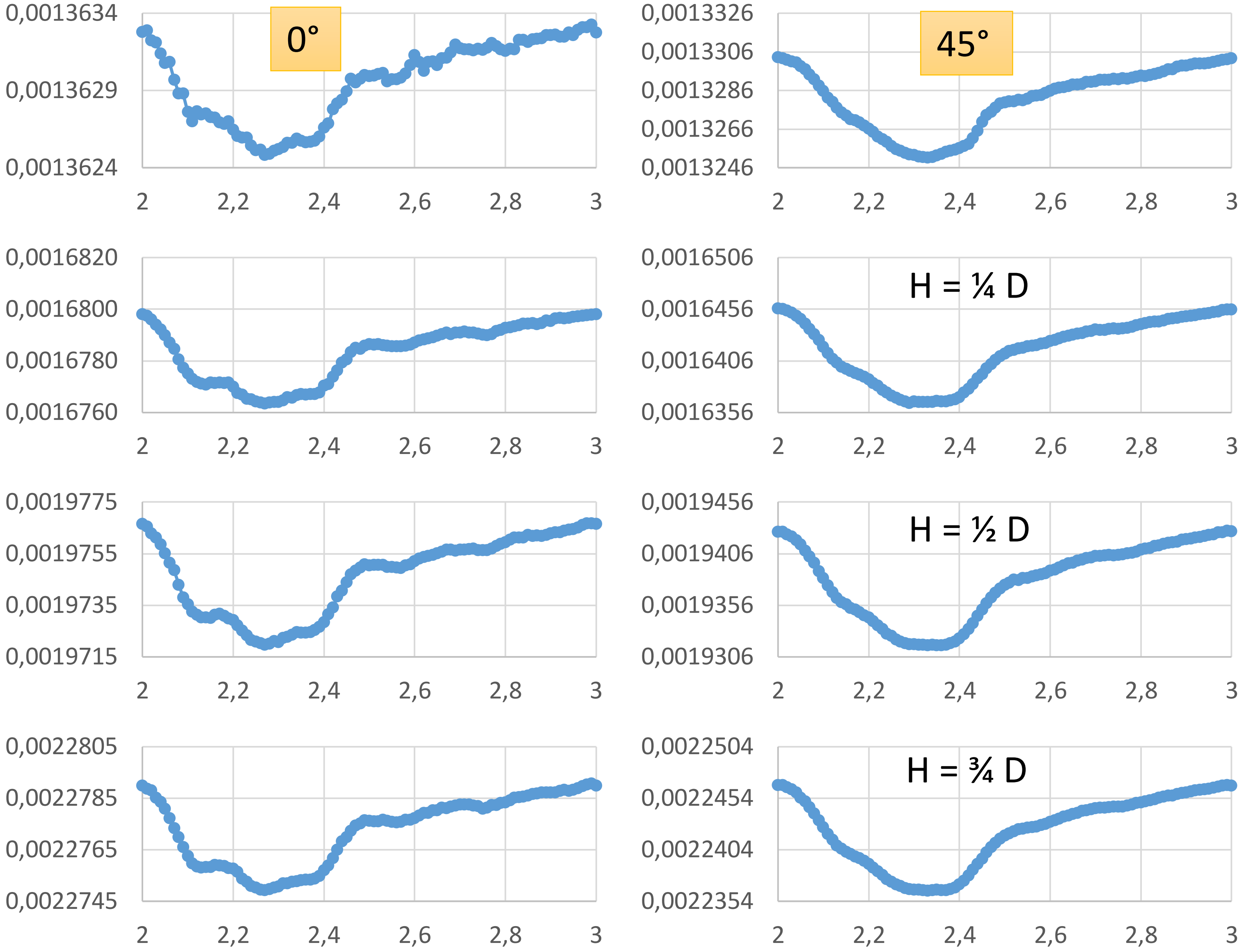

Willmore functional

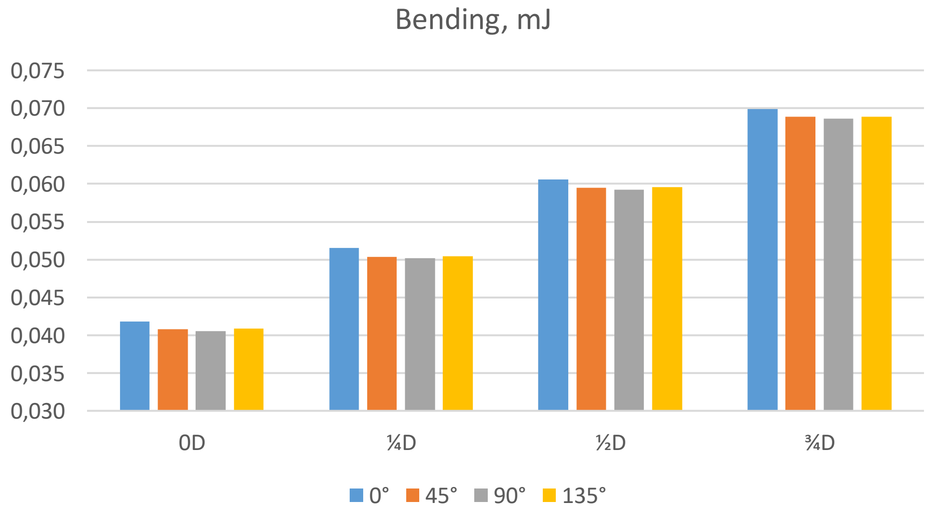

Decreases with angle

Simulation results: Kinetic energy

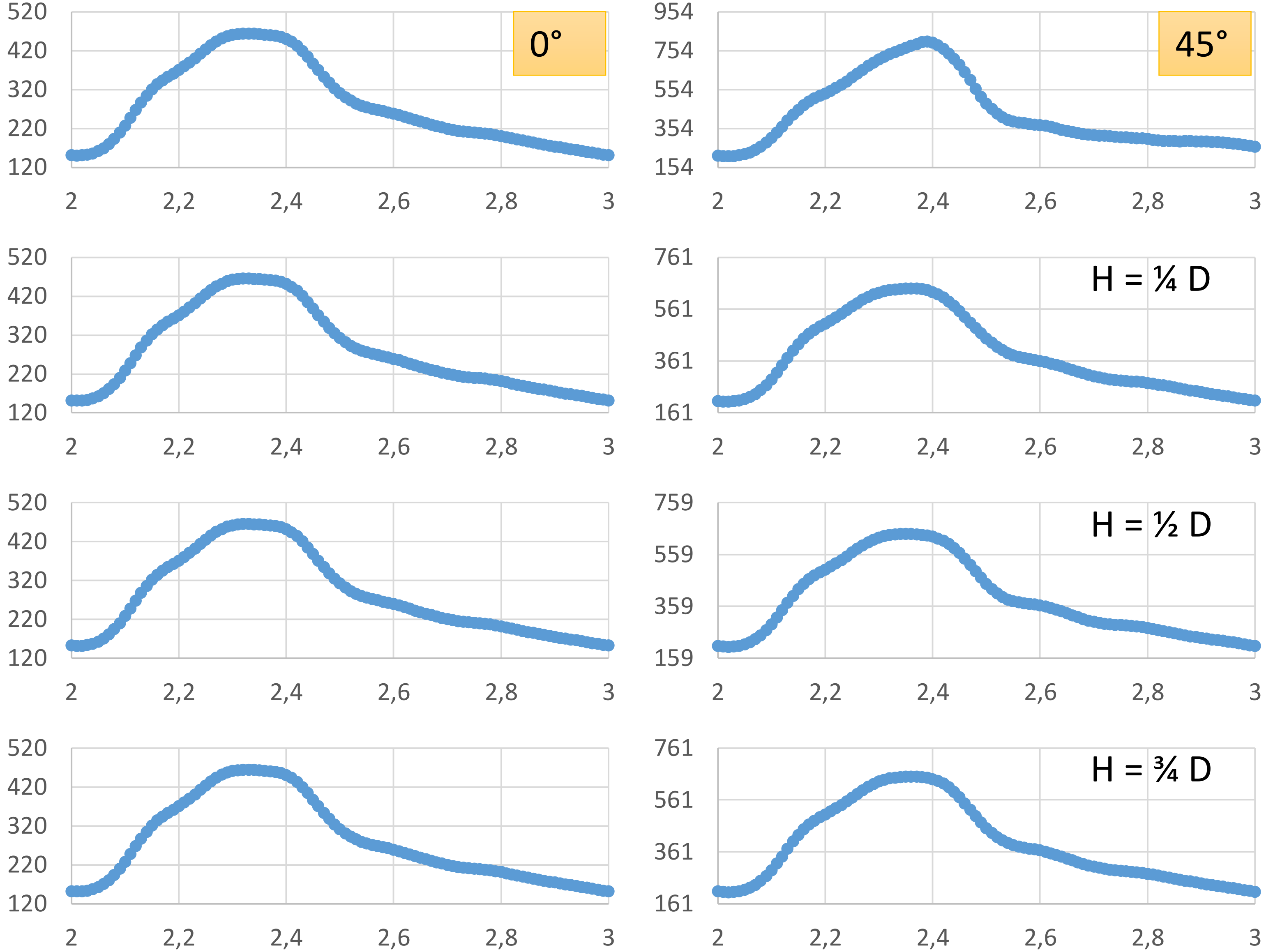

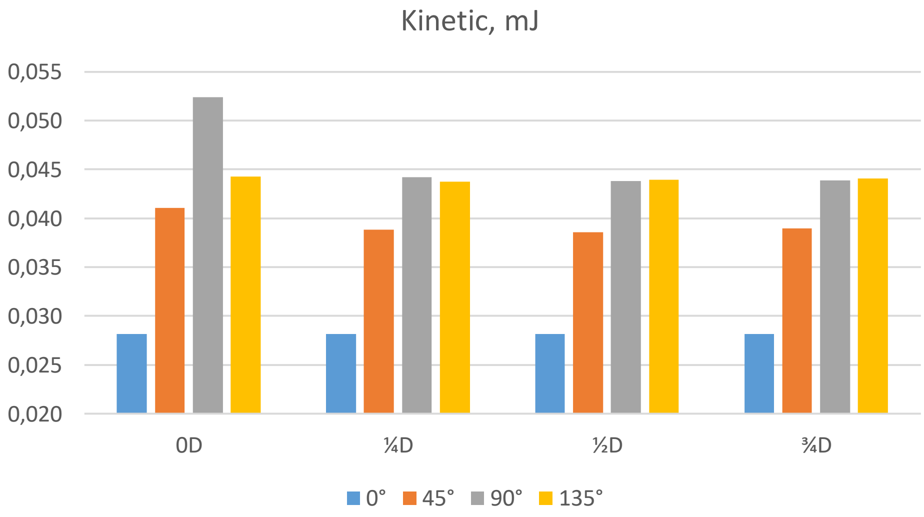

Simulation results: Viscous dissipation

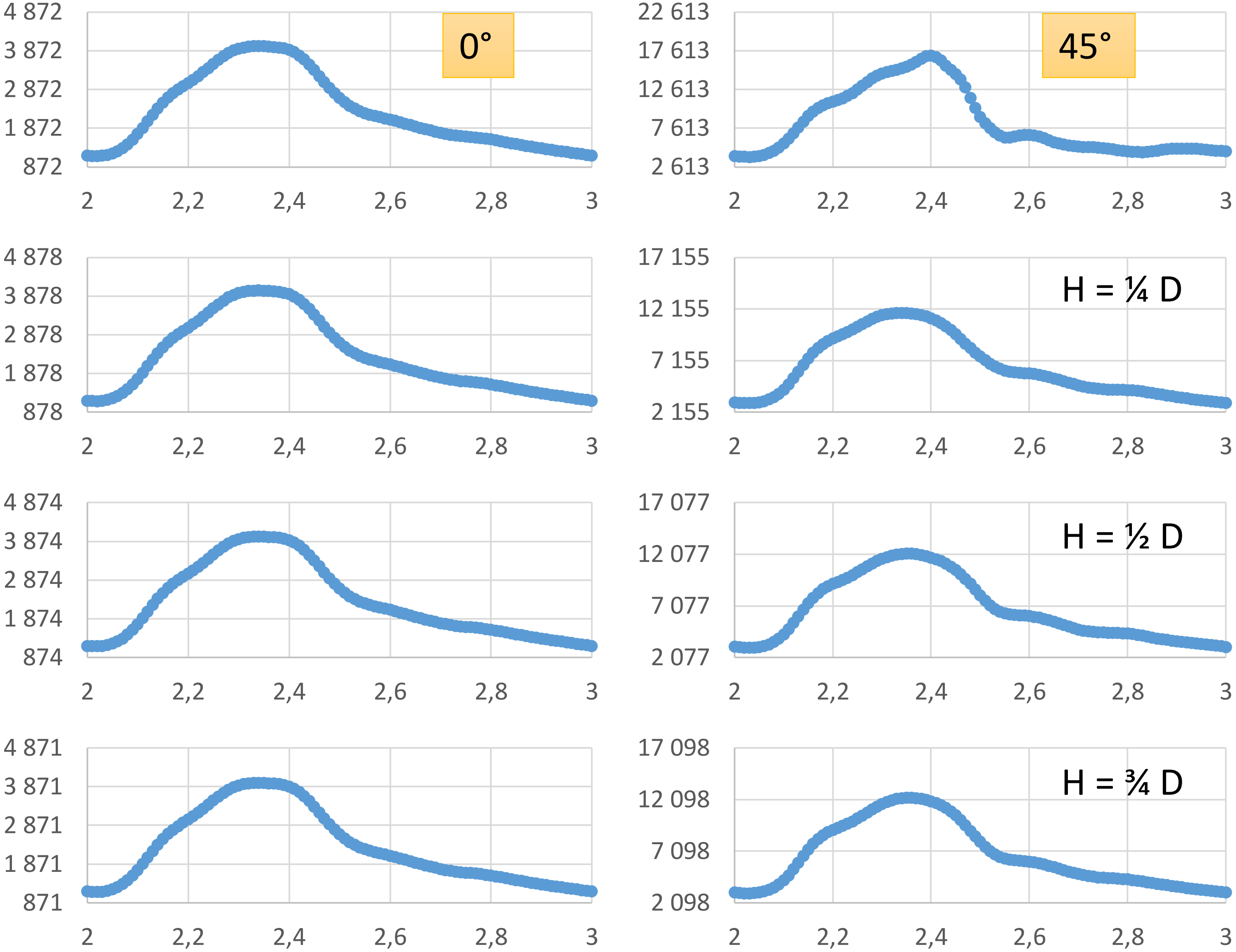

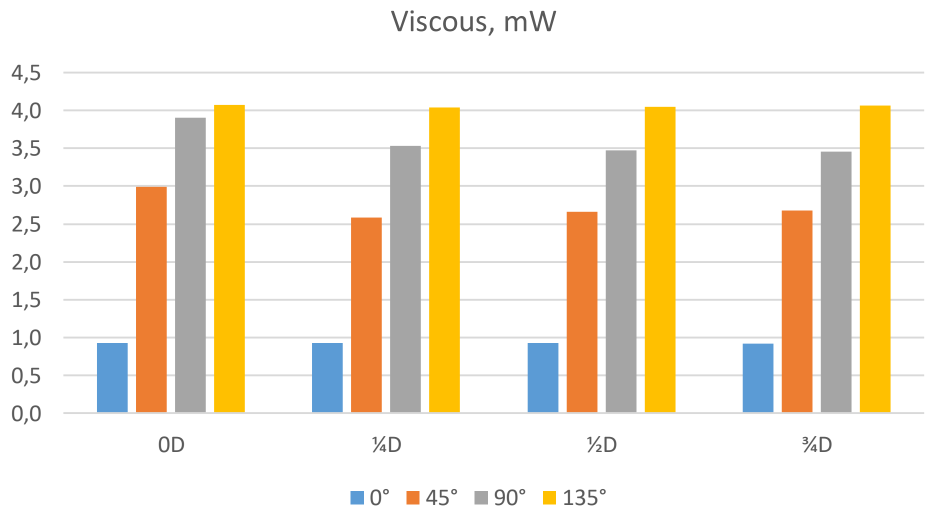

Energy: 0°

E_e $E_\mathrm{e} + E_\mathrm{k}$ $E_\mathrm{e} + E_\mathrm{k} + E_\mathrm{b}$ E_ν

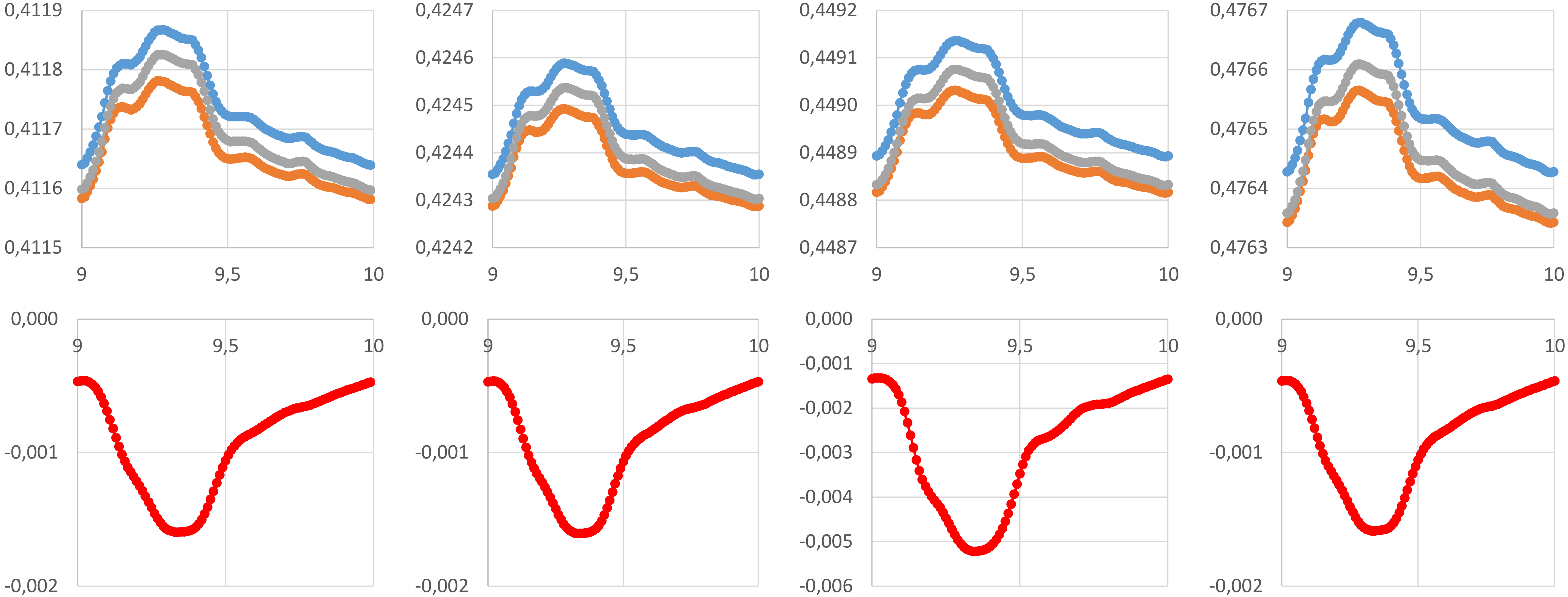

H = 0 D H = ¼ D H = ½ D H = ¾ D

Energy: 45°

E_e

$E_\mathrm{e} + E_\mathrm{k}$

$E_\mathrm{e} + E_\mathrm{k} + E_\mathrm{b}$

E_ν

$E_\nu + E_\Gamma$

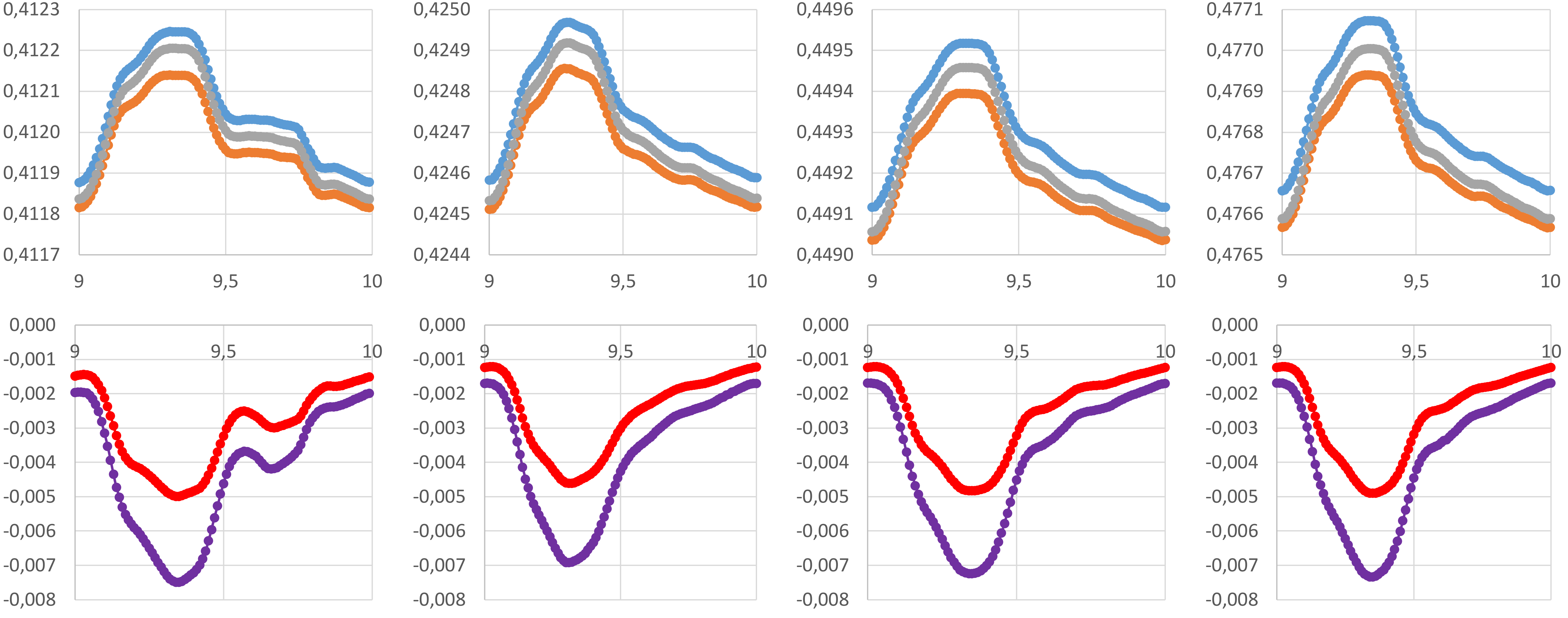

H = 0 D

H = ¼ D

H = ½ D

H = ¾ D

The impact of energy components: Percentage from the total

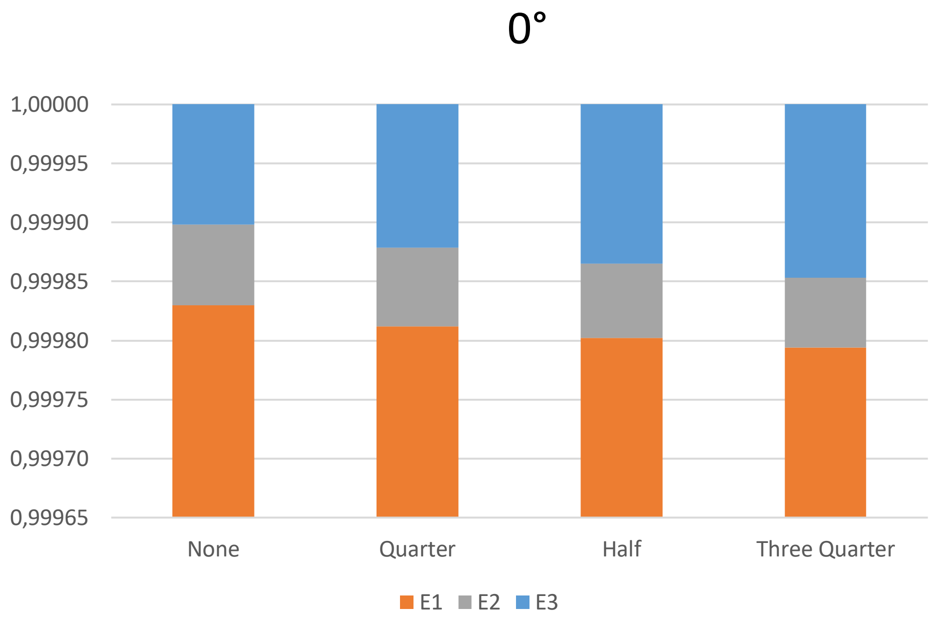

E_b

E_k

E_e

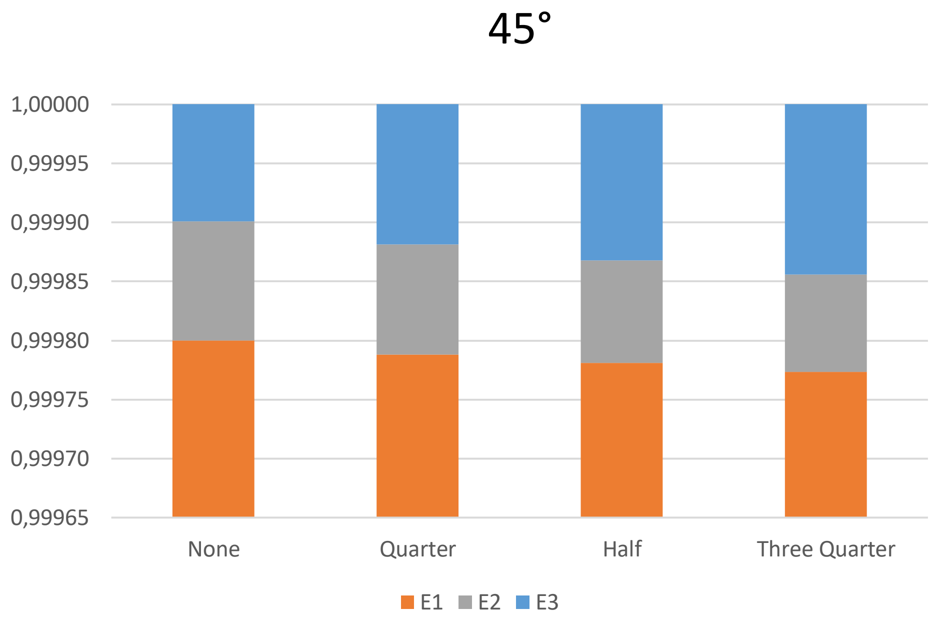

Velocity–pressure diagrams

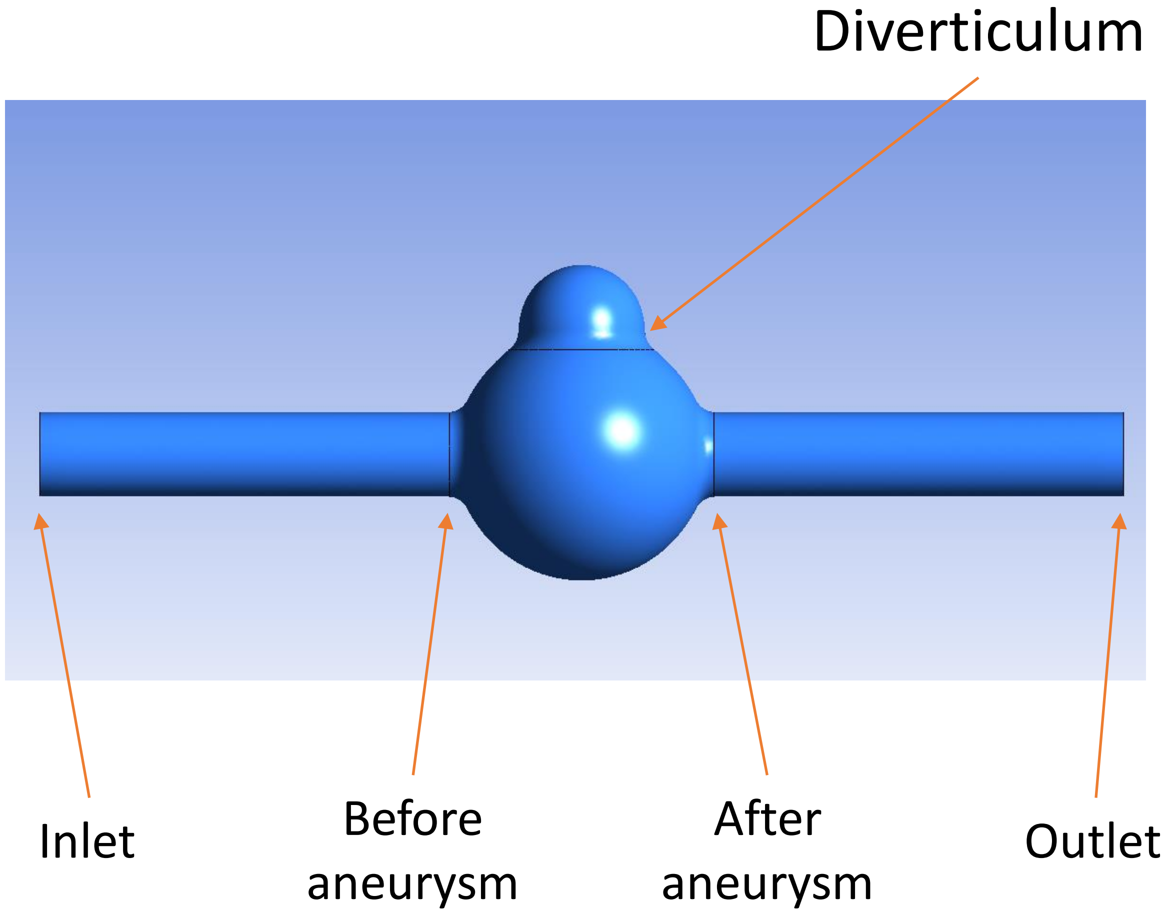

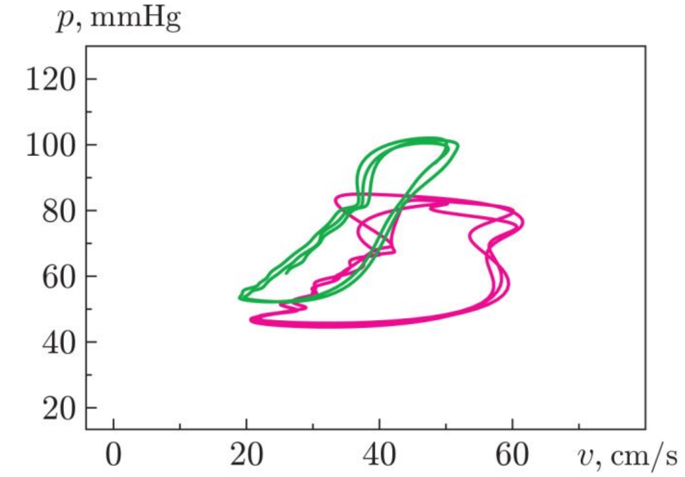

Velocity–pressure diagram for blood flow in cerebral aneurysm (BEFORE the treatment and AFTER the treatment)

Velocity–pressure diagrams: 0°

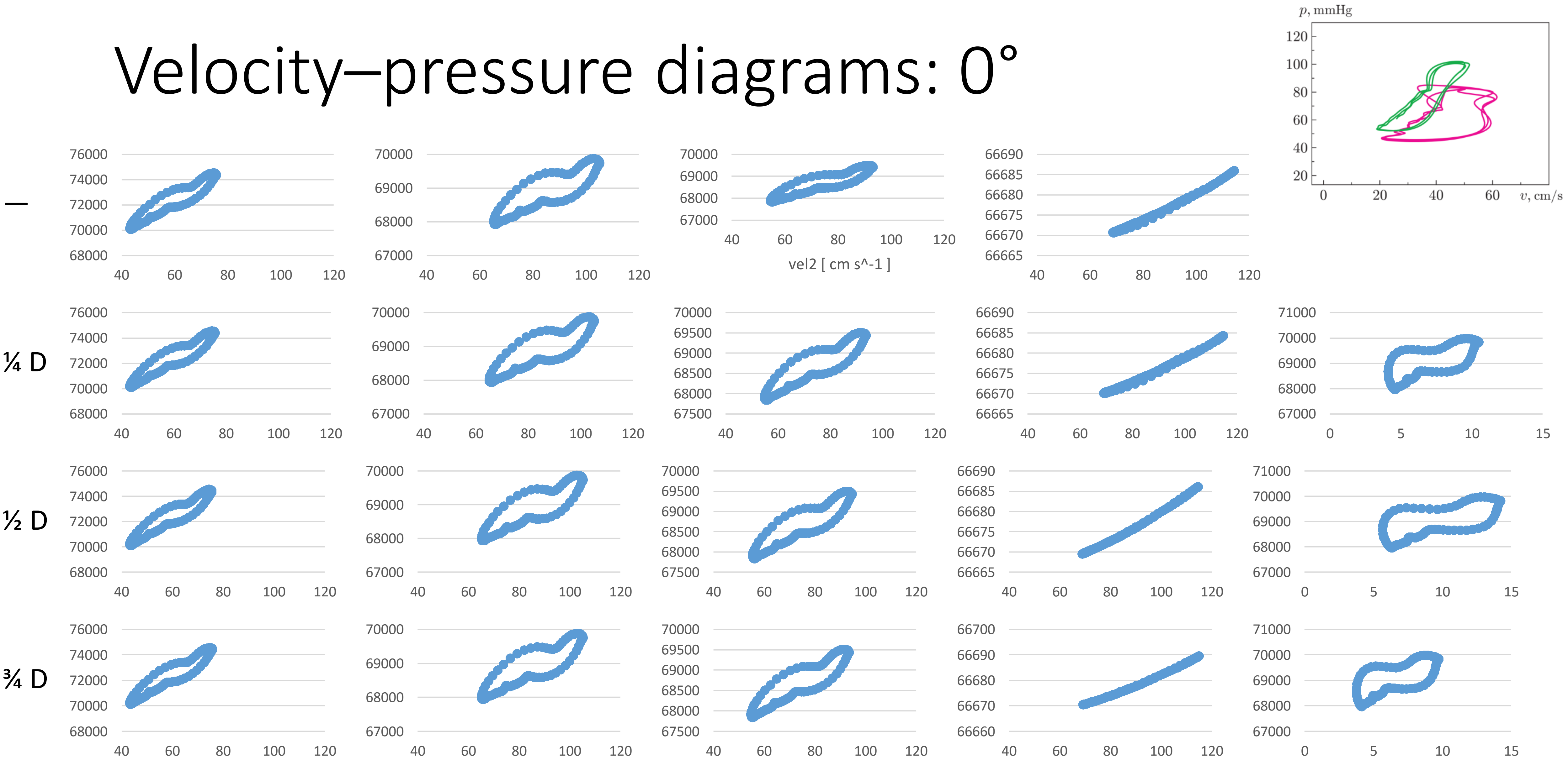

Inlet

Before aneurysm

After aneurysm

Outlet

Diverticulum

Velocity–pressure diagrams: 45°

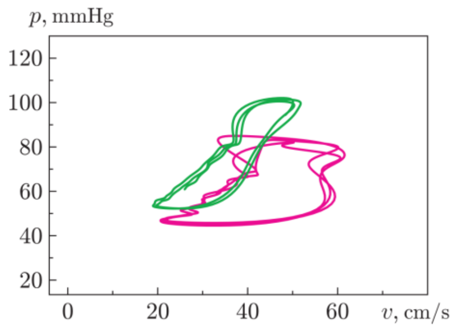

—

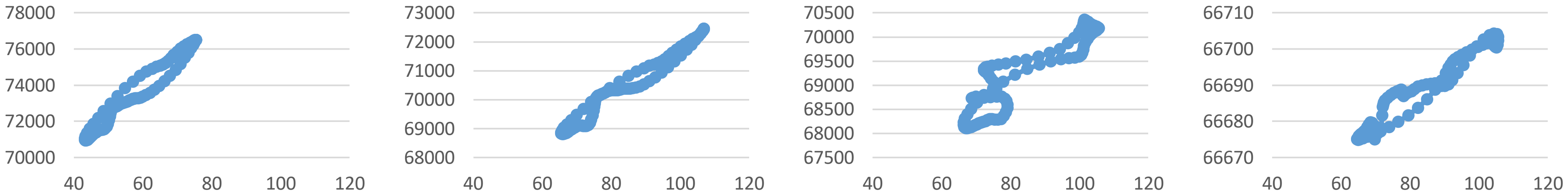

¼ D

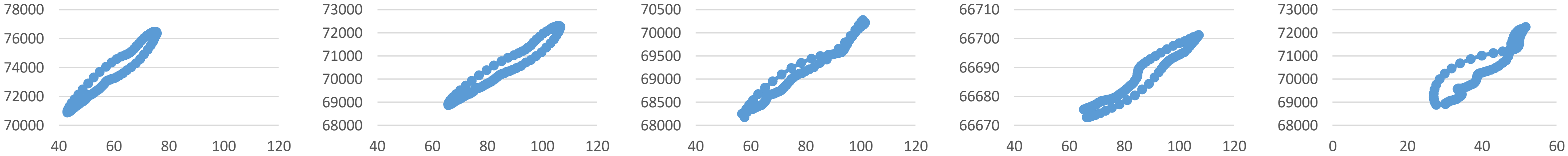

½ D

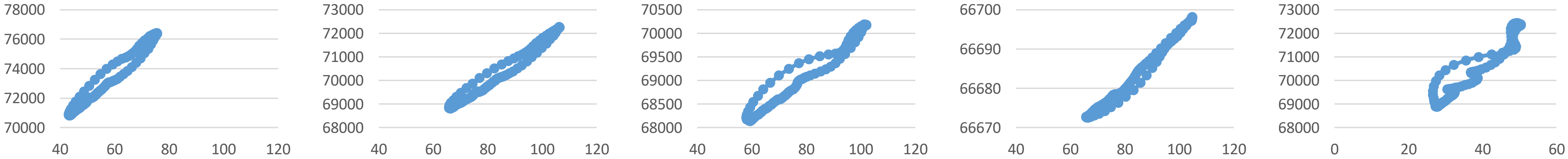

¾ D

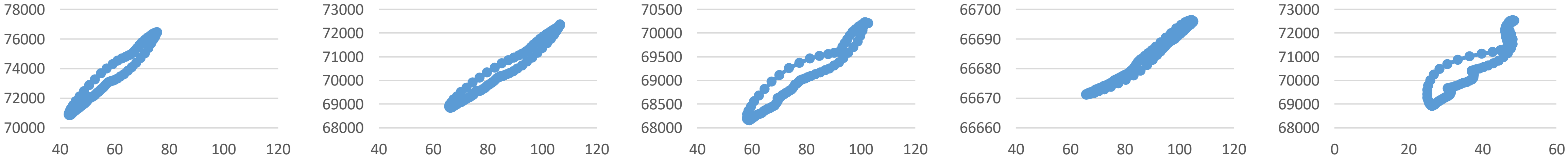

Inlet

Before aneurysm

After aneurysm

Outlet

Diverticulum

Conclusions

1. A computational framework for calculating the total energy of hydroelastic system is created.

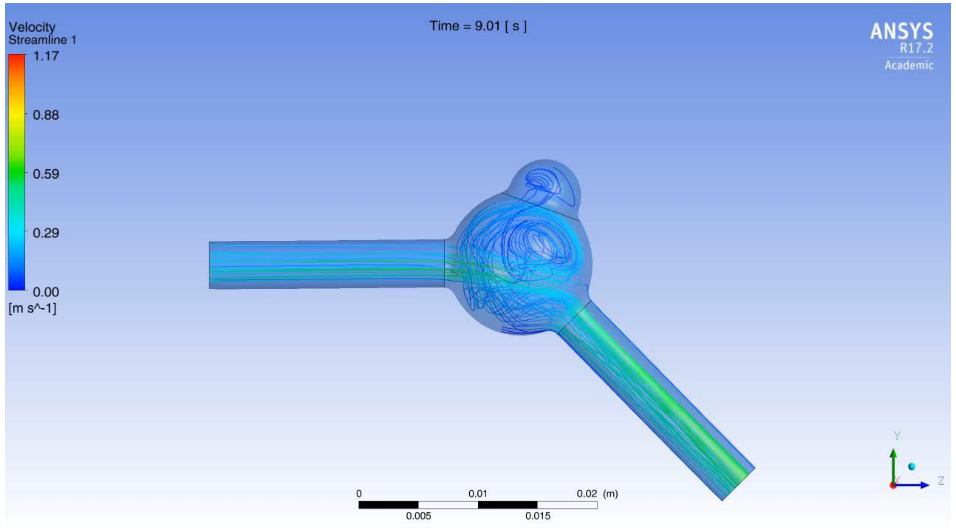

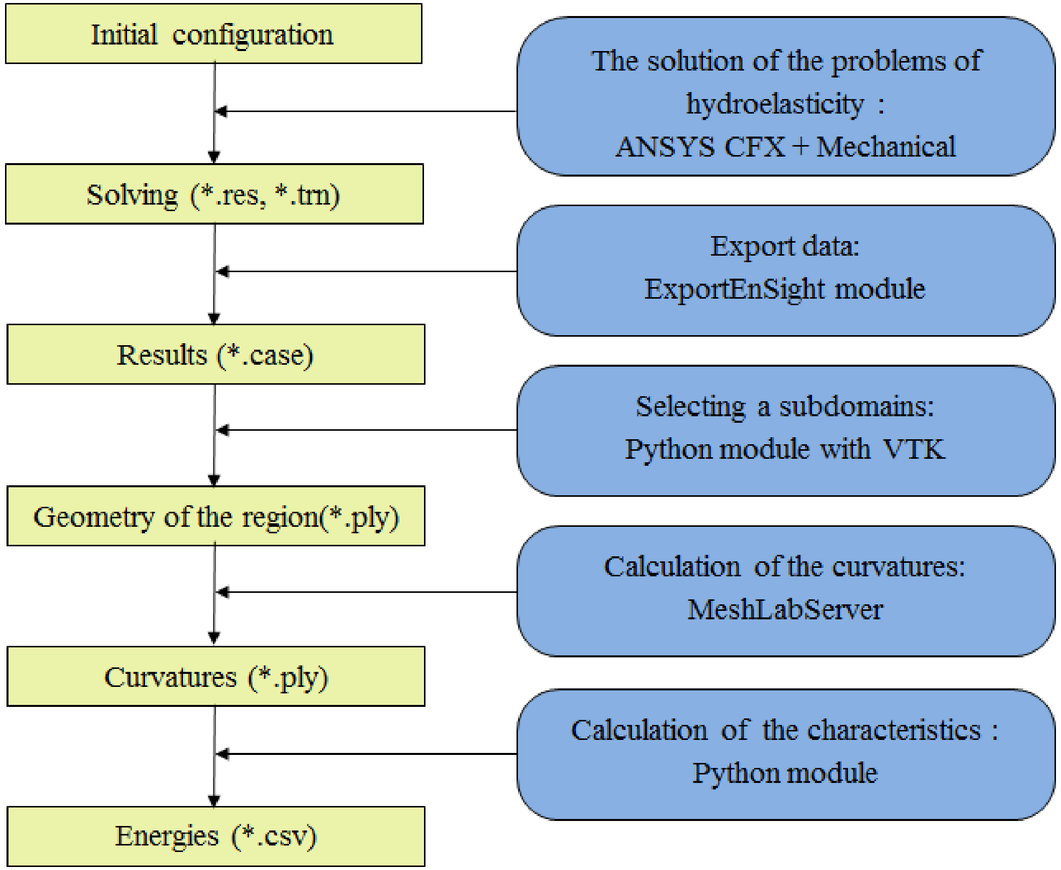

Initial configuration

Solving (*.res, *.trn)

Results (*.case)

Geometry of the region(*.ply)

Curvatures (*.ply)

Energies (*.csv)

The solution of the problems of hydroelasticity : ANSYS CFX + Mechanical

Export data: ExportEnSight module

Selecting a subdomains: Python module with VTK

Calculation of the curvatures: MeshLabServer

Calculation of the characteristics : Python module

Conclusions

2. Kinetic energy of the fluid is comparable with the bending energy of the interface

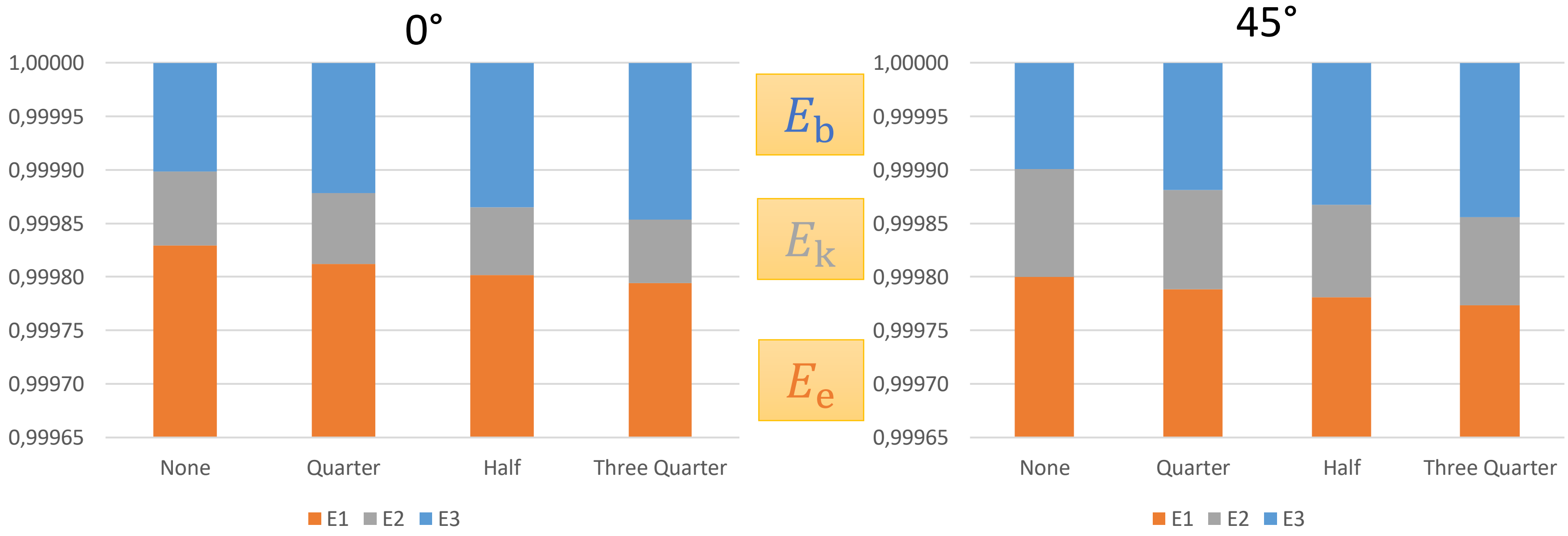

Conclusions

3. Calculation in 3D simulation FSI real diagrams “pressure-velocity” (p-v) for cerebral arterial aneurysm- BIRD-like diagram

¼ D

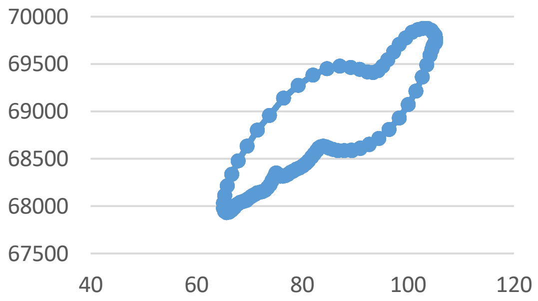

Before aneurysm

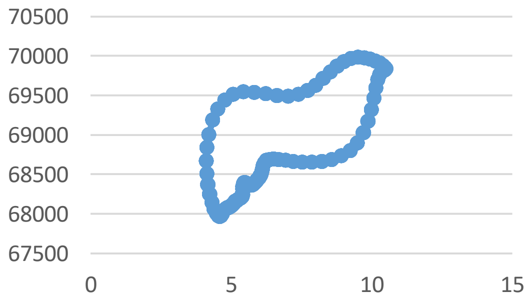

Diverticulum

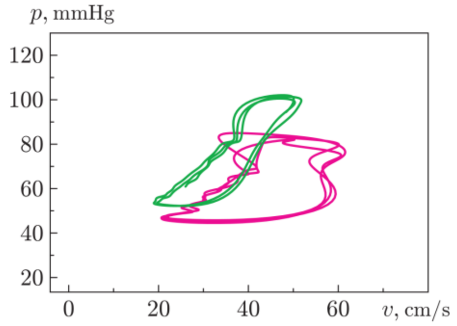

Conclusions

4. Modification of (p-v) diagrams along vessel: nonlinear oscillation near AA, linear far from AA

0°
½ D

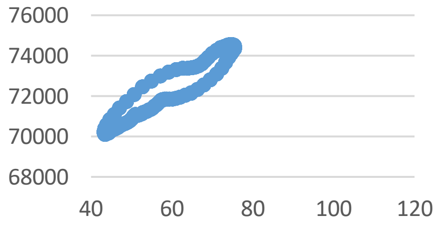

Inlet

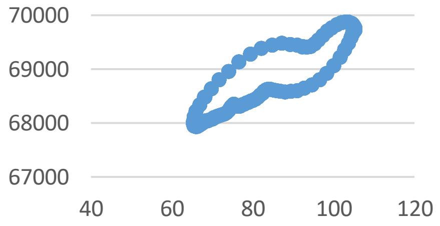

Before aneurysm

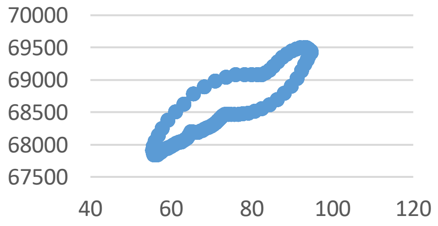

After aneurysm

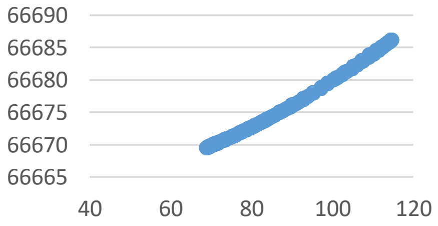

Outlet

Conclusions

5. Diverticulum in AA stabilizes fluid motion

45°
After
aneurysm

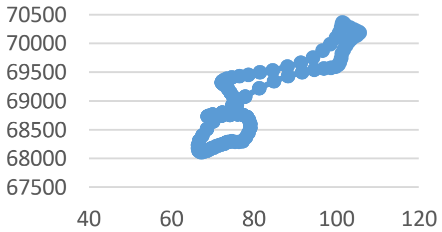

0 D

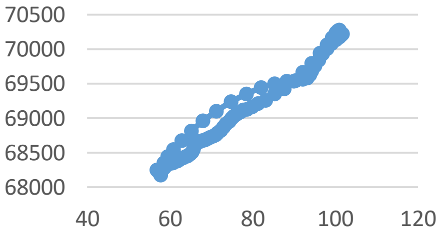

¼ D

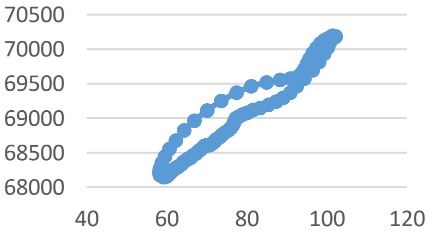

½ D

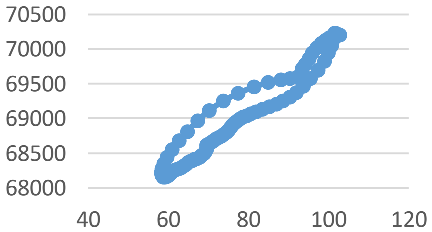

¾ D

Conclusions

1. A computational framework for calculating the total energy of hydroelastic system is created.
2. Kinetic energy of the fluid is comparable with the bending energy of the interface
3. Calculation in 3D simulation FSI real diagrams “pressure-velocity” (p-v) for cerebral arterial aneurysm — bird-like diagram
4. Modification of (p-v) diagrams along vessel: nonlinear oscillation near AA, linear far from AA
5. Diverticulum in AA stabilizes fluid motion

Acknowledgements

- More collaborators for another research area:

Krivoshapkin A.L.

Orlov K. Yu.

Kislitsyn D.S.

Acknowledgements

ЦЕНТР БУРДЕНКО

- Our collaborators for the research:

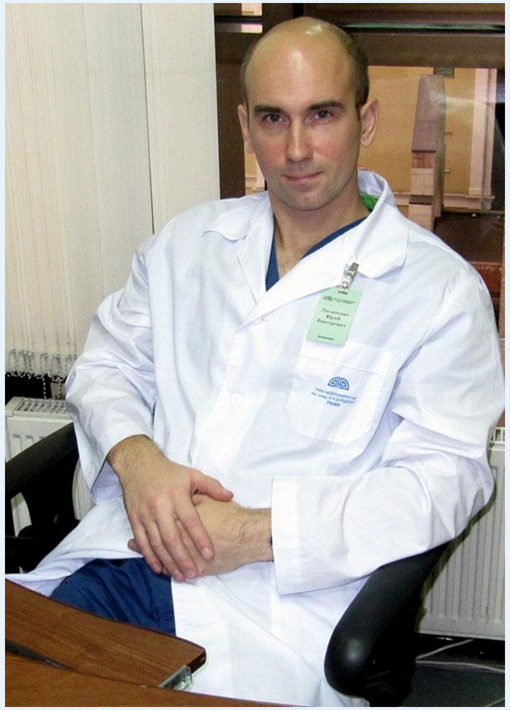

Pilipenko Yu.V.

Acknowledgements

ФЕДЕРАЛЬНЫЙ ЦЕНТР
НЕЙРОХИРУРГИИ
НОВОСИБИРСК

- Our collaborators for the current research:

Dubovoy A.V.

Ovsyannikov K.S.

Thanks for your attention!